Understanding Human Physical Contact and Peripheral Neural Responses in Social Touch Communication

---

A

Dissertation

Presented to

the faculty of the School of Engineering and Applied Science

University of Virginia

---

in partial fulfillment

of the requirements for the degree

Doctor of Philosophy

by

Shan Xu

December 2024

APPROVAL SHEET

This

Dissertation

is submitted in partial fulfillment of the requirements
for the degree of

Doctor of Philosophy

Author: Shan Xu

This Dissertation has been read and approved by the examing committee:

Advisor: Gregory J. Gerling

Advisor:

Committee Member: Sara Lu Riggs

Committee Member: Afsaneh Doryab

Committee Member: Seongkook Heo

Committee Member: Sarah McIntyre

Committee Member:

Committee Member:

Accepted for the School of Engineering and Applied Science:

Jennifer L. West, School of Engineering and Applied Science

December 2024

Abstract

In daily social activities, we often touch others in natural and intuitive ways to share thoughts and emotions—such as tapping to get one's attention, shaking hands to express gratitude, or caressing to soothe one's anxiety. Indeed, it has been widely reported that social affective touch is of critical importance for both human development and social connections. Nowadays, many efforts are attempting to replicate social touch communication using actuated haptic displays. However, it remains challenging to render the rich and subtle emotional expressions delivered by human touch. To achieve this goal, more needs to be understood regarding how touchers exactly adapt their contact strategies to various emotional meanings and social dynamics, and how such different physical skin contact elicits distinct sensory and perceptional responses. Specifically in this work, we addressed this gap by precisely quantifying the social touch delivery using 3D computer vision, analyzing emotional perception using psychophysics, and modeling the underlying peripheral neural coding using machine learning. First, we developed a high-resolution 3D tracking system utilizing a depth camera to capture physical skin contact delivered by bare hands. Time-series contact attributes were calculated including contact area, indentation depth, contact velocities, etc. The tracking system was systematically validated for measurement accuracy and its applicability in social touch scenarios. With this quantification capability, we then conducted psychophysical user studies and correlated perceptions of emotional valence and arousal with contact attributes. Social factors such as relationship status were also analyzed, where we found that while emotion recognition accuracies are similar across couples and strangers, valence and arousal ratings are significantly higher for couples. This discrepancy could be related to couples' fine-tuning of their contact delivery. Next, to further investigate the neurophysiological mechanism of social touch, we conducted microneurography experiments to record single peripheral tactile neurons in response to human touch stimuli. Classification analyses revealed that SA-II and HFA afferent subtypes can effectively decode social touch expressions, with their most informative firing patterns identified accordingly. Our results also show that peripheral neurons decode social touch expressions at time scales 1-2 orders of magnitude longer than those needed for non-social touch. Overall, this work uncovers the details of social touch communication from the perspective of contact delivery, neural pathways, and resulting emotional perception. These insights contribute to future design of haptics that achieve high effectiveness and realism in mediated social touch communication.

Keywords—Social touch, affective touch, emotion communication, tactile perception, 3D tracking, psychophysics, microneurography

Contents

1 Overview

The sense of touch provides us with the means to interact with our surrounding environments. We rely on it in our daily activities, from the basic sensation of shape or texture to the dexterous manipulation of tools. In addition to such discriminative functionalities, touch also plays an important role in communicating social intentions and emotional sentiments. Indeed, evidence is gathering that some emotions can be easily recognized through our sense of touch alone [1]–[4]. Meanwhile, as subtle and complex contact changes are embedded in human-delivered touch, how those changes govern the communication of different social meanings are still not fully understood. From the perspective of touch expression, precise measurements of human-to-human contact are difficult to capture. Among prior efforts using manual annotation or automatic trackers [1]–[3], [5], [6], constraints exist such as low resolution, limited quantifying metrics, or block of direct contact. From the aspect of emotional perception, touch receivers are sensitive to even subtle changes of contact, such as tapping with different frequencies or velocities could communicate distinct meanings from calm to anger. In addition, emotional perception is also subject to different social contexts under which touch communication happens, which makes it even more complex to investigate. Furthermore, from the perspective of neurophysiology, while peripheral nervous system serves as a key element for the perception of affective touch, prior studies mainly focus on stroking contact delivered by mechanical stimuli such as brushes. The firing properties of those afferents in the scenario of naturalist human-to-human touch need to be further explored.

Therefore, the objective of this work is to uncover the details of social touch communication from all three perspectives of human-delivered physical contact, peripheral neuronal functionalities, and resulting emotional perception. More specifically, we seek to measure hand-to-forearm contact using a customized high-resolution 3D visual tracking system (Fig.1.1, Chapter 1). The touch receivers' emotional perception and recognition performance are analyzed over the subtle changes of the touchers' contact delivery, along with the influence of social factors (Fig.1.1, Chapter 2). Moreover, the functional role of different peripheral afferent subtypes in responding to skin contact and mediating emotional percepts are modelled through microneurography experiments as well as mathematical and machine learning analyses (Fig.1.1, Chapter 3).

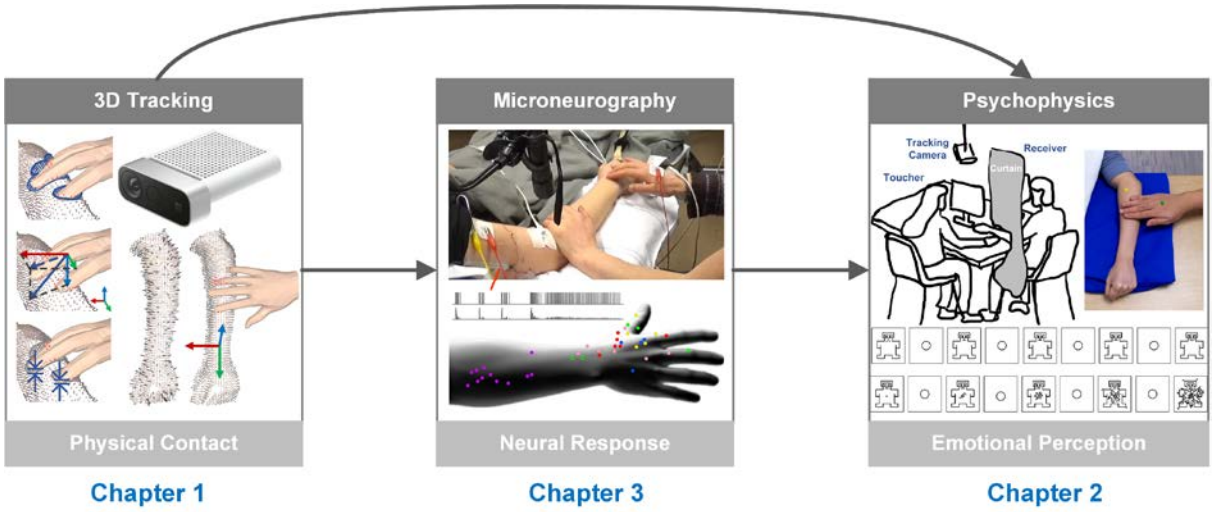

Figure 1.1. Research scope of this dissertation project.

2 Background

Discriminative touch and affective touch

The sense of touch affords the function of discriminating external stimuli by perceiving physical properties of pressure, vibration, temperature, etc., [7], [8]. We rely on such discriminative touch modality for sensorimotor control and decision-making while exploration or manipulation, such as holding or lifting a bottle of water, comparing the softness and ripeness of fruits, or writing a letter by typing on the keyboard or writing with a pen. However, this discriminative functionality of touch cannot fully explain the affective percepts of touch during especially social interactions. In daily activities, we often use touch to express social intentions, comfort friends, bond with teammates, or calm down a crying child. Even the briefest contact from another person could elicit strong emotional experiences, from a supportive tap on the shoulder by a friend, to an unexpected nudge by a stranger. Physical contact could sometimes convey the vitality and immediacy of emotion more powerfully than language. However, the emotional aspects of other senses, such as vision and audition, have attracted more research attention than the ones of touch. In the meanwhile, further investigation of human affective touch also faces challenges due to the difficulties in monitoring and quantifying skin contact attributes that change simultaneously and irregularly.

Quantification of physical contact in human-to-human touch

Focusing on the affective touch of stroking, mechanical or thermal stimuli have been broadly used such as brushing devices [9]–[11]. In so doing, stroking movements can be well controlled and precisely recorded. However, device-delivered stimuli do not fully express the natural and subtle complexities inherent in human-to-human touch. This can result in disconnect with the everyday, real-world interactions for which our sensory systems are finely tuned. Moving towards measuring human-delivered touch, initial efforts used qualitative, manual annotations to describe contact [1], [2], [12], [13]. While adaptable to a wide range of touch interactions and settings, this method is constrained by the time complexity, potential subjectivity of human coders, and a courser set of metrics levels. As a result, automated techniques have been introduced, such as motion trackers [4], [5] and pressure mats [14], [15], with each their own capabilities and limitations. For instance, electromagnetic trackers capture the movements of only a few points, thus is lack of the geometry information, and emits electromagnetic noise incompatible with other biopotential recording equipment. Pressure sensors inhibit direct skin-to-skin contact, where even thin films are shown to attenuate touch pleasantness [16]. Another approach is optical tracking, which includes infrared stereo techniques [4], [17], [18], motion capture systems [19], depth sensing cameras [20], [21], or multiple camera systems such as 3D DeepLabCut [22]. Compared with the other techniques, depth cameras can provide rich and accurate shape information with a concise setup. While depth cameras have been widely used in hand tracking and 3D reconstruction [23], [24], measurement of human-to-human contact interactions is still a pretty new application.

Emotional perception from human touch interaction

We regularly vary the gestures we use to convey different intentions. Yet a more interesting observation is that people can also reuse the same gesture to communicate multiple, distinct messages. For example, stroking might convey both love and sadness, while shaking might convey both happiness and anger [1], [2]. As those examples indicate, distinct sentiments may be shaped by the subtlety in one's touch delivery [18], while what are those subtle contact changes haven't been quantified yet. Meanwhile, we also do not understand whether receivers actually perceive emotions from these touch expressions, as opposed to intuitively discriminating and associating touch expressions as 'codes' with the messages. Classic theory on emotion dictates two dimensions are at play, i.e., valence and arousal, which refer to the pleasantness and the intensity of emotion [25]. As a point of comparison, under the brush stroke to the forearm and hand, changes in velocity govern the sensation of pleasantness with an inverted U-shape relationship [9]. In human affective touch interaction, whether and how contact changes tune the perceived valence and arousal states need to be further explored. Moreover, affective touch typically exhibits distinct

characteristics under various social contexts, such as gender, culture difference and relationship status [26]. Since social touch exists upon the touch initiator and receiver, the relationship between the two individuals might impact their communication strategies. Indeed, it has been found that emotional messages could be more accurately delivered to the partner than a stranger especially for self-focused emotions [3].

Peripheral neural response to physical skin contact

The discriminative modality of touch on hairy skin is classically described as being mediated by five different types of myelinated mechanoreceptive afferents with fast-conducting Aβ fibers [7], [27]. Three of the five types are rapidly adapting afferents, which respond to a temporally or spatially dynamic components of contact[28]. More specifically, rapidly adapting Pacinian corpuscle (PC) units have a single zone of maximum sensitivity in their receptive fields and also respond to taps remote from the receptive field center. Rapidly adapting hair follicle afferent (HFA) units can be activated by deflection of single hairs and have large receptive fields. Rapidly adapting field (Field) units have large receptive fields with a number of zones of high sensitivity [27]. The other two afferent types are slowly adapting [28], which continue to fire during a static component of contact. Slowly adapting type I (SAI) receptive fields contain a number of regions of high sensitivity. Slowly adapting type II (SAII) receptive fields usually have a single zone of maximum responsivity [27]. On the other hand, the affective modality of touch is found to be associated with low-threshold slowly conducting C-tactile afferents (CT). Those afferents can be preferentially activated by gentle tangential stroking contact, which is aligned with the sensation of pleasantness[9]. Recently, evidences have shown that single Aβ afferent is also capable of distinguishing emotions delivered by touch [29]. However, compared with CT afferents, it's still unclear how Aβ afferents encode different patterns of contact attributes underlying affective percepts, such as the changes of velocities and the variation of valence and arousal states.

3 Chapter 1. Quantify Human-to-Human Physical Contact in Social Touch Communication

3.1 Introduction

Social and emotional communication by touch is important to human development in daily life. It contributes to brain and cognitive development in infancy and childhood [30], and plays a role in providing emotional support [31], and forming social bonds [32]. For example, being touched by one's partner mitigates one's reactivity to psychological pressure, as observed in decreased blood pressure, heart rate, and cortisol levels [26]. Behaviors such as compliance, volunteering, and eating habits are also positively improved [26]. Moreover, several works now indicate that particular social messages and emotional sentiments can be readily recognized from touch alone [1]–[4], [18]. Despite their importance and ubiquity, we have just begun to quantify the exact nuances in the underlying physical contact interactions used to communicate affective touch.

To decompose how physical contact interactions evoke sensory and behavioral responses, most prior studies employ highly controlled stimuli, which vary a single factor at a time. In particular, mechanical and thermal interactions are typically delivered to a person's skin using robotically driven actuators [9], [10], [33]–[37]. For example, brush stimuli swept along an arc have been widely adopted to mimic caress-like stroking, while controlling their velocity, force, surface material, and/or temperature. Using such stimuli, C-tactile afferents are shown to be preferentially activated at stroke velocities around 1-10 cm/s, which align with ratings of pleasantness [9], [10], [37]. Beyond experiments to examine brush stroke, more complex interactions have been delivered via humanoid robots and robot hands [35], [36]. However, device-delivered stimuli do not fully express the natural and subtle complexities inherent in human-to-human touch. This can result in disconnect with the everyday, real-world interactions for which our sensory systems are finely tuned.

Measuring and quantifying free and unconstrained human-to-human touch interactions is complex and challenging. In particular, the physical interactions are unscripted, unconstrained, and individualized with rapid and irregular transitions. Indeed, multiple contact attributes often co-vary over time, e.g., lateral velocity, contact area, indentation depth. Therefore, in moving toward quantification, the initial efforts used qualitative, manual annotation to describe touch gestures, and their contact intensity and duration [1], [2], [12], [13]. While adaptable to a wide range of touch interactions and settings, qualitative methods

are constrained by the time required to analyze the data, the potential subjectivity of human coders, and a courser set of metrics and classification levels. For instance, contact intensity is typically classified in only three levels as light, medium, strong. As a result, automated techniques have been introduced, such as electromagnetic motion trackers [4], [5] and sensorized pressure mats [14], [15], with each their own capabilities and limitations. For instance, electromagnetic trackers capture the movement of only a handful of points, thus unable to monitor complex surface geometry, and can emit electromagnetic noise incompatible with sensitive biopotential recording equipment. Pressure sensors and mats inhibit direct skin-to-skin contact, when even thin films are shown to attenuate touch pleasantness [16]. Three-dimensional optical tracking methods have also been employed, such as infrared stereo techniques [4], [17], [18], motion capture systems [19], and stereo cameras with DeepLabCut [22]. While these methods are specialized in tracking joint positions of hands and limbs, they do not capture the shape and geometry of body parts, since the infrared cameras lack sufficient accuracy on depth, motion capture systems only track pre-attached markers, and stereo matching of multiple cameras often fail with texture-less surfaces. In contrast, depth cameras can provide high spatial resolution point clouds and allow shape extraction of texture-less body parts, such as a forearm. Depth cameras, as well, are more readily set up without calibration, afford minimum magnetic interference, and can be located at a larger distance from the area of interest. While depth cameras have been used in hand tracking and 3D reconstruction [23], [24], they have not been used to measure contact interactions in human-to-human touch.

While defined to a degree, we are still deciphering those physical contact attributes vital to social touch communication. In such settings, human touch interactions tend to include gesture, pressure/depth, velocity, acceleration, location, frequency, area, and duration [1], [2], [38], [4], [5], [12]–[15], [17], [18]. To understand the functional importance of specific movement patterns, certain attributes such as spatial hand velocity have been further decomposed into directions of normal and tangential [4] or forward-backward and left-right [5]. Moreover, simultaneous tracking of multiple contact attributes is needed for understanding naturalistic, time-dependent neural output of peripheral afferents. For example, a larger contact area should recruit more afferents, larger force or indentation should generate higher firing frequencies, and optimal velocity in tangential direction should evoke firing of C-tactile afferents [9], [17], [39].

Herein, we develop an interference-free 3D visual tracking system to quantify spatiotemporal changes in skin-to-skin contact during human-to-human social touch communication. Human-subjects experiments evaluate its ability to discern unique combinations of contact attributes used to convey distinct social

touch messages and gestures, as well as the identities of the touchers. Moreover, the system's spatiotemporal accuracy is validated against measurements from independent devices, including an electromagnetic motion tracker, sensorized pressure mat, and laser displacement sensor.

3.2 3D Contact Tracking System

This work introduces a 3D visual tracking system and data processing pipeline, which used a high-resolution depth camera to quantify contact attributes between the bare hand of a toucher and the forearm of a receiver. As illustrated in Fig. 3.1, the tracking system captured the 3D shape and movements of the toucher's hand and the receiver's forearm independently but simultaneously within the same camera coordinate system. Physical skin contact was detected between the hand and forearm based on interactions of their 3D point clouds. Seven contact attributes were derived over the time course of touch, which were contact area, indentation depth, contact duration, overall contact velocity, and its three orthogonal velocity components.

3.2.1 3D Shape and Motion Tracking with Depth Camera

The tracking procedure extracts the detailed 3D shape of the touch receiver's forearm. By merging the camera's RGB and depth information, an RGB-D image was derived and then converted into a dense point cloud per frame. The point cloud was cropped and down sampled to balance information and computation costs. To obtain a clean point cloud of the forearm without background, neighboring points around the forearm were first removed. Two removal methods were used alternatively based on the experimental setup (Fig. 3.1). If the receiver's forearm was placed on a flat surface, such as a table, the points within that flat surface could be removed in a shape-based manner using the plane model segmentation algorithm provided by the Point Cloud Library (PCL) [23]. In the second case, if a monochromatic holder was set underneath the forearm, such as a cushion, then the points of that holder could be removed by color-based segmentation in the HSV color space. Next, the 3D region growing segmentation algorithm [23] was applied to separate the rest point cloud into multiple clusters according to the smoothness and distance between points. Since neighboring points around the forearm were removed in advance, points farther away in the background were assigned to separate clusters instead of being blended with the arm. Finally, by setting a relatively large smoothness threshold, all arm points could be grouped into one cluster despite the curvature of the forearm shape.

In human-to-human touch scenarios, the receiver's forearm is frequently occluded by the toucher's hand. Given that a blocked arm region is nearly impossible to capture, only the shape of the forearm prior to

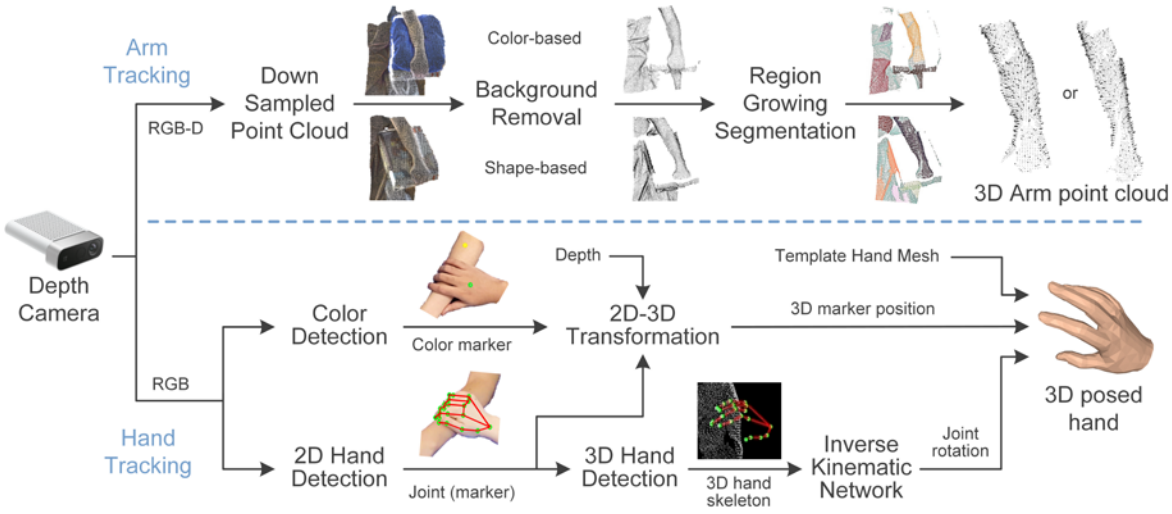

Figure 3.1. 3D visual tracking setup and data workflow. The toucher's hand and receiver's forearm are tracked using one depth camera (Microsoft Azure Kinect). Forearm shape is extracted as a point cloud while the hand mesh is animated by the gestures and movements of the toucher's hand.

the contact was extracted. More specifically, the forearm point cloud was extracted before the beginning of each contact interaction to update its shape and position. During the contact, its position was refreshed in real-time according to the 3D position of the color marker on the arm, though its shape was not updated during the contact. Once the forearm was shape updated, the normal vector $\boldsymbol{n}_{arm}^{i}$ of each arm point $\boldsymbol{p}_{arm}^{i}$ was calculated and updated as well to facilitate further contact detection and measurement.

The hand tracking procedure was developed to capture the posture and position of the toucher's hand by combining depth information with a monocular hand motion tracking algorithm [40]. The algorithm is robust to occlusions and object interactions, which is advantageous in hand-arm contact. The monocular tracking algorithm contains two neural network modules to predict the 3D location and rotation of all 21 hand joints. In the first module of the hand joint detection network, features extracted from the 2D RGB image were first fed into a 2-layer convolutional neural network (CNN) to detect the probability of the 2D position of all joints. Then, another two 2-layer CNN was used to predict the 3D position of hand joints based on 2D features and 2D joint position estimates. In the second module of the inverse kinematic network, a 7-layer fully connected neural network was designed to derive the 3D rotation of each joint. Finally, the parametric MANO hand model [41] was employed to incorporate 3D joint rotations to animate the hand mesh following the shape and pose of the toucher's hand.

The rendered hand mesh was expressed in the local hand coordinate without the spatial information of the hand position. Therefore, depth information is incorporated here to locate the hand mesh in the camera coordinate, according to the movement of any hand joint or the color marker on the back of the hand (Fig. 3.1). Specifically, the 2D position of the color marker was detected in the in the HSV, while the 2D position of the joint was retrieved from the detected 2D hand. The depth value of the hand joint or marker was derived by transforming the depth image to the RGB coordinate, which was then used to obtain its 3D position following the camera projection model. By identifying the corresponding point of that marker or joint in the hand mesh model, the posed hand mesh was moved in real-time following the toucher's hand movements.

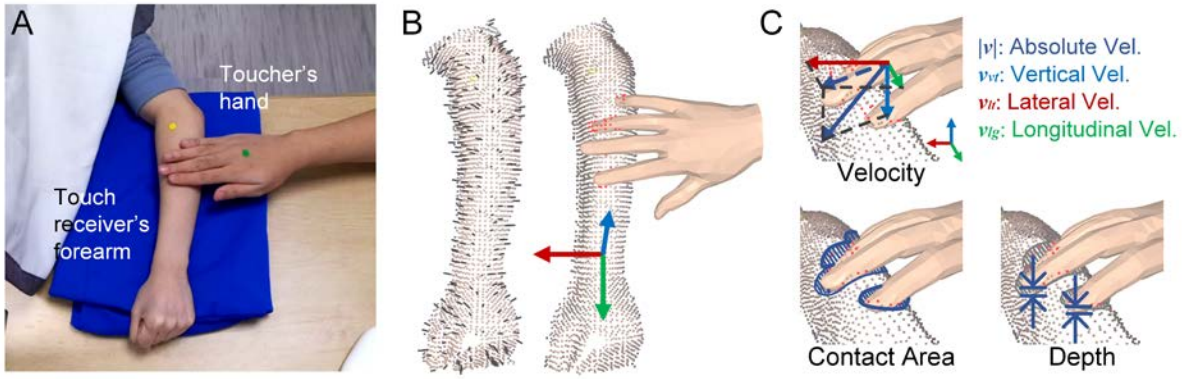

Figure 3.2. Definition of contact attributes. (**A**) Color image from video recorded by depth camera. Two color markers were placed on the toucher's hand and the receiver's forearm respectively to support motion tracking. (**B**) 3D forearm point cloud and hand mesh. Short black line segments represent the norm vector of arm points; red points on the forearm represent the region contacted by the hand. In the arm coordinate, the vertical axis (blue) is designated along the vertical direction pointing right upward, the longitudinal axis (green) is parallel with the arm direction from elbow to wrist, and the lateral direction is perpendicular to the two axes pointing to the internal side of the forearm. (**C**) Six time-series attributes include absolute velocity, which is the absolute value of spatial contact velocity; three orthogonal velocity components corresponding to the three axes of the arm coordinate; contact area, which is the overall area on the forearm being contact; and the indentation depth as the average depth applied on the forearm by the hand.

3.2.2 Calculation of Contact Attributes

Hand-arm contact was measured in a point-based manner, which afforded higher resolution compared with a geometry-based method [4]. First, a contact interaction between the hand and forearm was detected when at least one vertex point of the hand mesh was underneath the arm surface. More specifically, for each hand vertex point $\boldsymbol{p}_{hand}^{i}$, its nearest arm point $\boldsymbol{p}_{arm}^{i}$ was found first. Then, as detailed in Equation (1), if the angle between the vector $\boldsymbol{p}_{hand}^{i} - \boldsymbol{p}_{arm}^{i}$ and the normal vector $\boldsymbol{n}_{arm}^{i}$ of arm point $\boldsymbol{p}_{arm}^{i}$ is larger than or equal to 90 degrees, this hand vertex is marked as underneath the arm surface.

$$F_{contact} = \begin{cases} 1 & \forall (\boldsymbol{p}_{hand}^{i} - \boldsymbol{p}_{arm}^{i}) \cdot \boldsymbol{n}_{arm}^{i} \leq 0 \\ 0 & \exists (\boldsymbol{p}_{hand}^{i} - \boldsymbol{p}_{arm}^{i}) \cdot \boldsymbol{n}_{arm}^{i} > 0 \end{cases} \quad (1)$$

Physical contact attributes were calculated when hand-arm contact was detected. Indentation depth is measured as Equation (2). In particular, N_C is the number of hand vertex points contacted with the forearm. For each contacted hand point $\boldsymbol{p}_{hand}^{i}$, its indentation depth d^i is approximated as half the distance between $\boldsymbol{p}_{hand}^{i}$ and its nearest arm point $\boldsymbol{p}_{arm}^{i}$. The half scale was used because the line between two points might not be perpendicular to the arm surface. The overall indentation d deployed by the hand to the forearm is defined as the average indentation depth of all N_C contacted hand points:

$$Depth = \frac{\sum_{i=1}^{N_C} \left\| \boldsymbol{p}_{hand}^{i} - \boldsymbol{p}_{arm}^{i} \right\|_2}{2N_C} \ . \quad (2)$$

Contact area is measured as the summed area of all contacted arm points. As shown in Equation (3), the unit area S^i for one arm point is calculated as a sphere whose radius is the average neighbor distance, and π is round to 3. Within the arm point cloud of N_{all} points, the average neighbor distance l_{nbr}^{i} is calculated as the average distance of all points to their nearest neighbor points:

$$Area = 3N_C \left(\frac{\sum_{i=1}^{N_{all}} l_{nbr}^{i}}{N_{all}}\right)^2 \ . \quad (3)$$

In addition to cutaneous contact attributes, the velocity of hand movement was quantified when contact was detected. The absolute contact velocity V_{abs} is measured as the modulus of the spatial hand velocity $\boldsymbol{v}_{Hand}$:

$$V_{abs} = \left| \frac{\boldsymbol{p}_{Hand}^{t} - \boldsymbol{p}_{Hand}^{t-1}}{\triangle t} \right| . \quad (4)$$

In Equation (4), hand position $\boldsymbol{p}_{Hand}$ is represented by the position of the middle metacarpophalangeal joint. By defining another coordinate on the receiver's forearm (Fig. 3.2C), spatial hand velocity $\boldsymbol{v}_{Hand}$ is further decomposed in the arm coordinate as three velocity components V_{vt}, V_{lg}, V_{lt} parallel with its axis of the arm coordinate (Fig. 3.2C). The vertical axis $\boldsymbol{i}_{vt}$ of the arm coordinate is aligned with the vertical direction pointing upright. It could be obtained as the normal vector of a point on a horizontal surface, like a table, or the normal vector of a point on the top of the receiver's forearm. Vertical velocity V_{vt} is the hand velocity component in this direction:

$$V_{vt} = \boldsymbol{v}_{Hand} \cdot \boldsymbol{i}_{vt} . \quad (5)$$

The longitudinal axis $\boldsymbol{i}_{lg}$ is aligned with the direction of the arm bone, pointing from elbow to wrist. To derive this axis, the camera was orientated to display the forearm vertically in the 2D image. Then, the direction of the arm bone in the 2D image was set to be parallel with the y axis of the image coordinate. By projecting the y axis $\boldsymbol{y}$ of the camera coordinate onto the perpendicular plane of the vertical axis $\boldsymbol{n}_{vt}$, the longitudinal axis follows the direction of the projected vector:

$$\boldsymbol{i}_{lg} = \frac{\boldsymbol{y} - (\boldsymbol{y} \cdot \boldsymbol{i}_{vt})\boldsymbol{i}_{vt}}{\|\boldsymbol{y} - (\boldsymbol{y} \cdot \boldsymbol{i}_{vt})\boldsymbol{i}_{vt}\|_2} . \quad (6)$$

$$V_{lg} = \boldsymbol{v}_{Hand} \cdot \boldsymbol{i}_{lg} . \quad (7)$$

Lastly, the lateral axis $\boldsymbol{i}_{lt}$ is perpendicular to the plane of longitudinal and vertical axis, following the right-hand rule:

$$\boldsymbol{i}_{lt} = \boldsymbol{i}_{lg} \times \boldsymbol{i}_{vt} . \quad (8)$$

$$V_{lt} = \boldsymbol{v}_{Hand} \cdot \boldsymbol{i}_{lt} . \quad (9)$$

Compared with the overall hand velocity, these velocity components can quantify the directional nature of the hand movements.

Moreover, contact duration is measured as a scalar value for each hand-arm touch interaction, which is the sum of time over which contact was detected. Given the recording frequency f of the camera is 30 Hz and N_f is the number of frames per interaction, the contact duration is measured as:

$$Duration = \frac{\sum_{i=1}^{N_f} F_{contact}}{f} \quad . \qquad (10)$$

3.3. Experiment 1: Human-to-Human Affective Touch Communication

The first experiment was designed with the task of human-to-human emotion communication. Touchers was instructed to deliver cued emotional messages, e.g., happiness, sympathy, anger, to the touch receiver at the receiver's forearm using preferred gestures, e.g., tapping, holding, stroking. Recorded contact attributes were then used to differentiate delivered messages, utilized gestures, and individual touchers. Contact analysis was conducted on the platform with the Intel Core i9-9900 CPU, 3.1 GHz, 64 GB RAM, and a NVIDIA GeForce RTX 2080 SUPER GPU. The same platform was used for the second experiment.

3.3.1 Experimental Design

3.3.1.1 Cued Emotional Messages and Gesture Stimuli

Seven emotions of anger, attention, calm, fear, gratitude, happiness, and sympathy were selected as cued messages for touchers to express (Table 3.1). Those messages were adopted from prior studies and have been observed to be recognizable through touch alone [1]–[4], [18]. Among them, gratitude and sympathy are prosocial expressions that are more effectively communicated by touch compared with those self-focused. Anger, happiness, and fear are universal expressions that are commonly communicated by facial, vocal, and touch expressions. Attention and calm are also preferred messages in touch interactions and can be correctly interpreted significantly better than chance. For each of the cued messages, three commonly used gestures were adopted from prior studies [1], [3], [4], [18] (Table 3.1). Holding and squeezing were combined into one since they share a similar hand gesture and hand motion. Similarly, hitting was combined with the tapping gesture, but only for the message of anger.

Table 3.1. Available gestures for each cued emotional message in touch communication task

	Cued Emotional Messages						
	Anger (Ag)	Attention (At)	Calm (C)	Fear (F)	Gratitude (G)	Happiness (H)	Sympathy (S)
Gestures	Hit/Tap	Tap	Hold/Squeeze	Squeeze/Hold	Hold/Squeeze	Shake	Stroke
	Squeeze/Hold	Shake	Stroke	Shake	Shake	Tap	Tap
	Shake	Squeeze/Hold	Tap	Tap	Tap	Stroke	Squeeze/Hold

3.3.1.2 Participants

The human-subjects experiments were approved by the Institutional Review Board at the University of Virginia. Ten participants were recruited as touchers, including five males and five females (mean age = 23.8, SD = 5.0). Another five participants were recruited as touch receivers with three males and two females (mean age = 24.0, SD = 4.4). Five experimental groups were randomly assembled, where each group consisted of one male toucher, one female toucher, and one receiver. Each group performed two experimental sessions with one session conducted by the male toucher and another one conducted by the female toucher. Written informed consent was obtained from all participants.

3.3.1.3 Experimental Setup

To avoid visual distractions during the experiment, touchers and receivers sat at opposing sides of an opaque curtain. They were instructed to not speak to each other. As shown in Fig. 3.2A, a cushion was set on the table at the toucher's side upon which the receiver rested her or his left forearm. Cued emotional messages and corresponding gestures were displayed to the toucher on the computer screen. The toucher could select the gesture and proceed to the next message using the computer's mouse. Cued messages and the toucher's selection of gestures were also recorded. As illustrated by a snapshot of the experiment recording by depth camera (Fig. 3.2A), the camera was set in front of the cushion and orientated towards it.

3.3.1.4 Experimental Procedures

In each session, seven cued emotional messages were communicated with each repeated six times. The 42 message instructions were provided in random order. In each trial, one message was displayed on the screen with three gestures listed below. Touchers had five seconds to choose a gesture and report it on the computer display. For each cued message, the three provided gestures were identical but their order was randomized trial by trial. After that, the toucher delivered the message, by touching the receiver's forearm from elbow to wrist, using the right hand. Within each trial, only the chosen gesture was used. The use of other gestures or a combination of gestures was not allowed. For the same cued message across trials, touchers were free to use the same gesture or change to another gesture. A gesture could be deployed in any pattern of contact deemed appropriate by the toucher. No constraints or instructions were given for delivering the gesture, such as its duration, hand region employed, intensity, or repetition. At the end of a trial, by clicking the 'Next' button on the bottom of the computer display, the toucher initiated the next trial with a new message word and corresponding three gestures.

3.3.1.5 Data Analysis

Overall, 420 trials were performed in ten experimental sessions. Twelve trials were excluded from analysis as contact interactions were not properly recorded. Statistical and machine learning analyses were performed to examine the measured contact attributes.

To identify the contact pattern between touch gestures, paired-sample Mann–Whitney U tests were applied across gestures per contact attribute. For time-series attributes, the mean value was used. Since longitudinal velocity, lateral velocity, and vertical velocity are signed variables, the mean was derived from the absolute value of those variables. Contact duration as a scalar variable was directly compared across gestures. To evaluate which of the contact attributes could best identify or describe a certain type of touch gesture, the importance of each attribute in predicting that gesture was identified using a random forest classifier. The mean values of time-series attributes together with the scalar attribute served as inputs. For example, in predicting the stroking gesture, all trials were labeled in a binary fashion as delivering or not delivering this gesture, instead of being labeled as the four gesture types. Seventy-five percent of trials were randomly assigned as the training set and those remaining were assigned as the test set. The permutation method was used to derive the importance of attributes. The value was obtained as the average of 100 repetitions of classification, with 10 permutations per classification.

3.3.2 Results

3.3.2.1 Physical Contact Attributes in Human-to-Human Touch

Human-to-human physical contact interactions between social messages, gestures, and individual touchers were quantified by their contact attributes. As shown in Fig. 3.3A, exemplar data for the four touch gestures (shake, tap, hold and stroke) exhibit distinct patterns across the contact attributes, consistent with expected hand movements per gesture. In particular, the stroking gesture was characterized by regular patterns in longitudinal velocity, which implies slow and repetitive movements along the direction of the forearm. For the shaking gesture, velocity attributes depicted large changes in frequency and relatively lower amplitude. Meanwhile, velocities in all three directions changed simultaneously, indicating a spatial direction in the movement of the toucher's hand. The tapping gesture was quantified as discontinuous, large-amplitude spikes of short contact duration. Compared with other touch gestures, holding gesture exhibited relatively stable contact with minimal changes. With further inspection into each gesture, contact patterns with subtle differences could also be captured across emotional messages. Such as in the shaking gesture, happiness was delivered with higher velocities

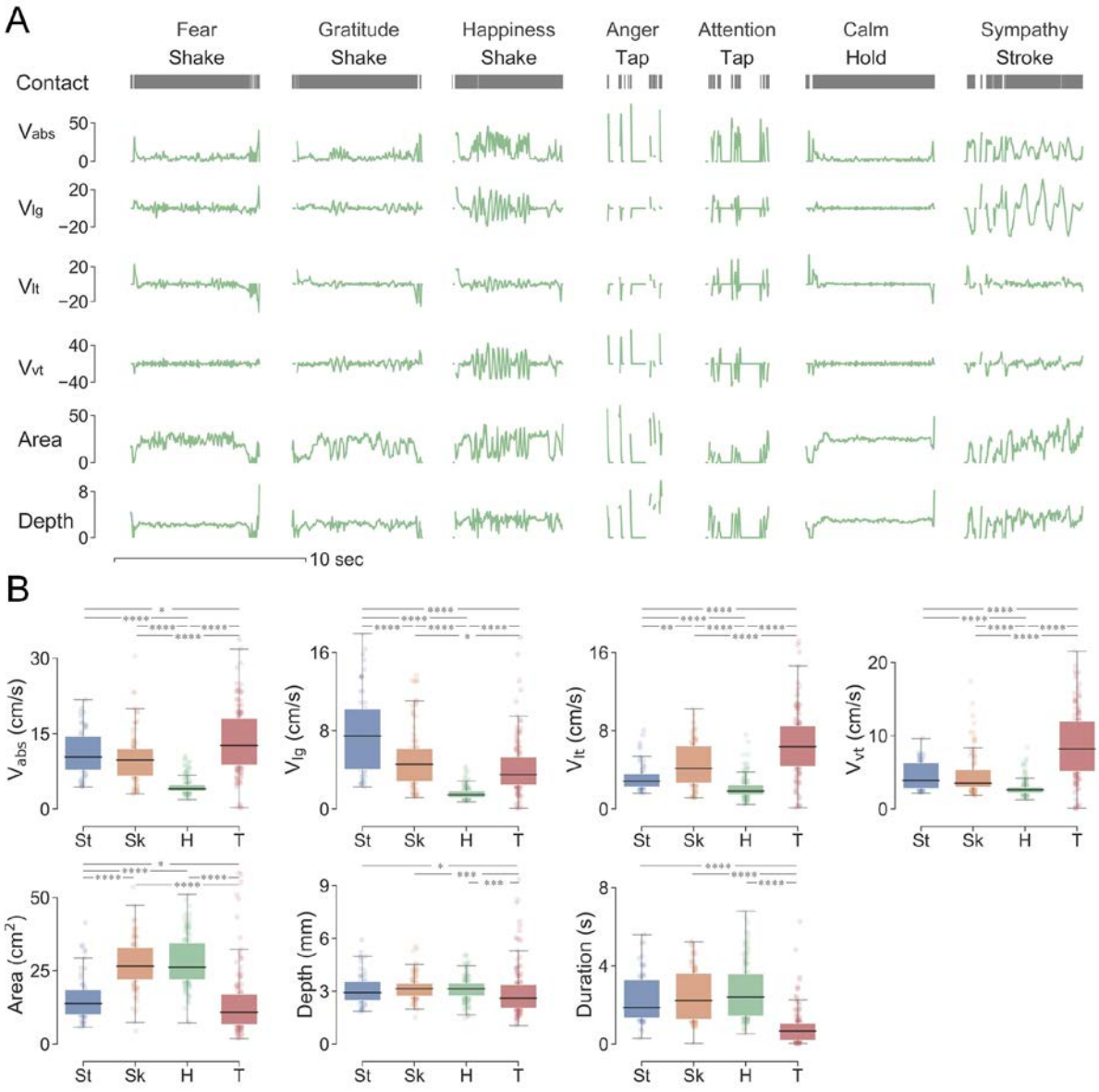

Figure 3.3. (**A**) Time-series recordings of each contact attribute across touch gestures and delivered messages. Distinct contact patterns were captured by the spatiotemporal changes of those attributes. The *Contact* variable represents the status of the being contacted or not. V_{abs} denotes the absolute contact velocity (cm/s), V_{lg} denotes the longitudinal velocity (cm/s), V_{lt} denotes the lateral velocity (cm/s), V_{vt} denotes the vertical velocity (cm/s), *Area* denotes the contact area (cm^2), and *Depth* denotes the indentation depth (mm). (**B**) Comparison of contact attributes across the four touch gestures. $*p < 0.05$, $**p < 0.01$, $***p < 0.001$, $****p < 0.0001$ were derived by paired-sample Mann–Whitney U tests.

compared with the expression of fear. Within the tapping gesture, shorter but more intensive contact was recorded when expressing anger compared with attention.

As shown in Fig. 3.3B, the four touch gestures were statistically differentiable according to several of their contact attributes. For instance, absolute contact velocity can differentiate all gesture pairs except for that of stroking and shaking. With the contact attribute of longitudinal velocity, stroking was differentiable from shaking as it afforded higher longitudinal velocity. This also aligns with hand movements during stroking that are typically along the direction of the forearm. Both shaking and tapping gestures exhibited significantly higher longitudinal velocities than the holding gesture. With the lateral velocity, significant differences were derived among all four gestures, where tapping and shaking gestures afforded higher amplitudes than stroking and holding. As for the vertical velocity, the tapping gesture was associated with significantly higher velocities than others, which aligns with its up-down movements. Across all velocity attributes, the holding gesture was significantly distinct from other ones.

For the contact area attribute, shaking and holding gestures exhibited significantly higher values than the stroking gesture, and then tapping. Indeed, participants generally used the whole hand to deliver holding and shaking, while only the finger digits for stroking and the fingertips for tapping. Moreover, with indentation depth and contact duration, tapping was distinct amongst the gestures with significantly lower depth and shorter duration. Note the hand motion with the tapping gesture could be faster than the recording frequency of the camera, where one trial of contact might not be entirely captured and thus lead to a lower estimation of indentation depth.

3.3.2.2 Classification amidst Gestures, Messages, and Individuals

In Fig. 3.4, the contact attributes are shown to robustly classify touch gestures, delivered messages, and individual touchers at accuracies better than chance, which is 25%, 14.3%, and 10% respectively. For gesture prediction, the accuracy was 87% when the mean values of contact attributes were used as predictors (Fig. 3.4A). The prediction accuracy slightly increased to 92% when all relevant features were used as more information was included and was around 86% when predicted by the time-series data. In classifying delivered emotional messages, the accuracy was 54%, 57%, and 55%, for the three respective feature classes (Fig. 3.4C). Moreover, in classifying the individual touchers, the accuracies were 56%, 72%, and 77%, respectively. For the importance ranking of the contact attributes, those of longitudinal velocity, contact duration, and contact area were typically more important.

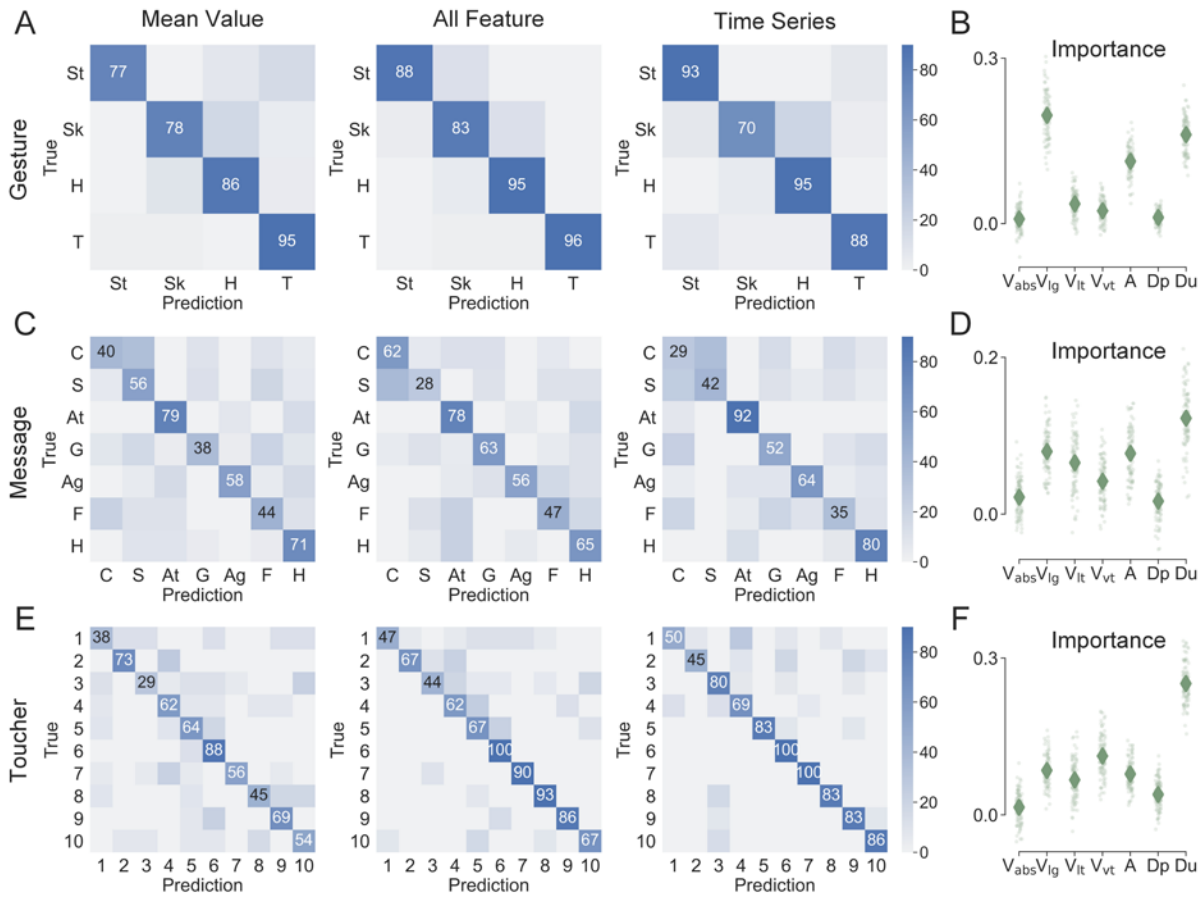

Figure 3.4. Classification of touch gestures, delivered messages, and toucher individuals using the mean value, all relevant features, and time-series data of contact attributes, respectively. The accuracy in prediction of (**A**) touch gestures, (**C**) delivered messages, (**E**) toucher individual are shown, as well as the importance of particular contact attributes in classifying (**B**) touch gestures, (**D**) delivered messages, (**F**) toucher individual. Numbers and colors in confusion matrices represent the prediction percentage. In the importance plots, the diamonds denote means; points denote importance values from 100 repetitions of classification.

3.4. Experiment 2: Technical Validation on the Visual Tracking Method

The second experiment was designed to validate the effectiveness of the 3D visual tracking system in measuring controlled human movements against those from independent devices, including an electromagnetic motion tracker, sensorized pressure mat, and laser displacement sensor. These techniques are used commonly in haptics studies [4], [5], [14], [15], [42], [43]. In this experiment, the observed contact attributes were compared within controlled touch conditions, e.g., stroking in different

directions at preset velocities, pressing with different parts of the hand varying in contact area, and tapping at different depth magnitudes.

3.4.1 Contact Velocity Validation Using Electromagnetic Tracker

3.4.1.1 Experimental Setup

Measurements of the directional components of contact velocity, including absolute velocity, longitudinal velocity, lateral velocity, and vertical velocity were validated against those of an electromagnetic (EM) motion tracker (3D Guidance, Northern Digital, Canada. 6 DOF, 20-255 Hz, 1.4 mm RMS position accuracy, 78 cm range; 0.5° RMS orientation accuracy, ±180° azimuth & roll, ±90° elevation range). Both tracking systems were operated simultaneously to capture controlled movements of the human hand touching the forearm. The transmitter of the 3D Guidance EM tracker was oriented to be aligned with the arm coordinate (Fig. 3.5A). The sensor of the EM tracker was attached to the toucher's back of the hand near the middle metacarpophalangeal joint.

3.4.1.2 Experimental Procedures

Table 3.2. Experiment procedure for validating contact velocity

	Gesture	Direction	Velocity Levels	Repeated Trials per Level	Trials in Total
1	Stroking	Longitudinal	Low, Medium, High	3	9
2	Stroking	Lateral	Low, Medium, High	3	9
3	Tapping	Vertical	Low, Medium, High	3	9
4	Holding	None	None	1	1 (long duration)
5	Shaking	Irregular	Irregular	1	1 (long duration)

Given velocity components were defined in different directions, five test gestures were designed in total. The first two test gestures were stroking contact along the forearm in longitudinal and lateral directions, respectively. The third test gesture involved tapping vertically to the surface of the forearm. The fourth gesture was holding without movement. The fifth gesture was shaking, which was delivered in an irregular and arbitrary way with different directions and velocities included. For the first three test gestures, each one was performed in three levels of velocities, from low to medium to high. Each velocity level was repeated for three trials. For example, the longitudinal stroking gesture was performed as three trials of stroking in the longitudinal direction with lower velocity, followed by three trials of stroking with medium velocity, and concluded by three trials of stroking with higher velocity. The direction of hand movement

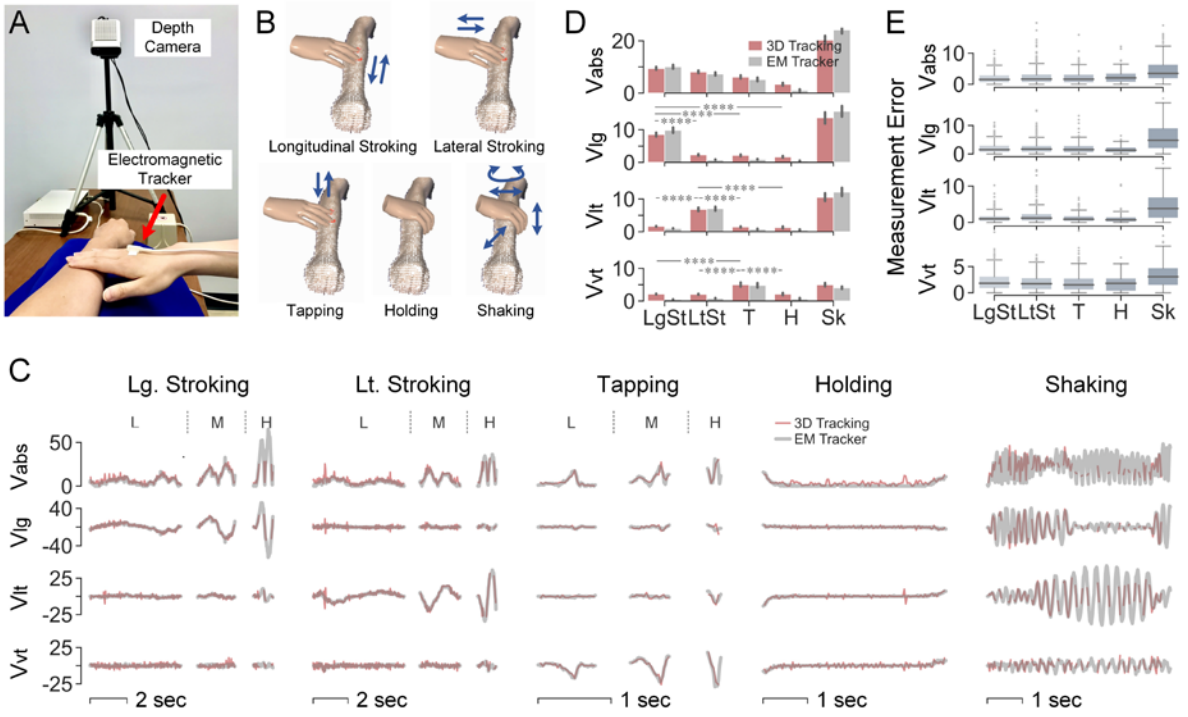

Figure 3.5. Validation of contact velocity measurements using EM tracker. (**A**) Experimental setup. (**B**) Five test gestures. (**C**)Velocity (cm/s) over time by the two tracking systems. For the first three test gestures, one trial is shown per force level, i.e., low, medium, and high force. (**D**) Mean values of velocities (cm/s) per test gesture. ****$p < 0.0001$ were derived by paired-sample Mann–Whitney U tests. (**E**) Errors (cm/s) of measured velocities between the two systems for each test gesture.

and level of velocity were behaviorally controlled by the trained toucher, who performed all three validation experiments. Shaking and holding gestures were performed only once but lasted for a longer time to collect enough amount of data for validation analysis.

3.4.1.3 Data Analysis

Similar to the 3D visual tracking system, the four velocity attributes captured by the EM tracker were derived from the original time-series position data. For either tracking system, the absolute mean value of each velocity attribute was calculated per test gesture. Mann–Whitney U tests were conducted across the test gestures based on mean velocity collected by the visual tracking system. Measurement errors between the two tracking systems were derived per attribute and test gesture. Since the sampling rates of the two systems differ, i.e., 30 Hz for the Azure Kinect camera and 60 Hz for the EM tracker, data

collected from the EM tracker was resampled to be synchronized. More specifically, the EM tracking data was first interpolated and sampled according to the timestamps of the 3D visual tracking data. Then, the error was calculated for each time point between the velocities from the two systems.

3.4.1.4 Results

In Fig. 3.5, velocities measured by the 3D visual tracking system were accurate when compared with the EM tracker. The time-series data from the two systems well overlapped amidst touch gestures (Fig. 3.5C) and the average velocities of the gestures were comparable between the two systems (Fig. 3.5D). Shaking delivered high velocities in all three directions, while velocity in a certain direction was significantly higher for hand movements along that direction. All four velocity attributes were significantly lower when the holding gesture was performed. As shown in Fig. 3.5E, the measurement error was 1-2 cm/s for the first four gestures and relatively higher at around 5 cm/s for the shaking gesture.

3.4.2 Contact Area Validation Using Pressure Mat

3.4.2.1 Experimental Setup

Contact area was measured simultaneously with the 3D visual tracking system and a sensorized pressure mat (Conformable TactArray SN8880, Pressure Profile Systems, USA, 7x14 cm, 12x27 sensing elements, 0.002 psi pressure resolution, 3.05 psi pressure range, 29.3 Hz). Note that contact was evaluated between the toucher's hand and the surface of the pressure mat which was overlaid on top of the bare forearm, for which it had been custom-designed (Fig. 3.6A). Based on pilot tests with the pressure mat, its measurement of contact area could be inaccurate due to the creases caused by pressing when the mat was put on the forearm. To attenuate this effect, a piece of single-face corrugated cardboard was placed between the forearm and the mat to generate a smooth and stiffer curved surface following the shape of the forearm.

3.4.2.2 Experimental Procedures

Table 3.3. Experiment procedure for validating contact area

	Test Gesture	Force Levels	Repeated Trials per Level	Trials in Total
1	Single-finger pressing	Low, Medium, High	3	9
2	Multiple-finger pressing	Low, Medium, High	3	9
3	Holding	Low, Medium, High	3	9
4	Shaking	Irregular	1	1 (long duration)

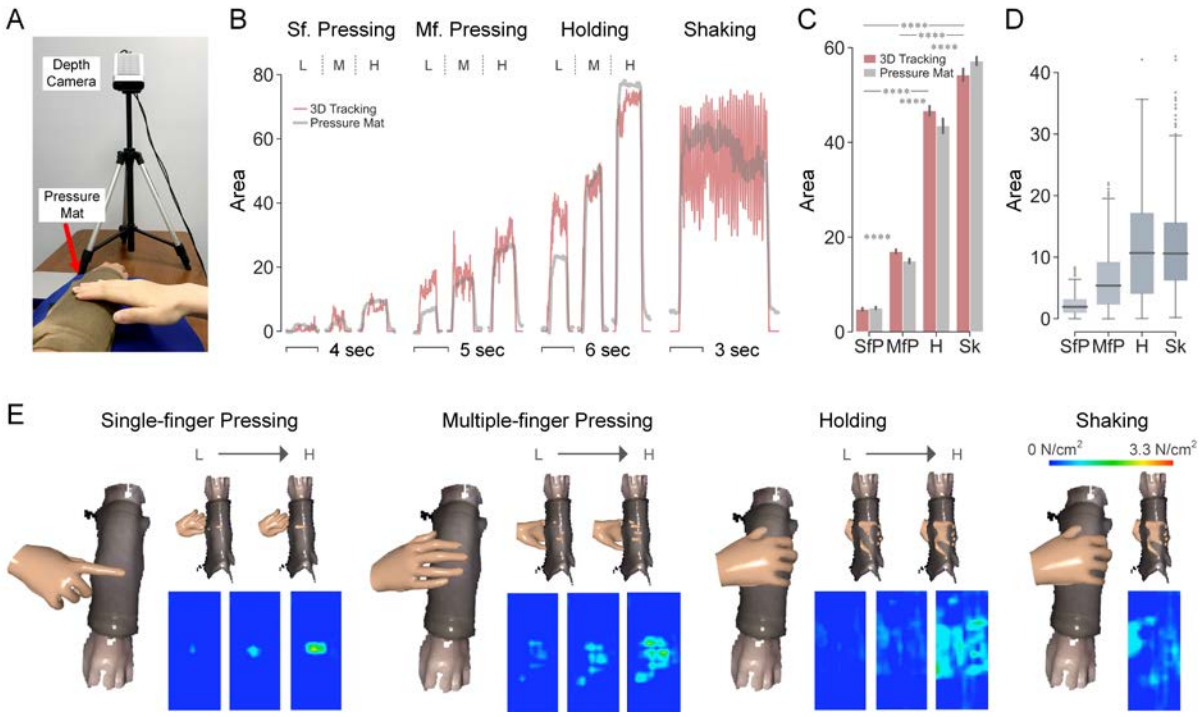

Figure 3.6. Validation of contact area measurements using sensorized pressure mat. (**A**) Experimental setup. (**B**) Contact area (cm^2) over time by the two systems. For the first three test gestures are shown one trial per force level, i.e., low, medium, and high force. (**C**) Mean values of contact area (cm^2) per test gesture. ****$p < 0.0001$ were derived by paired-sample Mann–Whitney U tests. (**D**) Differences of measured contact area (cm^2) between the two systems per test gesture. (**E**) Visualization of hand-arm contact in top view (left) and bottom view (top right) with heatmaps of contact pressure tracked by sensorized pressure mat across force levels (bottom right).

Four test gestures were employed. The first test gesture was single-finger pressing with the index finger. The second gesture was multiple-finger pressing with all fingers except for the thumb. The third gesture was holding and the fourth gesture was shaking. For the first three test gestures, three levels of force were applied from low to medium to high, to generate different levels of contact area within a gesture. Each force level was repeated for three trials. Per trial, the toucher's hand moved downward into the receiver's forearm and maintained pressure/hold at that force level for more than three seconds. For example, the single-finger pressing gesture was conducted for three trials of pressure using the index finger at a low force level, followed by three trials of pressure at a medium force level, and three trials of pressing with a higher force level. The shaking gesture was conducted for one trial with a long duration.

Any patterns of shaking could be applied in an irregular and arbitrary manner including different directions, velocities, etc.

3.4.2.3 Data Analysis

The average contact area per gesture was calculated for both measurement systems. Significance tests were performed across gestures based on average areas from the visual tracking system. The measurement differences between the two systems were derived from time-series recordings per gesture. To overcome the time discrepancy of sampling, data collected by the sensorized pressure mat was resampled to be synchronized with the visual tracking system.

3.4.2.4 Results

In Fig. 3.6B, the time-series contact areas captured by the 3D visual tracking system and the sensorized pressure mat well overlapped with each other across test gestures and force levels. While single-finger pressing (SfP) afforded the smallest contact area, larger multiple-finger pressing (MfP) was significantly smaller than holding (H) and shaking (Sk) (Fig. 3.6C). As shown in Fig. 3.6D, the measurement differences between the two systems were around 2 and 6 cm^2 for SfP and MfP, while increased to 11 cm^2 for holding and shaking.

3.4.3 Indentation Depth Validation Using Laser Sensor

3.4.3.1 Experimental Setup

Indentation depth was first validated using a laser displacement sensor (optoNCDT ILD 1402-100, Micro-Epsilon, Germany, 100 mm range, 10 µm resolution, 1.5 kHz). The sensor was mounted on a customized stand with the beam pointing downward. Given its capability of measuring the displacement of one point in only the vertical direction (Fig. 3.7A), a limited set of tapping gestures was evaluated in this setting. Other gestures were then tested with a separate validation procedure using the sensorized pressure mat (Fig. 3.7E).

3.4.3.2 Experimental Procedures

Two test gestures were examined with the laser sensor. The first gesture was multiple-finger tapping, where the movement of the tip of the middle finger was tracked. The second gesture was tapping with the palm, measured at one point on the back of the hand. Holding, shaking, and stroking gestures were not examined here since these gestures are typically not conducted in the vertical direction. Within each gesture, three force levels were employed, i.e., low, medium, high, and each repeated in three trials. The

toucher quickly tapped for four times within one trial. For example, the palm tapping gesture was conducted for three trials of four taps with the palm at a low force level, followed by three trials of four taps at a medium force level, and three trials of four taps at a high force level. The raw data collected by laser sensor contained displacements of both indentations into the skin and movements in the air. Therefore, the toucher conducted a 'zero contact' touch to the forearm at a minimally perceptible force prior to each test gesture.

Within the setting of sensorized pressure mat, the three test gestures performed were single-finger pressing, multiple-finger pressing, and holding. Each gesture was performed in three force levels, where each level was repeated for three trials.

Table 3.4. Experiment procedure for validating indentation depth

	Validation with Laser Sensor			
	Test Gesture	**Force Levels**	**Repeated Trials per Level**	**Trials in Total**
1	Multiple-finger tapping	Low, Medium, High	3 (4 taps per trial)	9
2	Palm tapping	Low, Medium, High	3 (4 taps per trial)	9
	Validation with Pressure Mat			
	Test Gesture	**Force Levels**	**Repeated Trials per Level**	**Trials in Total**
1	Single-finger pressing	Low, Medium, High	3	9
2	Multiple-finger pressing	Low, Medium, High	3	9
3	Holding	Low, Medium, High	3	9

3.4.3.3 Data Analysis

For the validation with laser sensor, average indentation depth at each force level was obtained by aggregating the two tapping gestures. Significance tests were conducted across force levels based on the average depth collected by the visual tracking system. Measurement errors between the two systems were derived from time-series recordings at each force level. The data from the laser sensor was resampled according to the 3D visual tracking system's results. For quick tapping gestures, slight temporal discrepancies between the two recordings could derive large differences. Therefore, the dynamic time warping method was used to match tracked movements. The measurement errors were obtained by comparing each pair of matched points from the two recordings.

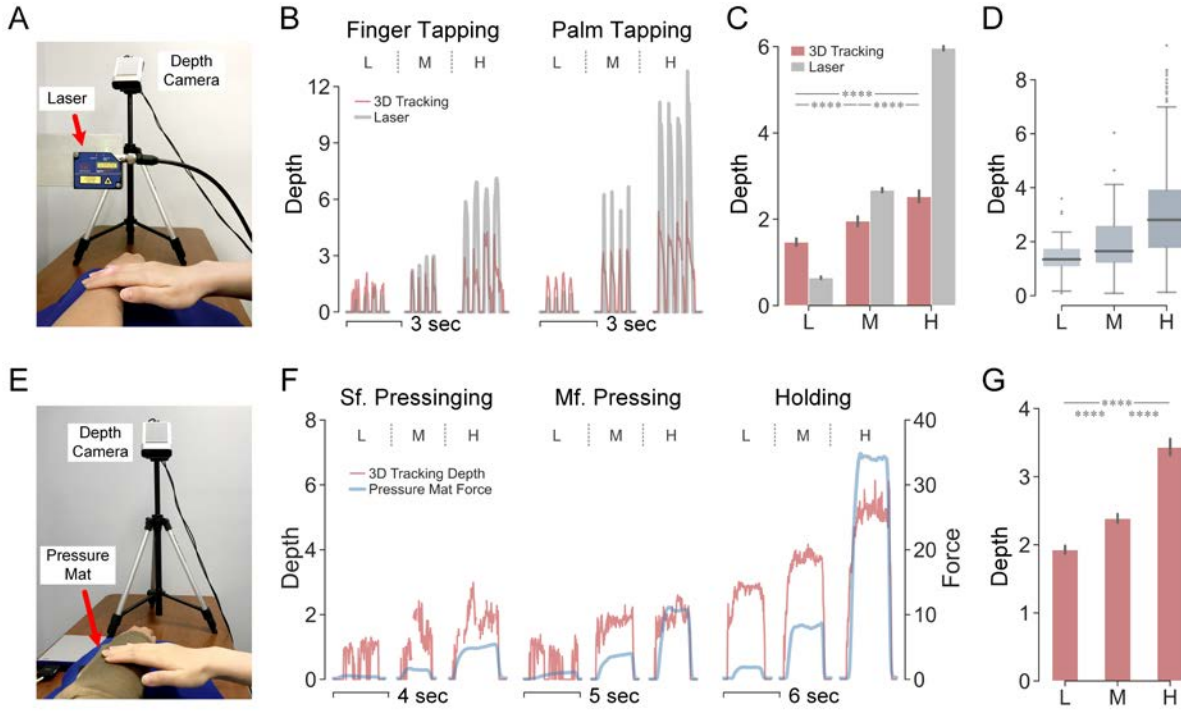

Figure 3.7. Validation of indentation depth measurements using laser displacement sensor and sensorized pressure mat. (**A**) Experimental setup with laser displacement sensor. (**B**) Indentation depth (mm) over time by the either system. For the two test gestures shown is one trial per force level, i.e., low, medium, and high force. (**C**) Mean values of indentation depth per test gesture. ****p < 0.0001 were derived by paired-sample Mann–Whitney U tests across force levels. (**D**) Errors of measured indentation depth between systems per force level. (**E**) Experimental setup with sensorized pressure mat. (**F**) Indentation depth (mm) collected by the 3D visual tracking system overlaps with overall force (N) collected by the sensorized pressure mat. Per test gesture, one trial per force level is shown i.e., low, medium, and high force. (**G**) Mean value of indentation depth per force level recorded by the 3D visual tracking system. ****p < 0.0001 were derived by paired-sample Mann–Whitney U tests across force levels.

Though no depth data could be captured by the pressure mat, the overall contact force was measured for correlation with indentation depth measured by the visual tracking system. By aggregating all test gestures, the average depth derived per force level was then calculated and compared.

3.4.3.4 Results

In Fig. 3.7, the patterns of indentation depth measured by the two systems were very similar especially for the temporal changes (Fig. 3.7B). Though differences could be observed between their overall amplitudes, their increasing trends were maintained across force levels (Fig. 3.7C). Therefore, the 3D visual tracking system affords the sensitivity to track slight changes in indentation depth, while the amplitude of changes is proportionally mitigated. Moreover, contact with different force levels could be easily differentiated by indentation depth amongst a variety of touch gestures. (Fig. 3.7C, 3.7G).

3.5. Discussion

To better understand human-to-human touch interactions underlying social emotional communication, an interference-free 3D visual tracking system was developed to precisely measure skin-to-skin physical contact by time-series contact attributes. The system was validated to capture and readily distinguish naturalistic human touches across delivered emotional messages, touch gestures, and individual touchers according to contact attributes. Compared with standard tracking techniques, similar accuracy of spatiotemporal measurements was achieved by this system, while multivariate attributes can be obtained simultaneously within one concise setup.

3.5.1 Deciphering Affective Touch Communication by Contact Attributes

As human affective touch is prone to be impacted by social and individual factors, such contact differences could be readily captured by this system via contact attributes. First, delivered emotional messages can be differentiated by contact attributes much better than chance (Fig. 3.4C). The accuracy of 54%, 57%, 55% was achieved when predicted by three different levels of information derived from contact attributes (Fig. 3.4C). Note that human receivers only achieve a comparable recognition correctness around 57% when a similar pool of messages were tested [4], [18]. It indicates that some contact information human receivers rely on in identifying emotional messages can be captured by this tracking system. Meanwhile, certain messages that were difficult to be discriminated by contact attributes might indeed be very similar in their social meanings and touch behaviors. Such as sympathy and calm, which are supposed to be close in the terms of contact quantification.

Furthermore, this tracking system can capture individual differences in affective touch as individual touchers were also easily distinguished. Prior studies highlighted that touch behavior in social communication could be influenced by many factors, such as age [30], gender [2], [44], cultural backgrounds [1], [45], relationship [3], or personalities [18]. While the personal information is easy to

obtain via questionnaires, the uniqueness of their contact performance is always challenging to collect. Prior attempts on individual difference typically focused on contact with engineered stimuli like silicone-elastomers [46], grooved surfaces in grating orientation tasks [47], or the contact with robots [48]. In those settings, contact can be well-recorded by built-in or attached sensors, which in contrast is impractical or interferential for human-to-human touch. As individual difference indeed plays a role in social emotion communication, this system could help bridge the gap by inspecting the differences from the aspect of skin contact quantification.

3.5.2 Improved Skin-to-Skin Contact Measurement by 3D Visual Tracking

The measurement accuracy of this system was validated by several standard tracking techniques. As shown in Fig. 3.5-3.7, time-series recordings of contact attributes aligned well with the data collected from independent devices, i.e., contact velocities from an EM motion tracker, contact area from a sensorized pressure mat, and indentation depth from a laser sensor. Those standard tracking methods typically afford high accuracy or resolution of measurements but are specialized for limited types of contact attributes. Therefore, when different attributes are needed at the same time, a complex combination of multiple devices is usually required. In contrast, the proposed tracking system captures most of those attributes simultaneously with a concise setup without calibration.

Moreover, the proposed 3D visual tracking system is compatible with wider applications as many limitations of standard tracking methods were overcome or avoided. More specifically, compared with the EM tracker, this system is free of electromagnetic interference and provides shape information instead of tracking the position of only few points. Compared with infrared motion trackers like the Leap Motion sensor, it covers a larger range of tracking and captures any 3D shapes in addition to hands and several basic geometric shapes. The motion capture system is superior in tracking movements but is expensive to set up and constrained by pre-attached markers. Sensorized pressure mat and other force sensors always block the direct contact and might not be reliable in area measurement due to spatial resolution constraints and the increasing zero drift over time. While the proposed tracking system is free of those issues mentioned above, limitations still exist. In particular, the attribute of contact force and pressure are unavailable although they contribute to contact interactions [35], [37], [42], [49]. Due to the constraint of recording frequency, fast movements might fail in tracking since the hand image could be blurred. Meanwhile, the forearm needs to be recorded parallel with the y-axis of the color image coordinate. In so doing, the spatial hand velocity can be decomposed into the three orthogonal directions without additional markers to define the arm coordinate.

3.5.3 Further Applications in Human-to-Human Touch Interaction

Human touch each other with different intentions and a wide range of emotional states. In the classic theory of emotion, three dimensions of valence, arousal, and dominance, are typically employed for emotion assessments [25], [50]. Indeed, using machine-controlled brush stimuli, the valence rating was reported to be tuned by the tangential stroking velocity [9], [10], [37], [51], [52]. In the scenario of naturalistic human touch, our measurements could further facilitate the quantitative analysis regarding other correlates between contact attributes and the three emotional dimensions.

From the perspective of neurophysiology, changes in the skin's mechanics caused by physical contact could elicit different responses of peripheral afferents [39], [43], [53]. For example, the firing frequency of C-tactile afferents is associated with the stroking velocity in an inverted-U shape relationship [9], [10], [54]. Other Aβ afferents are suggested to support the identification of distinct emotional messages delivered by touch [17]. Moving forward into this direction, measurements of naturalistic human contact can aid in uncovering how exactly afferents respond to such contact and contribute to different emotional percepts.

Affective touch is also believed to impact physiological arousal such as blood pressure, heart rate, respiration, ECG, EEG, and hormone level [26], [55]. Especially for infants, touch delivered by caregivers contributes to their social, cognitive, and physical development [38], [56], where the underlying contact details would be meaningful to quantify. Additionally, many physical therapies, such as massage, rely on specific manipulation of the muscle and tissue of patients delivered by professional therapists. Those therapies create health benefits including relieving stress and pain, promoting blood circulation, and boosting mental wellness [57]. While the underlying mechanism is waiting to be further explored with the aid of physical skin contact tracking.

4 Chapter 2. Identify Subtle Contact Changes and Corresponding Emotional Perceptions Across Social Contexts

4.1 Introduction

Human-to-human touch is essential to social communication, particularly in expressing emotions. For example, those in intimate relationships convey love and sympathy, often preferring touch over facial expressions, body postures, or movements [58]. Social and affective touch is also critical in cognitive development throughout infancy and childhood, providing emotional support and forming social bonds [30]. Moreover, works are now indicating that social meaning is readily identified from touch alone [1]–[4].

Certain touch interactions may underlie how we communicate social and emotional sentiment. To understand contact deployed in human-to-human touch, prior efforts have relied on human observers to annotate a toucher's gestures, contact duration, and contact intensity [1], [2], [12]. While touchers regularly vary their gestures to convey different intentions, a more interesting observation is that they often reuse the same gesture to communicate multiple, distinct messages. For example, stroking might convey both love and sadness, while shaking might convey both happiness and anger [1], [2]. To capture details finer than possible with a proctor, computerized tracking systems have been introduced. Such systems utilize sensors, cameras, and electromagnetic trackers [4]–[6], [14], [17], [18] to quantitatively capture pressure and positional attributes that underlie human-to-human contact.

However, we still do not understand whether receivers actually perceive emotions from these touch expressions, as opposed to intuitively discriminating and associating touch expressions as 'codes' with the messages. Classic theory on emotion dictates two dimensions are at play, i.e., valence and arousal, which refer to the pleasantness and the intensity of emotion, respectively [25]. As a point of comparison, under the brush stroke to the forearm and hand, changes in velocity govern pleasantness, with an optimal speed range around 1-10 cm/s [9]. In other experimental paradigms, changes in valence and arousal have been examined when participants observe images of social and non-social touch [59] and in physical interactions with robot hands [35]. Here, in human-to-human interaction, we focus on whether slight changes in direct skin contact alter the valence and arousal perceived by receivers.

Moreover, as intimate touch is more prevalent and natural, social touch has also been widely investigated in close relationships, especially for romantic couples [4], [5], [18], [26], [60]–[62]. Physiological,

psychological, and brain responses collected from touch receivers indicate that touch delivered by a partner can lower one's heart rate and blood pressure, elicit more positive and pleasant affect, as well as induce brain responses related to pain and emotion regulation [26], [60]. In addition, physical touch behaviors of couples have been observed [4], [5], [18] and verified as being intuitively understood [18]. Other efforts have evaluated touch delivery among strangers [1], [2], [60], wherein receivers respond less consistently and favorably [60]. Together, these studies illustrate that romantic social touch is indeed effective and beneficial to the physical and mental wellbeing of receivers. Indeed, the fact that the majority of prior studies explicitly consider relationship status implies its importance.

To better understand the role of relationship status, direct comparisons are needed between individuals with distinct types of social bonds. From online self-report studies, we see that when the strength of one's emotional bonds increase, the body regions permitted for social touch increase proportionally [45], [63]. Moreover, the frequency and desire to touch increase with interpersonal intimacy [64]. In terms of affective responses, touch from one's partner is reported to be more pleasant and comfortable than with less closely bonded individuals [45], [65], [66]. Similar results are also reported in human-subjects experiments, where partner's touch elicits more pleasant responses [67]. When it comes to the communication of emotions, couples recognize a wider range than strangers, especially self-focused emotions [3].

As skin contact is the primary interface for social touch, it has been widely reported that pleasantness, as well as neural responses of C-tactile (CT) afferents, follow an inverted U-shape curve relative to stroking velocity [9]. Such inspiration causes us to hypothesize that a romantically involved toucher might modulate her or his contact interactions to alter her or his receiver's perception. However, the physics of such contact changes has seldom been quantified, where velocities have been compared across relationship status for only the stroking gesture [68], and vibration of the toucher's finger has been analyzed between touching themselves or another person [69].

Herein, by developing an interference-free visual tracking system to quantify contact attributes, we investigate if slight distinctions in skin-to-skin contact tune both receivers' recognition of a cued message (e.g., anger, sympathy) and their ratings of its emotional content (i.e., arousal, valence). The impact of relationship status is also analyzed. More specifically, experiments are conducted where emotional messages are delivered by touching a receiver's forearm. Responses from receivers are first compared among romantic couples and strangers. Measured skin contact is then correlated with perceptual performance. Finally, relationship status is evaluated relative to other contextual factors.

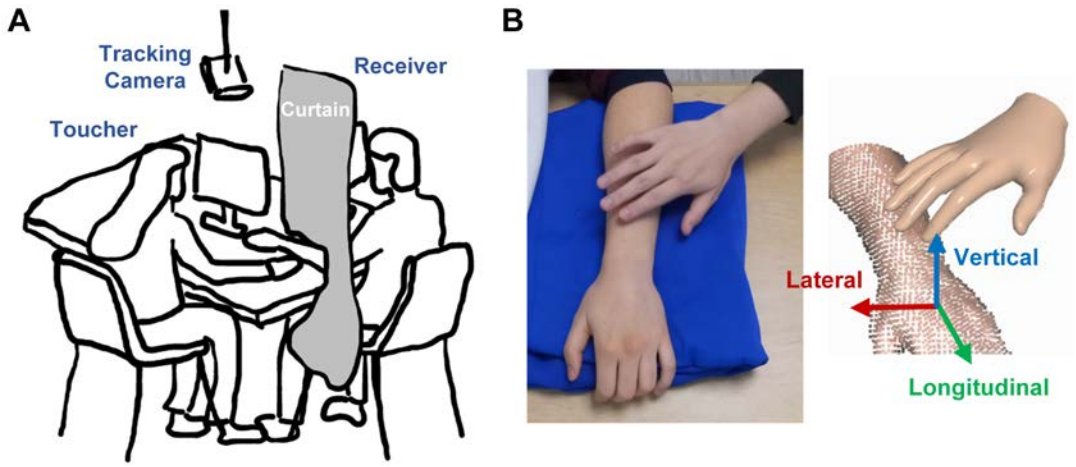

Figure 4.1. (**A**) Experimental setup. Touchers and receivers were separated by an opaque curtain with no verbal or visual communication. Instructions and questions were displayed on the screen for participants to interact. A depth camera tracked contact interactions. (**B**) One frame captured by the depth camera and the resultant 3D visualization of tracked contact.

4.2 Experimental Methods

4.2.1 Participants

Five couples in romantic relationships were recruited (5 males, 5 females, age = 23.8 ± 5.0). Per couple, a stranger participant was recruited separately and grouped with that couple, making five stranger participants in total (3 males, 2 females, age = 24.0 ± 4.4). The study was approved by the Institutional Review Board at the University of Virginia, and all participants granted consent to participate.

4.2.2 Experimental Setup

As shown in Fig. 4.1A, one toucher and one touch receiver were involved in the emotion communication task. Two participants sat at opposite sides of an opaque curtain to eliminate visual communication and were instructed to avoid verbal communication. A cushion was set on the toucher's side, where the receiver rested her or his left arm on and could not see the contact interaction delivered by the toucher. Touch instructions and perceptual questions were displayed to the toucher and receiver separately on two computer displays. Participants were instructed to use a mouse to interact with the experiment's user interface. A depth camera was aimed at the receiver's arm to capture hand-arm interactions.

4.2.3 Emotional Message Stimuli

As shown in Table 4.1, seven emotional messages were adopted from prior studies as instructions for touchers [1]–[4], [62]. Those messages have been reported to be recognizable and preferable to

Table 4.1. Emotional messages and associated gestures

Message	Gestures		
Anger (Ag)	Hit/Tap	Hold/Squeeze	Shake
Happiness (H)	Shake	Tap	Stroke
Fear (F)	Hold/Squeeze	Shake	Tap
Gratitude (G)	Hold/Squeeze	Shake	Tap
Sympathy (S)	Stroke	Tap	Hold/Squeeze
Attention (At)	Tap	Shake	Hold/Squeeze
Calm (C)	Hold/Squeeze	Stroke	Tap

communicate in social touch. In addition, three commonly used gestures [1]–[4], [62] were selected per emotional message and provided to touchers. Gestures of holding and squeezing were combined as a single option due to similar hand poses and contact patterns. Similarly, hitting was added to the tapping option for the anger message to better fit its natural expression.

4.2.4 Experimental Procedures

For each group of three participants, including a couple and a stranger, four experimental sessions were designed. Two of the sessions were conducted by the couple, with their roles as toucher/receiver reversed between sessions. The other two sessions were conducted with the stranger as the receiver and either of the couple participants assigned as the toucher alternatively. Therefore, twenty sessions were completed in total, where ten romantically involved participants delivered contact to both their partner and the stranger. Participants were aware of who the other participant was before each session. Note that experimental sessions between couples were conducted before strangers to moderate the reluctance of physical contact between strangers, which might have an influence on the toucher's contact performance. Within each session, seven emotional messages were conveyed with each message repeated six times. The forty-two message instructions were provided to the toucher in a random order.

Per experimental trial, one emotional message was displayed to the toucher with three corresponding gestures listed with a random order. The toucher selected only one gesture by clicking it and then expressed the message by touching the receiver's forearm using the selected gesture. No constraints were

given regarding how to deliver a gesture. Any contact patterns the toucher considered as that gesture could be used. For the same message across different trials, touchers were also free to choose either the same gesture or different ones. After contact was delivered, touchers clicked another button to inform the receiver to answer the perceptual questions. The first question was to identify the emotional message they recognized from the contact. It was a seven-alternative forced choice question with the same seven messages provided to touchers. The next two questions rated perceived levels of valence and arousal. Both affective ratings were collected using the Self-Assessment Manikin (SAM) with nine levels [70]. Valence represents pleasantness, which ranges from least to most pleasant. Arousal represents emotional intensity, which ranges from least to most intense. After all questions were answered, the receiver clicked a button to inform the toucher to proceed to the next trial. Participants could fully control the pace of the experiments.

4.2.5 Measurements of Hand-Arm Contact

As classic tactile sensor would barrier the direct contact between the toucher and receiver [16], we decided to quantify contact interactions using a 3D visual tracking system. The 3D shape and movements of the toucher's hand and touch receiver's forearm were tracked using the Azure Kinect depth camera (30 Hz, Microsoft, USA). Contact interactions between the hand and forearm were quantified using a customized point-cloud based algorithm [71]. Six time-series contact attributes were derived when hand-arm contact was detected, which includes absolute spatial contact velocity, contact area, indentation depth, three orthogonal velocity components in longitudinal, lateral, and vertical directions (Fig. 4.1B) [71], [72]. Per experimental trial, the mean value of the six time-series contact attributes was used to derive scalar measurements. In addition, the overall contact duration of one trial was collected as the seventh contact attribute.

4.3 Data Analysis

Analyses were conducted to investigate the impact of relationship status on social touch in terms of emotional perception, contact delivery, and their correlation. In addition, the impact caused by relationship status was further compared with that of other factors in the context of social touch, i.e., gesture, emotional message, and individual toucher. Note that seven of 840 trials were removed due to poor tracking quality.

4.3.1 Contact Delivery Across Emotional Messages

For the data collected from couples and strangers combined, we first calculated the proportions of messages delivered by touchers and recognized by receivers separately, when the same touch gesture was used. The message recognition matrix was then calculated per touch gesture. Then we performed Mann–Whitney U tests to evaluate differences in contact attributes across messages given the same gesture. Since receivers might interpret messages different from those intended, this test was conducted per gesture for both delivered and recognized messages, where only the results for recognized messages were shown here. Benjamini-Hochberg correction was applied to the multiple testing for each attribute within a gesture by controlling the false discovery rate. In cases where a message was recorded for less than 15 trials with a gesture, it was excluded from analysis due to the low statistical power.

4.3.2 Impact of Relationship Status on Emotional Perception

The recognition accuracy of all communicated emotional messages were first counted in the format of separate confusion matrices for couples and strangers. Mann–Whitney U tests [73] were applied to compare the participants' recognition accuracies of each message between couples and strangers. The total number of trials each emotional message was recognized by receivers was also counted and compared.

Affective ratings of valence and arousal reported by receivers were further compared between couples and strangers. The ratings were first grouped by delivered gestures and recognized emotional messages. Since receivers were different participants between the touch communication of couples and strangers, Mann–Whitney U tests were conducted to compare ratings between the two relationship statuses. Cohen's D effect sizes [74] were then calculated and reported for significantly different pairs. With multiple tests implemented, the Benjamini-Hochberg method [75] was applied for post-hoc correction.

4.3.3 Impact of Relationship Status on Contact Delivery

The impact from relationship status on contact delivery may be twofold: gesture preference and contact attributes. For gestures, the total number of trials that each gesture was used by couples and strangers were counted and compared. The distribution of each contact attribute was then compared between couples and strangers. Since the same participant delivered contact to both the partner and the stranger, linear mixed effects model [76] was used for significance tests with relationship being the fixed effect and participants' intercept being the random effect. F-tests and p-values for the fixed-effect term using Satterthwaite degrees of freedom were reported [76]. The partial η^2 effect sizes [77] were calculated for

significantly different pairs. Benjamini-Hochberg method was used for post-hoc multiple testing correction.

4.3.4 Impact of Relationship Status on Correlations between Contact Attributes and Affective Ratings

As widely reported by neuropsychology studies, an inverted-U shape pattern is observed between the pleasantness sensation and log-transformed stroking velocities. Therefore, linear mixed effects model was used for both linear and quadratic regressions to characterize correlations between contact attributes and affective ratings with all gestures aggregated. Contact attribute was treated as the fixed effect, while both touchers and receivers were treated as random intercepts. F-tests for the fixed-effect term using Satterthwaite degrees of freedom and the partial η^2 effect sizes were reported. Only combinations with notable differences between couples and strangers are elaborated upon in Results.

Similar analyses were further conducted for the stroking gesture, where the distribution of contact attributes and valence ratings were examined. The linear mixed effects model was applied to compare contact attributes between couples and strangers with Benjamini-Hochberg post-hoc correction. Only attributes with notable differences between couples and strangers were reported.

4.3.5 Comparing the Impact of Relationship with Other Factors in Social Touch

We compared the variation of contact attributes caused by relationship status with that of the other three contextual factors: gestures, emotional messages, and individual touchers. The metric var was developed to quantify the variation caused by a certain factor. In this case, the other three factors should remain the same. For example, var of relationship status represents the contact variation caused by switching from touching the partner to the stranger, when the same toucher used the same gesture to express the same emotional message. For another example of gesture, var represents the contact variation caused by switching among different gestures when the same toucher expressed the same emotional message under the same relationship status.

Detailed derivation of this metric is explained as follows using the factor of gesture as an example. $N_c = 140$ conditions were first identified, which came from all combinations of the other three factors, i.e., seven messages multiplied by ten touchers and two relationship statuses. Since contact was quantified as seven-dimensional contact attributes, its variance is defined as a covariance matrix. To obtain a scalar metric for comparison, the contact variation was formulated here as the trace, i.e., the sum of eigenvalues, of the covariance matrix of multi-dimensional contact attributes. Therefore, for each

condition c_i, contact variation caused by changing gestures was written as $var^{c_i} = \text{tr}(\text{Cov}(\boldsymbol{att}^{c_i}))$. To better calculate eigenvalues of the covariance matrix, the dimension of contact attributes was reduced using principal component analysis (PCA) by taking only the first two principal components (PCs), so that $\boldsymbol{att}^{c_i} = \left[\boldsymbol{PC}_1^{c_i}, \boldsymbol{PC}_2^{c_i}\right]^T$. The number of data points in $\boldsymbol{att}^{c_i}$ equals to the number of gestures used in condition c_i. Per gesture, $\boldsymbol{PC_1}$, $\boldsymbol{PC_2}$ were derived as the mean value over all trails under that gesture. Note that conditions with only one gesture were removed since there was no variation. Therefore, var of gesture was finally derived as the mean of $N_{valid} = 67$ valid conditions: $var = \sum_{c_i}^{N_{valid}} var^{c_i} / N_{valid}$.

The var of the other three factors was calculated following the same procedure. The total number of conditions N_c was 80, 56, and 280 for the emotional message, individual toucher, and relationship status, respectively. After removing conditions with only one record, the number of valid conditions N_{valid} was 69, 36, and 88 for the three factors. In order to compare the contact variation introduced by the four factors, Mann–Whitney U tests were conducted with Benjamini-Hochberg post-hoc correction.

4.4 Results

4.4.1 Same Touch Gesture Communicates Multiple Messages

Touchers were able to use the same gesture to deliver multiple cued messages. Touch receivers were able to identify the similar sets of messages delivered by touchers, with discrepancies in only the relative proportions of delivered and recognized messages (Fig. 4.2A). In specific, touchers deployed stroking to deliver calm (32.9%), sympathy (41.1%), and happiness (24.7%). Touch receivers identified the same three messages, though calm (41.8%) was recognized in a relatively greater proportion than it was delivered. With the shaking gesture, touchers used it for fear (32%), happiness (29%), gratitude (21%), and attention (10%). Likewise, receivers perceived shaking as fear (39%) and attention (33.5%), with the other two messages recognized less often. With holding and tapping gestures, the proportions between touchers and receivers were nearly equivalent.

Recognition of messages is shown as a confusion matrix per gesture (Fig. 4.2B). When stroking was used, messages of calm and sympathy were apt to be confused, with happiness more easily recognized (53%). With the shaking gesture, fear was much more effectively communicated. With the holding gesture, calm (52%) and fear (45%) were recognized with higher accuracy relative to sympathy and gratitude. The tapping gesture was readily capable of getting one's attention (93%) or delivering anger (81%).

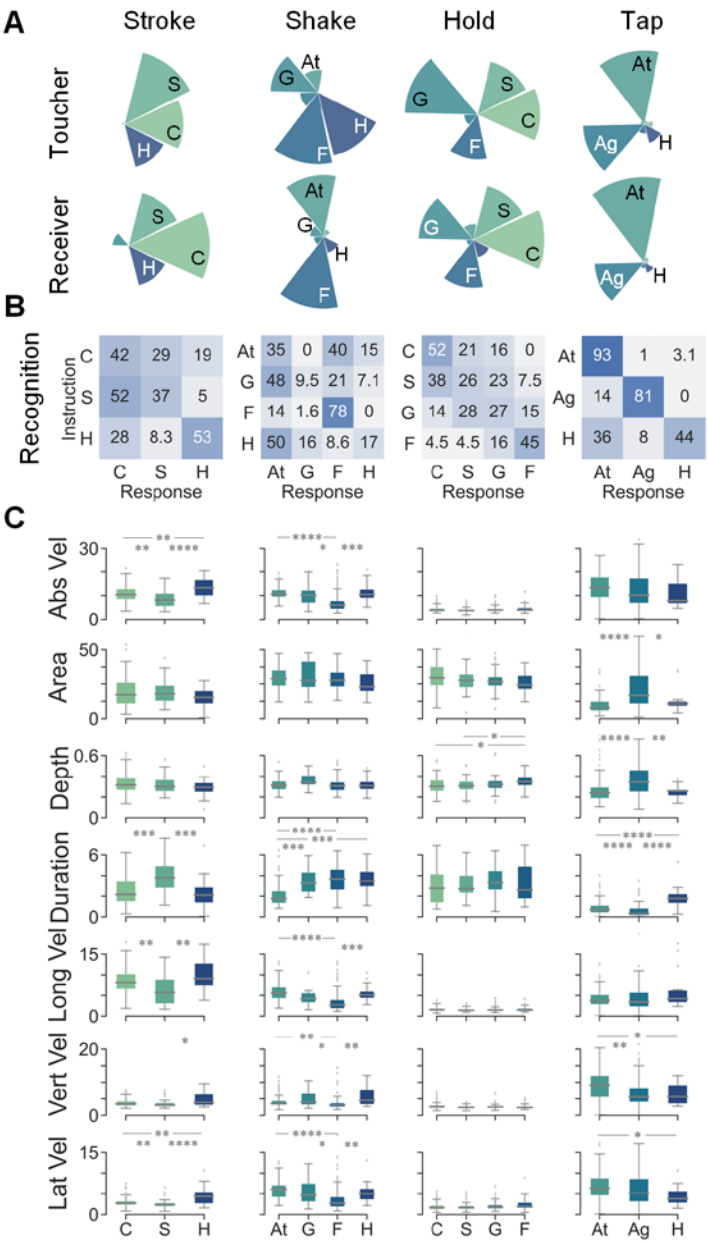

Figure 4.2. Messages communicated per gesture. (**A**) The proportion of messages delivered by touchers and recognized by receivers, respectively. Seven cued messages were listed in Table I. (**B**) The receiver's recognition rates of delivered messages per gesture. Within each cell, the value and color redundantly show the percentage of the recognized message. As noted, a few rarely conveyed messages were excluded, so the sum of each row may not total 100. (**C**) Absolute measurements per contact attribute, message, and gesture. Points denote trial data. *p < 0.05, **p < 0.01, ***p < 0.001, ****p < 0.0001 are derived by paired-sample Mann–Whitney U tests after Benjamini-Hochberg correction.

To convey different messages, touchers slightly varied their contact attributes, which could be distinguished by receivers. In specific, Fig. 4.2C shows the distribution of contact attributes across messages per gesture recognized by receivers. For example, with the stroking gesture, hand movements with significantly higher velocity were commonly associated with happiness. For the shaking gesture, fear was distinct from other messages with significantly lower velocity, resembling more closely a trembling motion than a vigorous shake. Given minimal hand motion with the holding gesture, only small changes in contact attributes were detected, yet fear could still be distinguished by its significantly greater indentation depth. With tapping, anger was also made distinct by utilizing significantly greater indentation depth. Practically speaking, the relative magnitudes of those contact attributes align with the expected practice of the cued messages, e.g., quicker stroking in happiness than sympathy and tighter holding in fear than calm. In Fig. 4.2C, we provided the overall contact profiles of all cued messages with the distribution of all contact attributes, where several attributes can significantly distinguish recognized messages.

4.4.2 Couples Perceive Higher Valence and Arousal

Among the seven emotional messages communicated, couples and strangers recognized each message at a similar level of accuracy. As shown in Fig. 4.3A, there was no statistically significant difference between couples and strangers in their recognition. Detailed recognition accuracies are shown in the confusion matrices in Fig. 4.3B. For most of the messages, their recognition accuracies were much higher than chance (14.3%). Moreover, as shown in Fig. 4.3C, strangers tended to recognize received contact as the attention message much more frequently than couples. While each message was expressed for 60 trials (14.3%) in total by touchers, attention was recognized by stranger receivers in 118 trials (28.9%).

In contrast to their comparable message recognition performance, romantically involved receivers reported higher ratings of valence and arousal than strangers. As shown in Fig. 4.3D, couples perceived

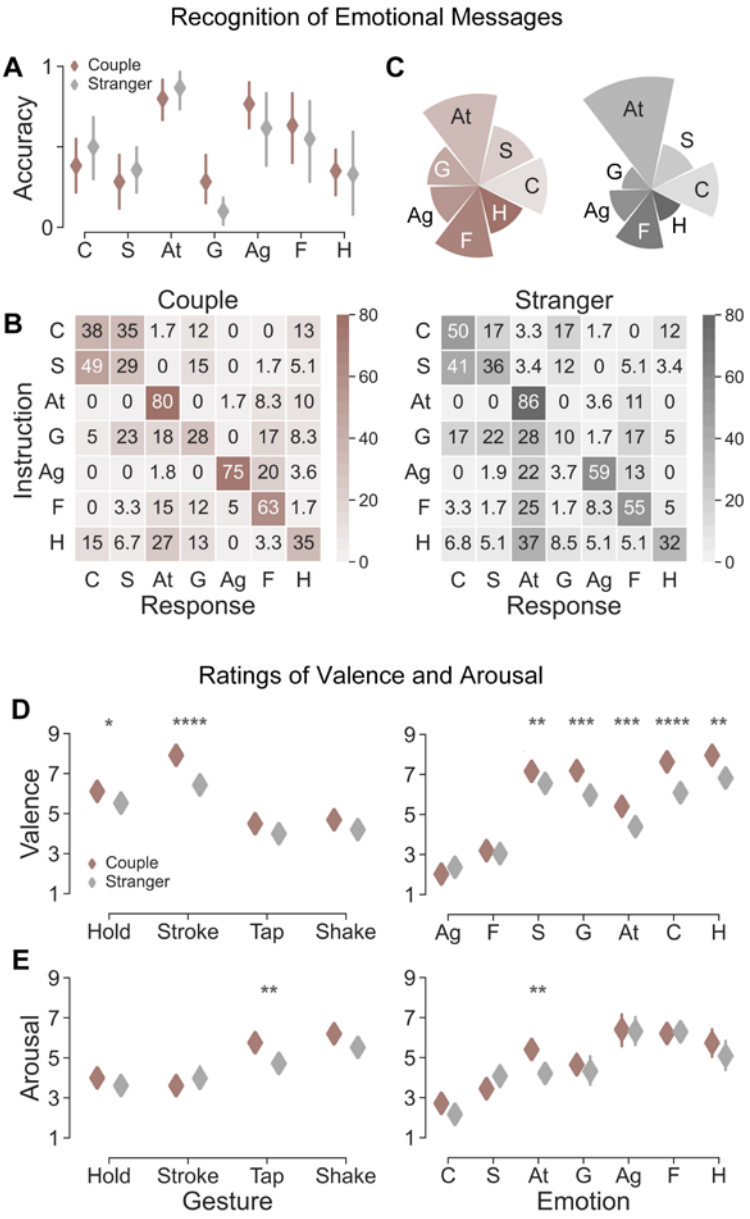

Figure 4.3. (**A**) Comparison of recognition accuracy of each emotional message between couples and strangers. Diamonds denote means, error bars denote 95% confidence intervals. **(B)** Confusion matrices of emotional message recognition for couples and strangers. (**C**) Frequency of recognized emotional messages for couples and strangers. (**D**) Valence ratings of each gesture and emotional message. (**E**) Arousal ratings of each gesture and emotional message. Diamonds denote means, error bars denote 95% confidence intervals. *$p < 0.05$, **$p < 0.01$, ***$p < 0.001$, ****$p < 0.0001$ were derived by Mann–Whitney U tests with Benjamini-Hochberg post-hoc correction. Cohen's effect sizes for significantly different pairs were 0.298, 1.20, 0.531, 1.03, 0.705, 1.07, 0.942, 0.396, 0.5 (from left to right, valence to arousal).

holding contact, and especially stroking contact, to be significantly more pleasant than strangers. In addition, among seven emotional messages, five of them, including sympathy, gratitude, attention, calm, and happiness, were reported to be significantly more pleasant by couples. For arousal ratings, the tapping gesture and attention message were perceived to be significantly more emotionally intense by couples than strangers (Fig. 4.3E).

4.4.3 Couples Deliver Contact in a Distinct Way

Touchers also changed gestures and contact attributes when switching between touching their partner and the stranger. As shown in Fig. 4.4A, couples selected all four gestures with similar frequencies, while strangers tended to use more tapping and holding gestures and avoided stroking gesture. From the distribution of contact attributes, couples delivered contact with significantly longer contact duration ($p < 0.0001$) and significant lower vertical velocities ($p < 0.01$).

4.4.4 Couples Exhibit Different Correlations between Contact Attributes and Affective Ratings

Correlations between valence/arousal ratings and contact attributes were also different across couples and strangers. As shown in Fig. 4.4B, an inverted-U shape relationship can be observed between valence ratings and spatial contact velocities for couples (quadratic regression, $p = 0.0135$, $\eta^2 = 0.02$). In contrast, quadratic regression shows a decreasing correlation between them for strangers (linear regression, $p < 0.001$, $\eta^2 = 0.03$). Meanwhile, the curve fitted for couples was overall above that of strangers in the same coordinate. A quadratic function was also fitted for valence ratings relative to contact durations for both couples ($p < 0.0001$, $\eta^2 = 0.09$) and strangers ($p < 0.0001$, $\eta^2 = 0.16$). The curve for strangers began to decrease at around 3 s. Yet the curve for couples kept increasing (linear regression, $p < 0.0001$, $\eta^2 = 0.06$). As for arousal, the ratings reported by couples increased when contact velocity increased (linear regression, $p < 0.0001$, $\eta^2 = 0.05$), while decreased for strangers (linear regression, $p < 0.0001$, $\eta^2 = 0.08$). More interestingly, when contact duration increased, arousal rated by couples decreased (linear regression, $p < 0.0001$, $\eta^2 = 0.04$), but increased for strangers (linear regression, $p < 0.01$, $\eta^2 = 0.02$).

Especially for stroking gesture (Fig. 4.4C), an inverted-U shape curve was fitted between valence ratings and longitudinal velocities for couples (quadratic regression, $p = 0.0482$, $\eta^2 = 0.07$). Yet quadratic regression exhibits a decreasing trend for strangers. Distributions of contact attributes and valence ratings are also shown as marginal kernel density estimation plots and box plots. Longitudinal velocities deployed by couples and strangers exhibit similar median values, but data from couples concentrate more around 8-10 cm/s, while that from strangers were distributed more evenly. Moreover, as valence ratings for

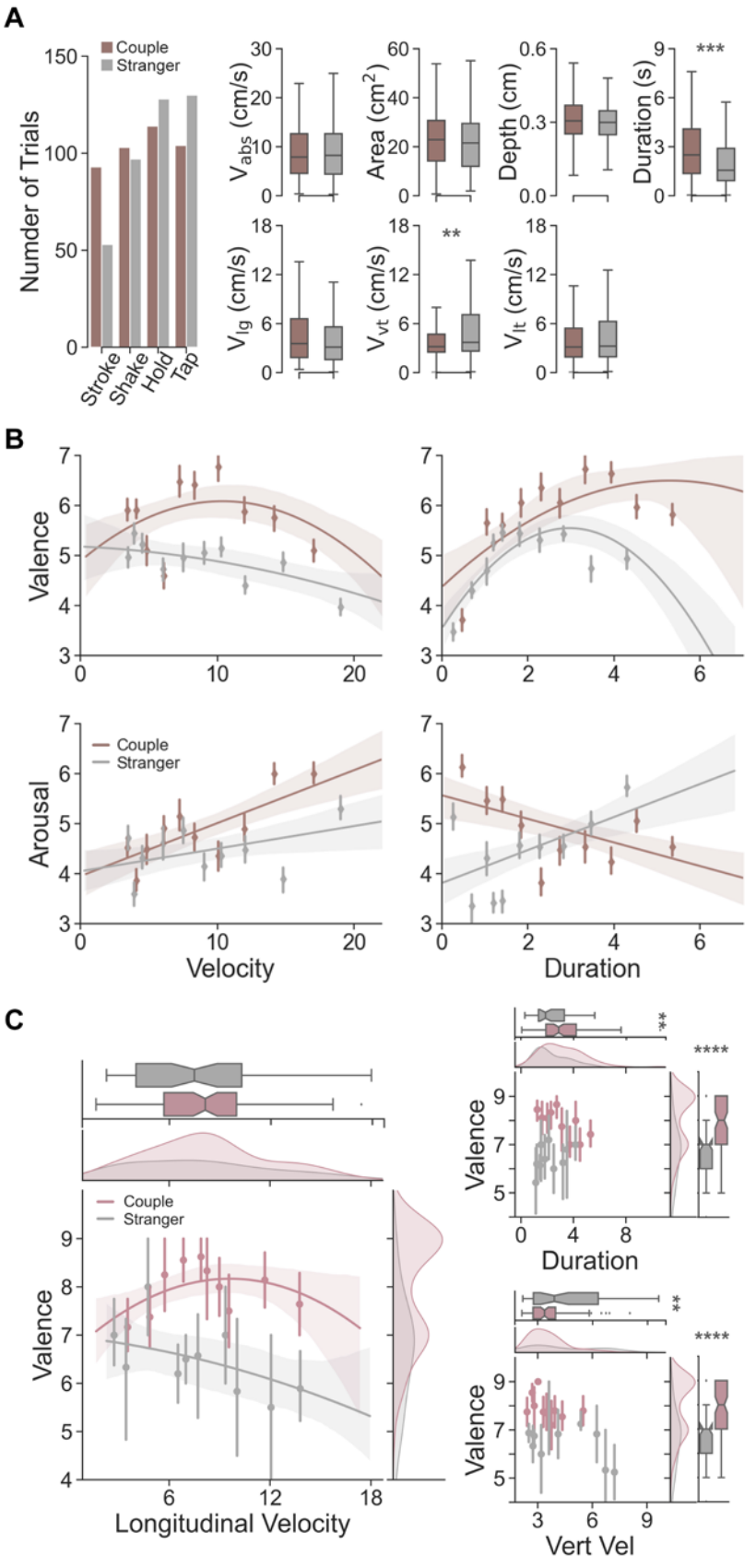
A
Couple
Stranger
Numder of Trials
Stroke
Shake
Hold
Tap
V_{abs} (cm/s)
Area (cm^2)
Depth (cm)
Duration (s)
***
V_{lg} (cm/s)
V_{vt} (cm/s)
**
V_{lt} (cm/s)
B
Valence
Arousal
Couple
Stranger
Velocity
Duration
C
Couple
Stranger
Valence
Longitudinal Velocity
Duration
Vert Vel
**
****

Figure 4.4. (**A**) Left: Total number of trials each gesture is selected by couples and strangers respectively. Right: The distribution of contact attributes deployed by couples and strangers. Vabs: absolute contact velocity, Vlg: longitudinal velocity, Vvt: vertical velocity, Vlt: lateral velocity. (**B**) Correlation between contact attributes and valence, arousal ratings across couples and strangers with all gestures combined. Quadratic regression was applied for valence and linear regression was applied for arousal. Bands around regression curves denote 95% confidence intervals. (**C**) Quadratic regressions between longitudinal velocities and valence ratings for the stroking gesture across couples and strangers. For regressions in panel B and C, data points denote means of raw data grouped by 10 even bins and error bars denote 95% confidence interval. For the comparison of contact attributes in panel A and C, **p < 0.01, ***p < 0.001, ****p < 0.0001 were derived by linear mixed effects model with Benjamini-Hochberg post-hoc correction. Partial η^2 effect sizes were 0.07, 0.02, 0.08, 0.07 for (A) duration, vertical velocity, (C) duration, vertical velocity, respectively.

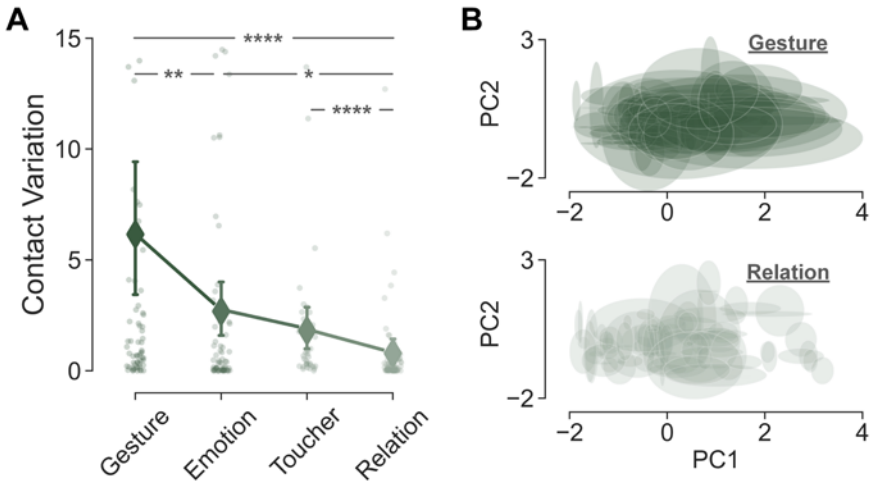

Figure 4.5. (**A**) Contact variation caused by varying a factor while the other three factors remain the same. Data points denote contact variations var^{c_i} of valid conditions. Diamonds denote means, which are contact variations var caused by factors. Error bars denote 95% confidence intervals. *p < 0.05, **p < 0.01, ****p < 0.0001 were derived by Mann–Whitney U tests with Benjamini-Hochberg post-hoc correction. (**B**) Contact variations of valid conditions visualized by two PCs of contact attributes. Ellipses are associated with data points in panel A, which are valid conditions defined above. The center of the ellipse denotes the mean value of PC1 and PC2 over all gestures/relationships within that condition. Semi-major and semi-minor axes are the standard deviations on PC1 and PC2, respectively. Larger area implies larger contact variation of the condition.

couples being significantly higher than strangers, contact durations ($p < 0.01$) and vertical velocities ($p < 0.01$) deployed by couples were sginificantly higher and lower than strangers, respectively.

4.4.5 Relationship Has the Least Impact on Contact Delivery

As shown in Fig. 4.5A, contact variation caused by relationship status was significantly lower than that of the three other factors. More specifically, the ranking of the impact from the highest to the lowest was: gesture > emotional message > individual toucher > relationship status. Contact variation var of each factor as calculated in III-D was represented as a diamond in Fig. 4.5A. Contact variations var^{c_i} of valid conditions were represented as data points in Fig. 4.5A, with two PCs from the contact attributes represented as ellipses in Fig. 4.5B. Those ellipses tied to relationship status exhibit smaller areas than those tied to gesture, indicating that relationship status leads to less variation in contact attributes.

4.5 Discussion

This work shows how relationship status influences our delivery and perception of social touches and emotions and how touchers subtly, but significantly, vary the magnitudes of their skin-to-skin contact to convey distinct social messages. Similar to prior studies [45], [65], [67], we find that romantically involved couples perceive social touch as emotionally more pleasant and intense than touch from strangers. Measurements of hand-forearm contact interactions illustrate that couples indeed deliver contact and perceive contact changes differently from strangers. For instance, in stroking contact, significantly more pleasant sensations perceived by romantic receivers may result from the fine tuning of contact attributes, including velocities preferential to C-tactile afferents, and contact delivered for longer durations of time with larger contact areas. To put these findings in context, however, compared with factors of gesture, emotional message, and individual toucher, one's relationship status introduces relatively less impact on the delivery of contact interactions. Notwithstanding, the findings suggest that finely tuned contact interactions do still modulate the affective percepts of receivers in significant ways.

4.5.1 Relationship Impacts Affective Percepts

By evaluating responses from touch receivers, we find that relationship status does not affect one's recognition of emotional messages, yet it does influence their affective percepts. In particular, in terms of valence ratings, in line with prior studies [45], [65], [66], contact from one's partner as opposed to a stranger, especially gentle stroking [67], was perceived as much more pleasant (Fig. 4.3D). Indeed, among all gestures, gentle stroking has been shown to be the preferred stimulus for C-tactile afferents, which may drive valence ratings [7], [9]. In terms of recognition, we found that universal emotions (anger, fear,

happiness) and prosocial emotions (gratitude, sympathy) were communicated by couples and strangers in similar ways (Fig. 4.3A). Such insignificance in recognition accuracy aligns with prior findings [3], and helps validate the feasibility of our experimental paradigm.

4.5.2 Relationship Impacts Contact Delivery that Modulates Affective Percepts

Analysis of physical contact illustrates that relationship status affects touchers' strategies. As noted, couples frequently choose the stroking gesture, which strangers avoid (Fig. 4.4A). Indeed, stroking is a more intimate gesture and might be considered inappropriate to strangers. Moreover, couples deliver contact with longer durations as compared with strangers of less than 3 s (Fig. 4.4A). Strangers also deploy higher vertical velocities, which could be related to their preference of tapping gesture, as well as being more abrupt in how they make contact overall, regardless of gesture.

On the receiver side, couple and stranger receivers respond distinctly to changes in delivered contact. Specifically, increased contact durations are perceived as more pleasant, less intense by romantically involved receivers, while valence drops and arousal rises for strangers after 3 seconds (Fig. 4.4B). This indicates that strangers do not prefer prolonged physical contact as natural and comfortable, and thus, when touching strangers, delivered contact does not typically last long.

Furthermore, our results indicate that touchers fine tune their contact delivery according to specific affective responses when relationship status changes. Specifically for the stroking gesture, an inverted-U curve of pleasantness is observed for couples with a peak around 8-10 cm/s longitudinal velocities (Fig. 4.4C), which aligns with preferred stroking velocities for CT afferents in brushing experiments [9]. Meanwhile, longitudinal velocities delivered by couples also concentrated around 8-10 cm/s. This alignment between the pleasantness curve and the velocity distribution indicates that couples may finely adjust their stroking velocities towards an optimal range of pleasantness. In contrast, valence ratings of strangers do not follow the inverted-U pattern and their longitudinal velocities distribute evenly without any peak. It indicates that strangers might be indifferent to deliver pleasant contact during social touch communication. Moreover, the specific stroking pattern of couples, i.e., longitudinal velocities with CT-targeted range, more gentle contact with lower vertical velocities, and longer contact durations, could be related to the bottom-up neural signaling of pleasantness, on top of the influence of relationship being a top-down contextual factor [30].

4.5.3 Impact of Relationship is Significant but Subtle

We find that relationship status introduces the least impact on contact delivery compared with other factors. Among prior studies in social touch, qualitative observation may hinder the comparison of contextual factors' relative importance. Herein, we measured their relative impact based on physical contact attributes. The ranking obtained for the four factors was of the following order: gesture > emotional message > individual toucher > relationship status. This order indicates that gesture types lead to highly differentiable physical contact attributes. Emotional and social meanings may also shape adjustments to contact patterns, and to a lesser extent individual differences in touch preferences. The most subtle contact variation, due to relationship status, might explain similar recognition performance between couples and strangers. However, although subtle, impact of relationship is still significant in shaping the delivery of contact attributes so as to modulate affective percepts.

5 Chapter 3. Investigate Peripheral Neural Coding of Human Social Touch Expressions

5.1 Introduction

Touch is an often used medium for facilitating social relationships and emotional interactions. For example, one might lightly tap another person to get their attention, or stroke a partner's arm to offer a sense of calm. Between people in close relationships, and even between strangers, many social touch expressions are intuitively understood [2], [4], [18], [78]. The appreciation of emotion is commonly thought to be a centrally mediated process performed by frontal and temporal brain structures that integrate a multitude of peripheral and cross-cortical sensory information [79]. However, the peripheral nervous system may already be organized to facilitate the selection and processing of potentially socially relevant stimuli [80]. Reliable signaling from peripheral afferents could form the basis of the somatosensory and affective perception in the central nervous system. In our evolutionary history, such peripheral encoding may also have acted as scaffolding for the development of cross-sensory, cortical processing of emotion [81].

Among peripheral tactile afferents, percepts tied to social and emotional touch are thought to be influenced prominently by C-tactile (CT) afferents [9], [82]. These afferents can be preferentially activated by light stroking contact at 1-10 cm/s velocities [9] with temperatures similar to human skin [10]. Their firing frequencies have been found to be proportionally correlated with subjectively perceived pleasantness [9], [10], and both follow an inverted U-shape curve along with stroking velocity with a peak around 1-10 cm/s. Such an inverted U-shape relationship between pleasant sensation and stimuli velocity has been widely and reliably reproduced on the population level [52], [72], [83], [84], and has been suggested to be related with the firing patterns of CT afferents. Recent work has, however, encountered difficulty in reproducing such trends among individual participants [51], which suggests a more complex view of pleasantness and affective touch and a plausible role of other afferent types. Meanwhile, the firing properties of CT afferents have mainly been characterized in response to controlled stimuli [9], [10], [51], [82], such as rotary actuated brushing, while less explored under naturalistic, human-to-human touch.

In contrast to CT afferents, low-threshold mechanosensitive (LTM) Aβ afferents have been investigated in a wider variety of scenarios, especially in relation to discriminative touch such as surface roughness perception or skin-object friction. Pre-defined, well-controlled mechanical stimuli have been used to

decouple and examine stimulus attributes, one at a time [39], [85]–[87]. Across these studies, different tactile cues, e.g., pressure, vibration, shape, texture, the deflection of hair follicles, etc., were shown to be mainly encoded by certain Aβ subtypes [39], [85]–[89]. Moreover, the perception of certain elementary cues has been invoked via the intraneural electrostimulation, e.g., slowly adapting type I and fast adapting units for pressure and flutter/vibration [90]–[92]. However, device-delivered stimuli do not reflect the full range of naturalistic touch we encounter in everyday life. Indeed, in discriminative touch scenarios that invoke multiple tactile cues, e.g., object manipulation [93] and natural textures [94], single Aβ subtypes provide overlapping and complementary information [95]. As multiple tactile cues vary simultaneously in human-to-human touch [4], [18], the analysis of their firing patterns becomes more difficult.

Here, we investigated how the spike firing patterns of Aβ and CT human peripheral afferents encode information about the mechanical inputs produced by human-delivered social touch expressions. Microneurography experiments were conducted to record from single unit, peripheral afferents in human participants with natural human touch as the stimulus. Six standardized social touch expressions were delivered, each composed of complex dynamic skin mechanical properties but with socially distinct meanings. We first characterized afferents' firing properties, i.e., firing frequency and number of spikes, for comparison to prior studies with well-controlled mechanical contact. Then, machine-learning classifiers were developed to examine the capability of each afferent subtype in differentiating the expressions, for comparison with perceptual studies. Two classification strategies were employed following the theory of temporal coding and rate coding of the neural firing [96], respectively. Moreover, with these models, we evaluated the classification performance of different segments of the neural recordings and their sensitivity to spike-timing noise, to identify the most informative firing patterns for each expression. Overall, the encoding performance of peripheral afferents and their firing properties in human-delivered social touch shed light on the information present at the periphery, which may affect the strategies available to the central nervous system for processing social intent, emotional state or affiliative alignment from physical skin contact.

5.2 Experimental Methods

5.2.1 Participants - Touch Receivers

Twenty healthy participants (23-35 years old with one exception of 50 years old) were recruited through local advertisement and a mailing list. All participants provided informed consent in writing before the experiment. The study was approved by the Swedish Ethical Review Authority (Dnr 2017/485-31) and complied with the revised Declaration of Helsinki.

5.2.2 Standardized Touch Expressions

Based on social touch communication between people in a close relationship, we used a previously developed set of six, standardized social touch expressions, including “attention,” “happiness,” “calming,” “love,” “gratitude” and “sadness” [18], [62]. Those expressions have been validated to be reliably and effectively recognizable by naïve stranger participants with accuracy similar or even higher than people with close relationships [18]. Experimenters were trained to deliver those standardized social touch expressions in the same way as in our preceding studies [18]. Since during microneurography, it is logistically difficult to simultaneously obtain direct psychological responses from participants, such as their subjective emotional perception, we connected the emotional meanings of those social touch expressions though this standardized expression set.

More specifically, the touch expression of “attention” comprised 4 bursts of 4-5 repetitive taps with the index finger, each burst lasting approximately 1.5 s, with approximately 1 s between. “Happiness” consisted of continuous random playful tapping using multiple fingers, and moving up and down the arm. “Gratitude” consisted of patting (3-4 pats with multiple fingers, lasting approximately 2 s) alternated with holding (long grasp with the whole hand, lasting approximately 2 s). “Calming” involved 4 repeated slow strokes down the arm with the whole hand, each lasting approximately 2 s, with approximately 0.5 s between. “Love” involved a continuous back-and-forth light stroking with the fingertips up and down the arm. Finally, “sadness” consisted of a sustained hold with firm but gentle squeezing.

5.2.3 Microneurography

Neural recordings were performed with equipment purpose-built for human microneurography studies from ADInstruments (Oxford, UK; setup 1) or the Physiology Section, Department of Integrative Medical Biology, Umeå University (setup 2). The course of the radial nerve just above the elbow was visualized using ultrasound (LOGIQ e, GE Healthcare, Chicago, IL, USA). A high-impedance tungsten recording electrode was inserted percutaneously and with ultrasound guidance it was inserted into the nerve. Where needed, weak electrical stimuli through that electrode were delivered to localize the nerve (0.02-1 mA, 0.2 ms, 1 Hz; FHC, Inc. Bowdoin, ME, USA). The electrode was insulated, except for the ~5 µm bare tip, with a typical length of 40 mm and shaft diameter of 0.2 mm. In addition to the recording electrode, an indifferent (uninsulated) electrode was inserted subcutaneously, approximately 5 cm away from the nerve. Once the electrode tip was intra-fascicular, minute movements were made to the recording electrode, manually or with a pair of forceps until a single afferent signal was isolated.

Each low-threshold mechanosensitive cutaneous afferent (all soft-brush sensitive) was classified by its physiological characteristics, as per the criteria used in [28], [97]. Briefly, individual Aβ low-threshold mechanoreceptors were separated into fast and slowly adapting types based on their adaptive responses to ramp-and-hold indentation of the skin. Three groups of fast adapting units were identified as follows: fast adapting hair follicle (HFA), responsive to hair deflection and light air puffs; fast adapting Pacinian corpuscle (FA-II), comprising a single spot of maximal sensitivity and robust response to remote tapping; fast adapting field (Field), comprising multiple spots of high sensitivity with no response to hair displacement or remote tapping of the skin. Two groups of slowly adapting units, i.e., type I (SA-II) and type II (SA-II), were identified where several features were examined including spontaneous firing, stretch sensitivity, and receptive field characteristics. In addition, an inter-spike interval pattern to sustained indentation (100 mN for 30 s) was tested. Coefficients of variation of inter-spike intervals for all SA-IIs (4 units) were in the range of 0.15 to 0.23. This was also measured for one SA-I and its coefficient of variation was 1.92. These values are consistent with previous observations [28], [91], [98]. Single muscle spindle (MS) afferents were identified by stretch of the receptor-bearing muscle along its line of action. These were not further classified into primary and secondary afferents.

Mechanical thresholds of all cutaneous afferent fibers were measured using Semmes-Weinstein monofilaments (nylon fiber; Aesthesio, Bioseb, Pinellas Park, FL, USA), except HFA whose preferred stimulus is hair movement so responses to light air puffs were determined. The monofilaments were applied manually with a rapid onset until the monofilament buckled: If a unit responded to the same (weakest) monofilament in at least 50% of trials, it was taken as the mechanical threshold. Based on prior work showing that 4 mN threshold divides the low threshold (<4 mN) and high threshold (≥ 4 mN) cutaneous afferent populations in hairy skin [91], [97], only those afferents with thresholds below 4 mN were considered. Further, any cutaneous afferent with a receptive field located at a site inaccessible for the delivery of expressions was discarded.

All neural data were recorded and processed using LabChart Pro for setup 1 (v8.1.5 and PowerLab 16/35 hardware PL3516/P, ADInstruments, Oxford, UK) and SC/ZOOM for setup 2 (Physiology Section, Department of Integrative Medical Biology, Umeå University). Action potentials were distinguished from background noise with a signal-to-noise ratio of at least 2:1 and were confirmed to have originated from the recorded afferent by a semi-automatic inspection of their morphology. For further details see [91].

5.2.4 Experimental Procedure

Participants were seated in a comfortable chair and pillows were provided to ensure maximal comfort. Designed standardized expressions were applied by trained experimenters to the receptive field of single neurons during microneurography recordings. The experimenter received audible spoken cues, first the cue-word, then a countdown (3, 2, 1, go). They were instructed to perform the touch starting from the "go"-signal until they heard a stop signal (3, 2, 1, stop), creating a continuous time window of touch for 10 s. Those cues could be heard by both experimenters and participants, but would not influence microneurography recordings, since peripheral tactile afferents do not receive top-down projections from higher-order neurons. The experimenter was first familiarized with the afferent's receptive field and was

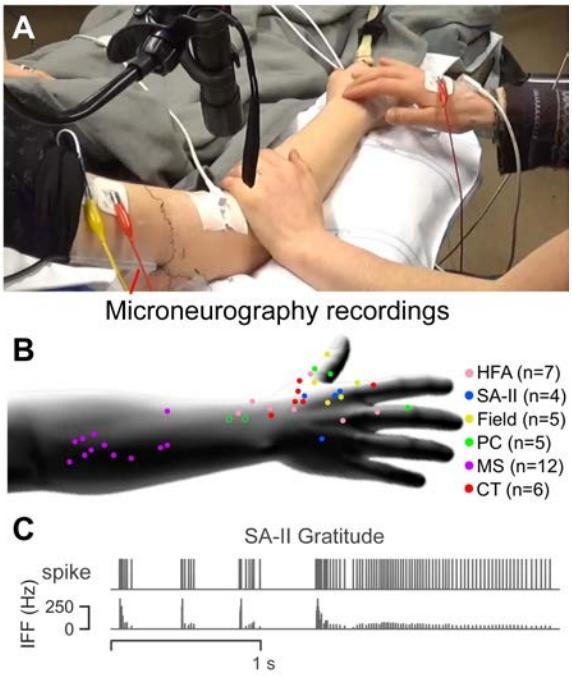

Figure 5.1. Experimental setup for microneurography experiments. (**A**) Standardized touch expressions were delivered over receptive fields of identified afferents by trained experimenters. Microneurography recordings were collected from the upper arm. (**B**) Multiple units were recorded for each of the six afferent subtypes. For cutaneous afferents, each dot represents the location of an individual receptive field. For two FA-II afferents in the forearm (open circles), the precise location of the receptive field was not documented. For muscle afferents, the dots are shown simply to illustrate where the gestures were delivered. The n-value denotes the number of units per afferent subtype. (**C**) An example microneurography recording of a SA-II unit when gratitude was delivered.

asked to touch an area of skin including but not limited to the receptive field (Fig. 5.1A). They were also required not to perform vigorous movements to avoid dislodging the recording electrode.

We recorded 41 low-threshold primary afferent units in total (Fig. 5.1B), which were classified into seven subtypes: Field (5 units), HFA (7 units), FA-II (5 units), SA-I (2 units), SA-II (4 units), CT (6 units), and MS (12 units). Among them, Field, HFA, FA-II, SA-I, and SA-II were classified as Aβ afferents. Since only two units were collected for SA-I afferents, we excluded this subtype from the dataset and kept the rest of 39 units. All cutaneous afferents were very sensitive to soft brushing and had mechanical (von Frey) thresholds of activation ≤ 1.6 mN. Per unit, each expression was conducted multiple times, comprising 751 trials in total, with the mean number of trials per unit being 19.26 and the standard deviation being 14.10. Specifically, we collected 128 trials for Field, 151 for HFA, 63 for FA-II, 127 for SA-II, 116 for CT, and 166 for MS. For the six emotion expressions, we collected 135 trials for attention, 124 for calming, 129 for gratitude, 124 for happiness, 119 for love, and 120 for sadness. All recordings were cropped to keep the first 10 s of data (which was the target duration for the trained experimenters) at a resolution of 1 ms. Microneurography data and models are available on Figshare: https://figshare.com/articles/dataset/Models_and_data/25739310.

5.3 Data Analysis

5.3.1 Afferent Responses to Elementary Touch Gestures

In our first analysis we characterized the firing properties of the afferents in human-delivered touch by comparing the mean instantaneous firing frequency (IFF) and the number of spikes across three elementary touch gestures (tapping, stroking, and holding). The elementary touch gestures were focused here to facilitate comparison with previous studies, summarizing the touch expressions to better align with the contact interactions examined by controlled stimuli, e.g., indentation, brushing, etc. In particular, attention and happiness expressions were grouped as the tapping gesture, calming and love expressions were grouped as the stroking gesture, and the sadness expression was counted as the holding gesture. The gratitude expression was left out since it consisted of both tapping and holding gestures.

Per expression trial, IFF was calculated only at the time point when a spike occurred, defined as the reciprocal of the time duration between the current spike and the previous spike. The mean IFF was derived over the whole 10 s neural recording and the number of spikes was counted from a 1 s chunk containing the largest number of spikes. The duration of 1 s was determined to avoid including long non-contact gaps within the expression. Since multiple emotion expressions and different touch gestures were

Figure 5.2. Example microneurography recordings of instantaneous firing frequency (IFF, Hz) collected from HFA and SA-II subtypes when six social touch expressions were delivered on the forearm. Sketches illustrate the standard contact delivery of those expressions. Touch gestures (tapping, stroking, and holding) used by the expressions are denoted.

recorded from the same afferent unit, the Linear Mixed Effects Model (LMEM) was used to perform significance tests on the pairwise comparisons of these variables across afferent subtypes and gestures. Partial η^2 effect size was calculated for each test and Post-hoc Benjamini-Hochberg method was used for multiple testing correction.

We further examined whether those afferent subtypes can classify touch gestures based on additional aggregated firing features. Five features were extracted as inputs from the 10 s recording of each trial, including the number of spikes, mean IFF, peak IFF, IFF variation, the number of bursts. IFF variation was calculated as the coefficient of variation of IFF, and the number of bursts was defined as the number of

spike bursts separated by gaps of inter-spike intervals larger than 1 s. The linear support vector machine (SVM) was implemented for classification with five-fold randomized stratified cross-validation repeated for 20 runs.

5.3.2 Touch Expression Classification

To evaluate the abilities of different afferent subtypes in discriminating the six expressions, we leveraged machine learning classifiers to predict delivered expressions from the neural spike trains. We first developed a one-dimensional convolutional neural network (1D-CNN) for time-series classification. This model was chosen following temporal coding theory [96], which suggests that stimulus information is coded by neurons through the timing and temporal pattern of firing activities. Full 10 s binary spike trains with the resolution of 1 ms were fed as inputs to take the full advantage of the temporal information. The model was trained and tested for each afferent subtype separately. Detailed structure and hyper parameters of the model were determined by cross validation grid search with data from all subtypes combined together. The final model structure contained five CNN layers and 16,646 trainable parameters in total. For each layer, 0.2 dropout was applied. The model was trained based on the loss of categorical cross-entropy with Early Stopping and the ADAM optimizer with a reducing learning rate starting from 0.001. Prediction accuracy was averaged over 20 repeats of five-fold randomly stratified cross validation to obtain more stable results.

To compare with the temporal coding based classification implemented by the CNN, we also employed a linear SVM model for rate coding based classification. Rate coding theory [96] follows that stimulus information is coded by aggregate descriptive features of neural firing, e.g., firing frequency, number of spikes. Therefore, instead of time-series spike trains, the same five firing features used in gesture classification, i.e., the number of spikes, mean IFF, peak IFF, IFF variation, and the number of bursts, were derived from 10 s neural recordings and used as inputs. Moreover, including a simpler model such as SVM is also beneficial since CNN model affords high computational power that might overshadow the encoding capability of each afferent subtype.

5.3.3 Expression Classification with Spike Train Segments

In order to identify the most informative segments of firing patterns that lead to high differentiation accuracies, we further conducted CNN classification on segments of spike trains per afferent subtype. A sliding window method incorporating window position and window length was applied to segment chunks from a given spike train for comparison. The sampling rates for window length were set at intervals of 0.1

s from 0.1 s to 4 s, and at intervals of 0.25 s from 4 s to 10 s, resulted 64 different window lengths in total. For each window length, five segments at different positions were derived according to five metrics with a sliding step of 1 ms, which includes the first segment, the segment with the largest number of spikes, the segment with the highest mean IFF, the segment with the highest IFF variation, and the segment with the highest IFF entropy. The IFF variation and IFF entropy here were calculated from step-interpolated IFF to better reflect the time-series pattern of touch expressions. Therefore, 320 different segment options were obtained in total to be compared.

For each afferent subtype, we first investigated the best window position metrics by conducting CNN with five-fold randomly stratified cross-validation repeated twice. Prediction accuracies of the five metrics were averaged across all window lengths, where Mann-Whitney U tests and post-hoc Benjamini-Hochberg correction were applied for pairwise comparison. Based on the best two window position metrics per subtype, we examined the prediction accuracies along with the window length by conducting CNN with seven repeats of five-fold randomly stratified cross-validation. We identified the saturation window length per subtype based on 90% of the highest accuracy from its accuracy curve fitted by fourth-order polynomial regression. Accuracy curves and saturation window lengths were further derived for all expressions per afferent.

According to the best window position and the saturation window length, the most informative firing segments were identified per afferent (group 1) and per afferent-expression combination (group 2). SVM classification was then conducted on the identified segments to examine if they also yield high prediction accuracies when using only five aggregated firing features and a linear model.

5.3.4 Expression Classification with Spike-Timing Noise

We aimed to further evaluate the contribution of the fine-grained temporal information present in the spike train to the accuracy of time-series classification. We therefore examined the spike-timing sensitivity of all afferent subtypes in classifying touch expressions. Random noise was added to all spike times across the full 10 s spike trains, which were then input to the CNN classifier. Noise following a Gaussian distribution was employed with mean equal to zero and standard deviation (SD) ranges from 0 to 100 ms with steps of 5 ms. The CNN model was trained per subtype with noise-free spike trains and was tested using recordings with noise added. Average accuracies were obtained per combination of afferent subtype and expression from five repeats of five-fold randomly stratified cross validation, with each level of noise tested by ten different sets of random noise.

5.4 Results

5.4.1 Firing Properties of Afferent Subtypes

Examples of collected neural recordings of SA-II and HFA afferents are illustrated in Fig. 5.2 for all six touch expressions. Despite the consistent delivery of the expressions, distinct firing patterns were observed between these two subtypes. For example, with the sadness and gratitude expressions, SA-II afferents

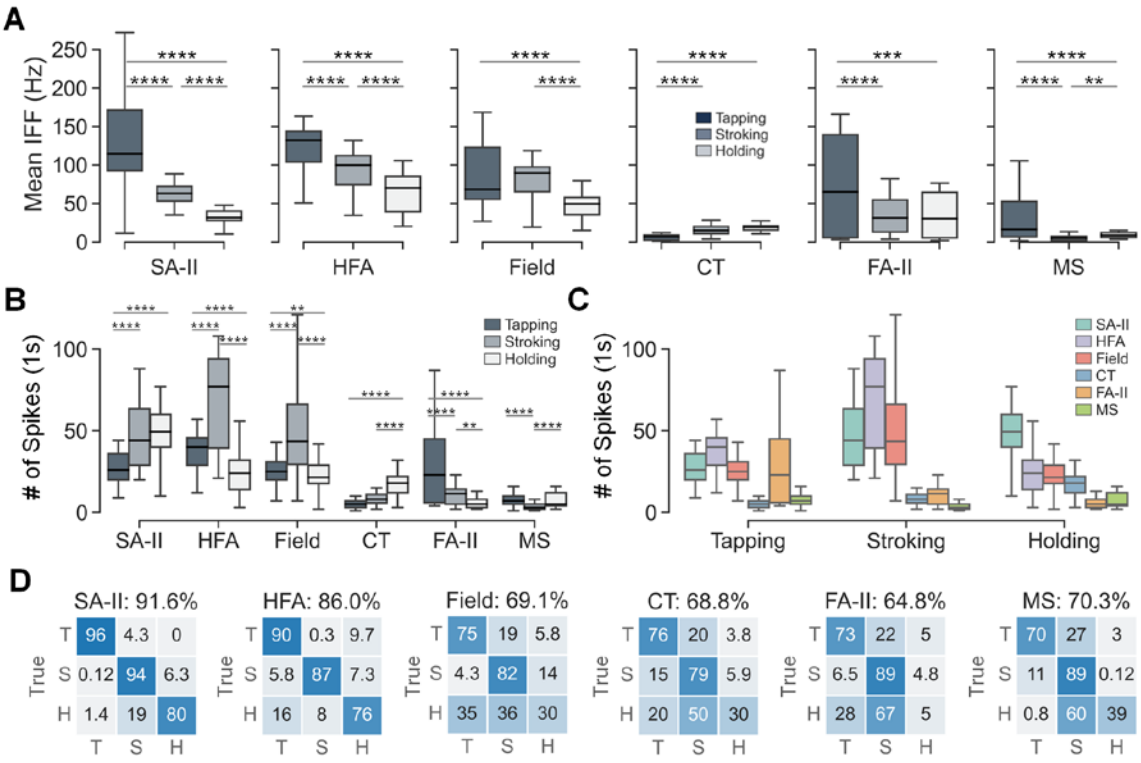

Figure 5.3. Neural firing properties of the six afferent subtypes in response to different touch gestures. (**A**) Distributions of mean IFF across gestures per afferent subtype. (**B**) Distributions of the number of spikes across gestures per afferent subtype. The number of spikes per trial was calculated from a 1 s duration with the largest number of spikes. (**C**) Distributions of the number of spikes across afferent subtypes per gesture. *$p < 0.05$, **$p < 0.01$, ***$p < 0.001$, ****$p < 0.0001$. Significance test results for panel C and partial η^2 effect sizes for panels A, B, and, C are provided in Supplementary Fig. 5.S1. (**D**) SVM classification of touch gestures per afferent subtype using five firing features extracted from 10 s recordings. "T" represents tapping, "S" represents stroking, and "H" represents holding. Numbers in the cells denote the percentage of classification results.

responded throughout contact with a sustained, slowly decaying firing pattern, while HFA afferents only responded to the onset and offset of the holding or when the hand position was adjusted.

Under human-delivered social touch, all afferent subtypes exhibited similar ranges of mean IFF and number of spikes (Fig. 5.3) compared with the same subtypes recorded with controlled stimuli [9], [27], [39], [85], [99]–[101]. More specifically, the mean IFFs of Aβ afferents (up to 300 Hz) were overall higher than those for CT and MS afferents (up to 50 Hz) (Fig. 5.3A), similar to prior studies using passive touch [9], [99], [101]. Also, the mean IFFs of SA-II, HFA, and Field afferents decreased when switching from fast tapping to stroking to static holding contact, yet increased for CT afferents (Fig. 5.3A). For stroking contact alone, it has been reported that the mean IFFs of Aβ afferents increased with higher velocity, while the mean IFFs for CT afferents decreased for velocities over 3 cm/s [9]. As for the number of spikes, HFA and Field afferents shared the same patterns, with stroking contact eliciting significantly more spikes and holding contact eliciting fewer spikes (Fig. 5.3B). Note that fewer spikes recorded from tapping contact may be due to the overall shorter contact duration relative to the other two gestures. In comparison, the numbers of spikes for SA-II and CT afferents were also high for slow and static holding contact, which agrees with the firing properties widely reported for these two subtypes [9], [27], [85]. Overall, such alignments in firing properties compared with those identified using controlled stimuli help validate the effectiveness of the designed microneurography paradigm and experimental procedure of human social touch.

Meanwhile, all Aβ afferents subtypes in the skin responded very well to tapping contact (Fig. 5.3C, p-values in Supplementary Fig. 5.S1), while SA-II responded with significantly more spikes for holding than other gestures and FA-II exhibited significantly fewer spikes for stroking than other gestures. These distinct properties suggest the potential complementary functional roles of those afferents when viewed as a population at higher levels of the nervous system. Moreover, when five aggregated firing features were used (see section III-A), the three elementary touch gestures can be well classified by all afferent subtypes (Fig. 5.3D) with the highest accuracies obtained by SA-II and HFA afferents.

5.4.2 Single Units of SA-II and HFA Afferents Effectively Classify Social Touch Expressions

Among the six afferent subtypes, SA-II and HFA achieved the highest accuracies around 70-80% in classifying the six touch expressions using the CNN with full spike trains as inputs (Fig. 5.4A). Note that the results may slightly vary across different runs due to the random train-test splitting and stochasticity of CNN model. Such accuracies are very close or even slightly higher than human recognition accuracy for

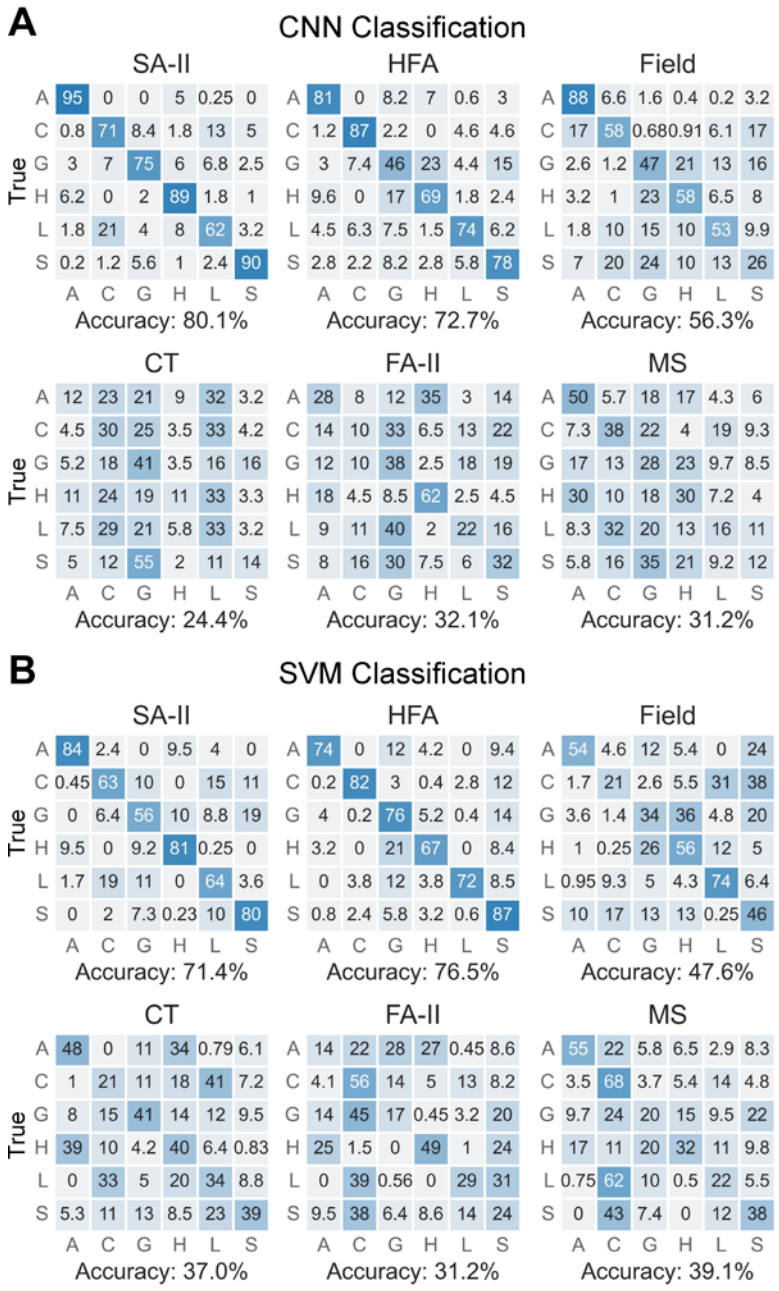

Figure 5.4. Classification results per afferent subtype using (**A**) CNN classifier with 10 s spike trains as inputs and (**B**) SVM classifier with five features as inputs. Numbers in the cells denote the percentage of classification results. The classification accuracy is markedly higher for SA-II and HFA subtypes, at levels observed in human perceptual experiments [4].

the same six standard touch expressions [18]. In comparison, Field afferents exhibited relatively lower accuracy around 56%, while the accuracy of CT, PC, and MS afferents were not far from the chance level

of 16.7%. Similar prediction results were also obtained in SVM classification when using five firing features (Fig. 5.4B). Classification accuracies as high as 70-80% were observed for SA-II and HFA subtypes while Field, CT, FA-II, and MS afferents exhibited lower accuracies. The consistency in classification performance between the two models implies that SA-II and HFA afferents convey the richest information in human social touch for at least the tested six touch expressions and are capable of encoding the mechanical skin deformations relevant to social touch expressions in an accurate and reliable way.

5.4.3 Most Informative Firing Patterns

Among the five window position metrics used in generating spike train segments, significantly different classification accuracies were observed among most pairs of metrics across all subtypes (Fig. 5.5B, p-values in Supplementary Fig. 5.S2B). For comparison purposes, we picked the best two window position metrics per subtype: the highest number of spikes and the highest mean IFF for SA-II, first and the highest number of spikes for HFA, and the highest number of spikes and the highest IFF entropy for Field, CT, FA-II, and MS. The accuracy differences among the window metrics were relatively small, such as 3.3% between the top two metrics for SA-II afferents, and 2.7% between the top two metrics for HFA afferents. Moreover, five accuracy curves along with the window lengths corresponding to the five window metrics also well overlapped with each other, especially for SA-II and HFA subtypes (Supplementary Fig. 5.S2C). It indicates that window position does not make a huge impact on the classification performance.

Per afferent subtype, the two top performing metrics were adopted for examining the influence of window length. Results show that classification accuracies for SA-II, HFA, and Field afferents saturate when window length approached 3.3 s, 3.8 s, and 5 s respectively (Fig. 5.5D). In contrast, accuracies for the other afferent subtypes began and remained consistently low. It implies that instead of the full 10 s, an average duration of 3-4 s of the neural responses of SA-II and HFA afferents provides sufficient information to differentiate those expressions. Further inspection into afferent-expression combinations shows that saturation window lengths varied between 2.5 s to 5.3 s across expressions for SA-II and HFA afferents, which is still a comparably limited range much less than 10 s.

The identified most informative firing patterns of SA-II and HFA afferents are shown in Fig. 5.6A, 5.6B for all expressions. We found that for expressions with multiple rounds of contact, e.g., attention and calming, at least one round of contact was always included, which captures the specific rhythm of the contact delivery across different expressions. Moreover, the variation of the saturation window length could be related to both contact stimuli and firing properties of afferent subtypes. For example, the unique

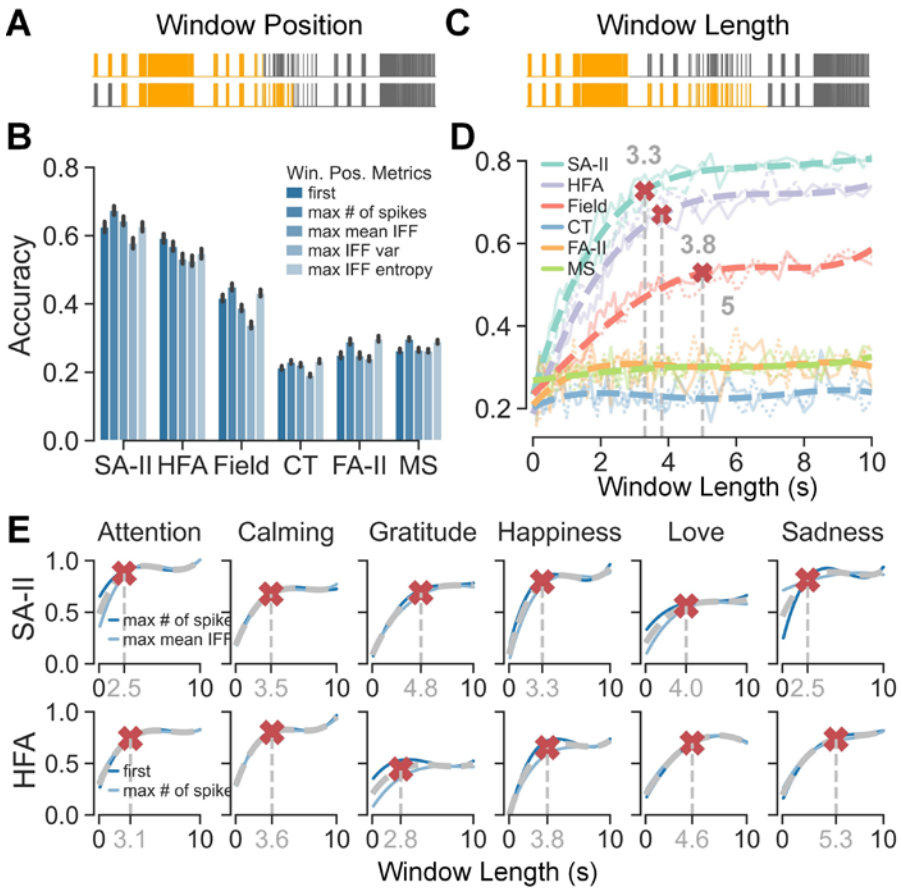

Figure 5.5. Comparison of CNN classification accuracies when using segments of spike trains derived from different window positions and window lengths. (**A**) An example of two window position options with the same window length. Gray traces are 10 s spike trains from the same trial, where highlighted spikes illustrate two different segments. (**B**) Classification accuracies across window position metrics averaged over all window lengths for each afferent subtype. Significance test results can be found in Supplementary Fig. 5.S2B. (**C**) An example of two window length options with the same window position. Gray traces are 10 s spike trains from the same trial, where highlighted parts illustrate two different segments. (**D**) Classification accuracies along with window length per afferent subtype. Accuracy curves were fitted using data from their best two window positions and fourth-order polynomial regression, shown as dashed curves. Red cross markers denote 90% saturation window lengths. Two lighter curves represent data from the two best two window positions. (**E**) Classification accuracies along with window length per afferent subtype per expression. Averaged accuracies from their best two window positions are shown as grey dashed curves and blue curves represent each of the best positions. Red cross markers denote 90% saturation window lengths.

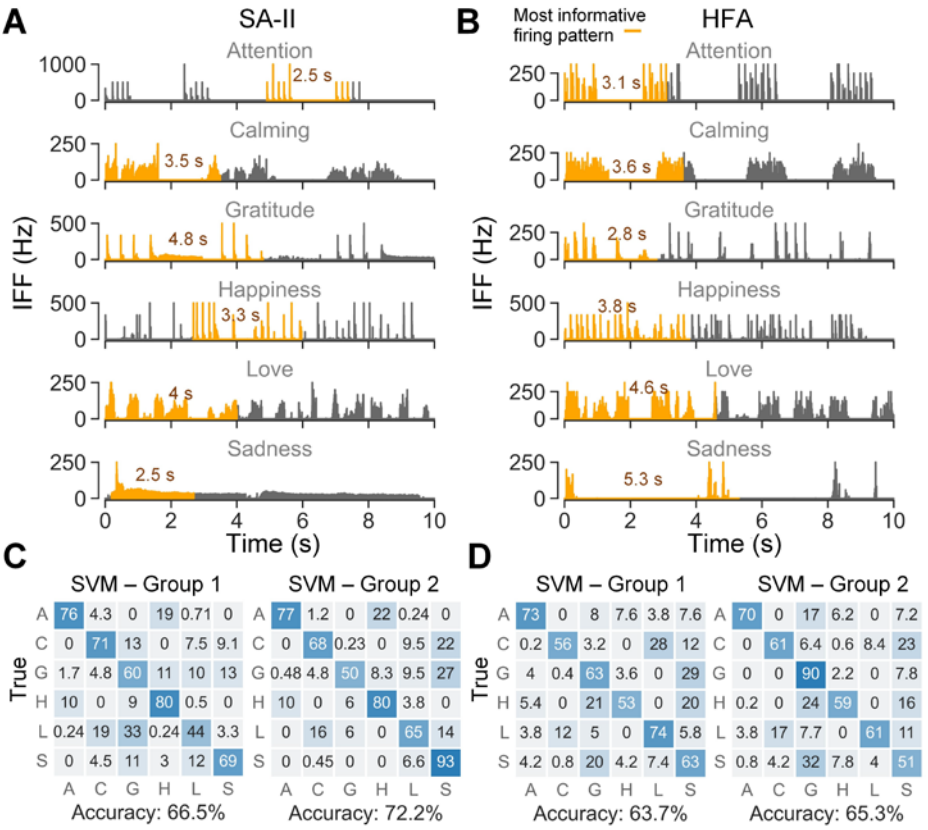

Figure 5.6. Examples of identified most informative firing patterns and SVM classification based on the identified segments. IFF traces highlighted in orange are the most informative segments determined by the best window position (SAII: max # of spikes, HFA: first, derived from Fig. 5.5B) and the saturation window length per afferent-expression combination (annotated as numbers near the highlighted segments, derived from Fig. 5.5E) for (**A**) SA-II subtype and (**B**) HFA subtype. Classification results using the SVM model for (**C**) SA-II subtype and (**D**) HFA subtype. Group 1 and group 2 refer to two groups of spike train segments derived by saturation window lengths per afferent subtype (Fig. 5.5D) and saturation window lengths per afferent-expression combination (Fig. 5.5E), respectively.

repetitive tapping pattern of attention expression might explain why it requires relatively less data than other expressions. Sadness exhibits the largest difference in saturation window length between SA-II and HFA (Fig. 5.5E). One explanation is the sustained low-frequency firing pattern of SA-II afferents under holding contact is easy to differentiate even within a shorter time. In comparison, the firing response of HFA to holding is similar to that of tapping contact such that more data including the non-response gap are needed to capture the unique dynamic of prolonged holding of the sadness expression (Fig. 5.6B).

Moreover, SVM classification using the identified most informative firing patterns show similar prediction accuracies as using the full 10 s recordings (Fig. 5.6C, 5.6D). Slightly higher accuracies were obtained by segments derived per afferent-expression combination (group 2). Such findings help validate the richness of information contained within identified segments of SA-II and HFA afferents' firing patterns.

5.4.4 Spike-Timing Sensitivity

We found that SA-II afferents were sensitive to spike-timing noise for attention, happiness, sadness, and gratitude expressions as their prediction accuracies dropped to approximately a chance level when noise higher than 50 ms SD was applied (Fig. 5.7B). Those four expressions were delivered by tapping and holding gestures, while expressions delivered by the stroking gesture, i.e., calming and love, were not influenced by spike-timing noise. HFA afferents were sensitive to spike-timing noise for only tapping-delivered expressions of attention and happiness. For other touch expressions delivered by holding or stroking gestures, their prediction accuracies did not drop when noise increased. Compared with HFA afferents, SA-II's unique spike-timing sensitivity to holding contact indeed align well with its unique sustained response to static contact. Except for SA-II and HFA afferents, other afferent subtypes were not sensitive to spike-timing noise across all expressions. Moreover, SA-II and HFA subtypes also exhibited tolerance to a lower level of spike-timing noise. More specifically, SA-II responses to tapping contact were tolerant to spike-timing noise up to 20 ms. In comparison, responses to holding contact began to be influenced at roughly 10 ms. For HFA afferents, responses to tapping contact exhibited noise tolerance up to approximately 15 ms. This tolerance could relate to the variability of human-delivered touch, the variability of firing patterns across units, and/or the prediction target of expressions being abstract and composite.

We then focused on SA-II afferents to investigate the potential cause of such high spike-timing sensitivity of certain afferent-expression combinations. Confusion matrices derived from CNN classification (Fig. 5.7C) show that the tapping contact with the attention expression was misclassified as stroking contact of the calming expression when 50 ms SD noise was applied, while holding contact of the sadness expression was misclassified as stroking contact of love when 25 ms noise was applied. Neural recordings with and without noise were next compared for those two confused cases (Fig. 5.7D). We found that, for attention expression, noise as high as 50 ms SD could flatten isolated spikes elicited by repetitive taps within one round of tapping. It thus changed the pattern envelope to a continuous chunk of firing with variable frequencies, which was similar to the firing pattern of calming delivered by stroking. As for the sadness expression, 25 ms SD noise already converted its sustained slowly decaying firing pattern into a spiky and

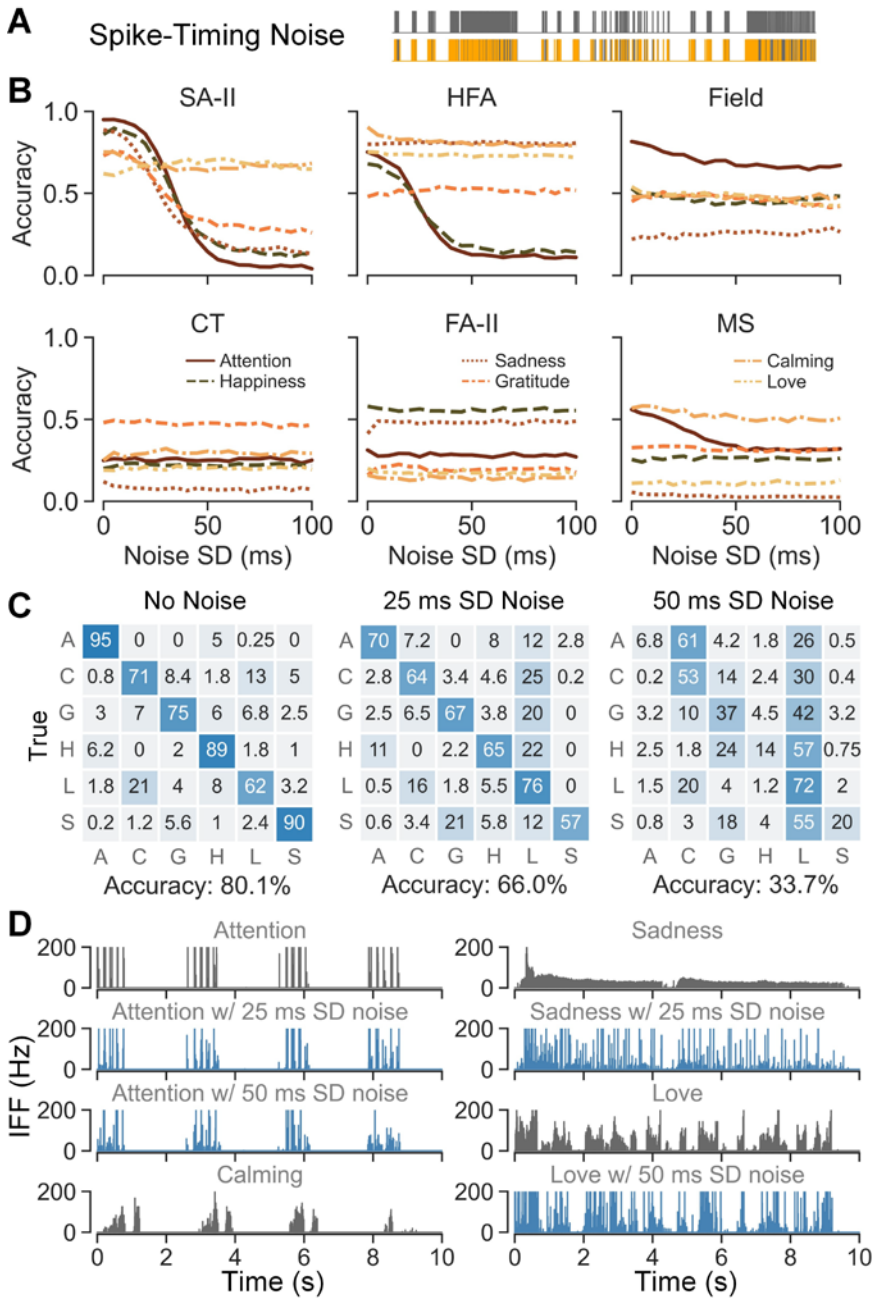

Figure 5.7. Spike-timing sensitivities across afferent subtypes in human social touch. (**A**) Spike trains from the same trial with (lower) and without (upper) spike-timing noise added. (**B**) CNN classification accuracies of six expressions relative to the standard deviation of added noise per afferent type. (**C**) CNN classification accuracies for the SA-II subtype using 10 s spike trains with different level of noise added. (**D**) SA-II recordings for the confused expressions when noise is added. The grey IFF traces are the original recordings and the blue IFF traces are recordings with noise added.

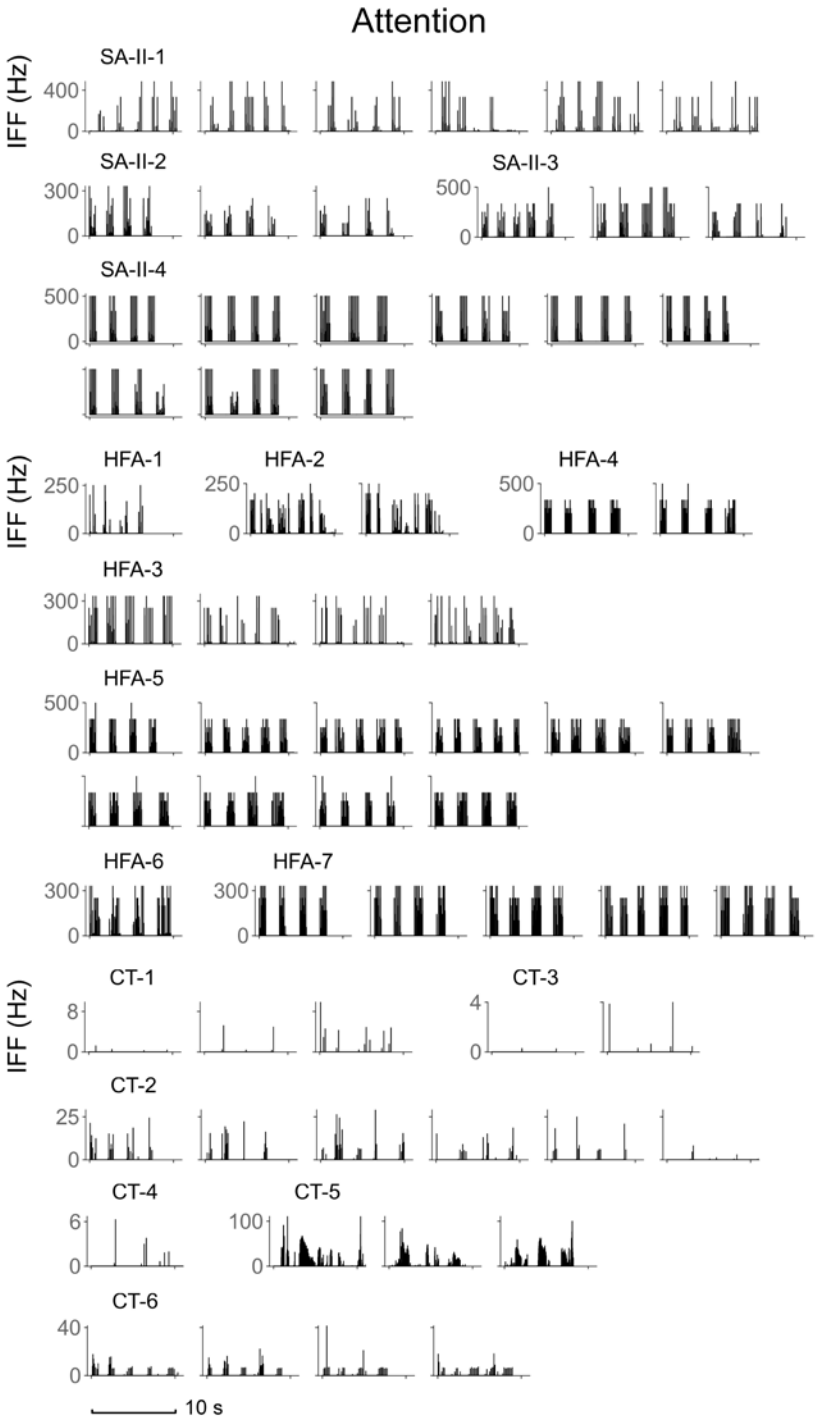

Figure 5.8. Neural recordings of SA-II, HFA, CT subtypes for the attention expression. All trials are shown here in the format of Instantaneous firing frequency (IFF, Hz).

irregular shape, which was similar to the firing pattern of love delivered by stroking. Here, attention and calming were mainly confused with the stroking of calming and love respectively, which could relate to their shared touch rhythm of having prolonged non-contact gaps or not. In contrast, since SA-II responses elicited by stroking contact were initially irregular, noise as high as 50 ms SD still did not cause a major change to the firing response of the love expression. Based on the observations, we hypothesize that the spike-timing sensitivity of those afferent subtypes could be strongly tied to the extent of changes in the envelope of their firing patterns caused by noise. This pattern envelope could be a more appropriate metric in capturing contact pattern at a macro level, such as touch gestures and contact rhythms when encoding touch expressions. In this scenario, millisecond-precision of single spike times might not be as informative due to robustness of the touch expressions and their social meanings.

5.5 Discussion

5.5.1 Microneurography Paradigm for Human-to-Human Touch

Distinct from traditional experiments that control the mechanical stimulus and vary a single feature at a time, we record from single peripheral afferents in a human-to-human touch paradigm, where multiple stimulus features, e.g., normal displacement, contact area, lateral velocity, vary simultaneously [4], [18], [71], [72]. Such naturalistic human touch interactions directly contribute to our emotional well-being and maintains our social connections [30], yet are technically difficult to replicate with actuated devices. Indeed, precisely controlled stimuli, such as rigid bodies indented in one dimension of depth or force [39], [86], [87], are more commonly employed in characterizing the firing properties of peripheral afferents. Recent efforts have begun to move toward more naturalistic contact interactions using brushing, puffs of air, and pinch, etc., [102], [103]. Natural textures have also been applied in recording monkey Aβ afferents [94]. However, each of these efforts still controls and varies a single stimulus feature at once, which is different from natural contact with co-varying features.

In this study, we move a step further into human-delivered touch, where the richness of contact dynamics could reveal classes of primary afferents that encode the combination of multiple features. In our tasks, such information could be relevant to social messages conveyed in touch expressions. More specifically, six standardized social touch expressions were delivered by trained experimenters. This affords reliable contact interactions [18] and retains the subtleness of human-delivered touch at the same time. Meanwhile, expressions were designed with specific touch gestures, which can be compared with similar mechanical stimulus contact, e.g., human-delivered stroking versus brush-delivered stroking, human-delivered tapping versus vibrating actuator indentation. Indeed, the firing properties we observed in

human touch (Fig. 5.3) share similar ranges and trends with those for controlled stimuli. It also demonstrates that similar states of skin contact and deformation could elicit similar responses across human touch and stimulus contact [83].

5.5.2 Social Touch Relevant Encoding across Afferent Subtypes

Both CNN classification using time-series neural recordings and SVM classification using five firing features show that SA-II and HFA subtypes outperform other subtypes (Fig. 5.4) and provide high differentiation accuracies similar to human perception [18]. Moreover, such accuracy is consistent in using either the full 10 s time course of the neural responses or the most informative firing patterns therein (Fig. 5.6C, 5.6D).

The SA-II and HFA afferent subtypes, due to particular physiological mechanisms, may be geared more to the inherent contact characteristics of social touch. One prominent commonality is their large, but not too diffuse, receptive fields [28], [104], [105], which may help in consistently capturing the range of contact dynamics given the size of touchers' fingers and hands and their lateral movements. The detailed sizes of receptive fields of those mechanoreceptive Aβ afferents have been reported by a series of microneurography studies [28], [104], [105]. In particular, Vallbo et al., [28] has recorded relatively large receptive fields for rapidly adapting units in the hairy skin of human forearm, with around 113 mm^2 for HFA and 78 mm^2 for Field afferents. On the hairy skin of human hands [105], median sizes were identified as 16 mm^2 and 28 mm^2 for SA-I and SA-II units respectively. In glabrous skin [104], the receptive field sizes of SA-II afferents have also been shown to increase considerably with indentation force, as compared with SA-I units. FA-II afferents that innervate Pacinian corpuscles, on the other hand, exhibited markedly larger receptive fields [105], which are almost too diffuse to map due to their extreme sensitivity [39]. Therefore, compared with other subtypes, the relative size of the receptive fields of HFA and SA-II afferents in hairy skin could contribute to their social expression encoding.

Furthermore, SA-II and HFA afferent subtypes are believed to be sensitive to a wide range of contact, including indentation [106], hair deflection [107], skin stretch [105], and shearing forces [85], [108], which are contact characteristics that human touch gestures tend to evoke. For example, both SA-II and HFA respond to tapping (vertical contact) and stroking (sheering contact) with distinct mean IFFs (Fig. 5.3A) and can easily differentiate those two gestures (Fig. 5.3D). In contrast, Field and FA-II afferents respond to these two directions of contact with non-differentiable firing frequencies (Fig. 5.3A). Moreover, SA-II and HFA afferents also precisely followed tapping contact with high IFF responses (Fig. 5.8), outperforming the other subtypes. Interestingly here, SA-II afferents are typically thought to mainly encode static/slow

movements and skin stretch [85], [108], but also responded very well to fast vertical contact delivered by human tapping. As for holding contact, as expected, SA-II afferents respond with sustained low-frequency firing patterns, which distinguish holding from other fast movements. HFA afferents did not respond to the sustained contact, but precisely captured the on-set and off-set of the hold gesture. Although this pattern of spike firing is similar to that of tapping, the unique prolonged touch rhythm of holding provides distinct temporal information. Meanwhile, those two subtypes also respond to the stationary holding gesture with a significantly lower mean IFF compared with other gestures. Overall, the capability of SA-II and HFA subtypes to differentiate the social touch expressions suggests that their neural responses well correspond to the range of stimulus input and mechanical skin deformation inherent in human-to-human touch interactions.

Focusing on the context of social touch, the afferent subtypes exhibited distinct sensitivities in encoding the two layers of information, i.e., gestures (lower level) and expressions (higher level). Based on the same five firing properties, all six subtypes could accurately differentiate the three gestures (Fig. 5.3D), whereas CT, FA-II, and MS afferents fail to separate the expressions (Fig. 5.4). It suggests that contact patterns of elementary touch gestures, e.g., tapping, stroking, and holding, can be captured to a certain extent by all afferent subtypes. While the same gesture can be slightly varied in terms of its contact delivery of velocity, indentation depth, contact area, etc. [72] to convey specific social meanings, such nuances may be less easy to capture for certain afferents. For example, attention and happiness delivered by tapping, and calming and love delivered by stroking, were frequently confused by CT, FA-II, and MS subtypes as they share comparable contact dynamics. This might also explain human receivers' misidentification of those expression pairs [18]. In comparison, SA-II and HFA subtypes are very sensitive to slight contact changes, as they classify gestures and expressions with relatively similar accuracies (Fig. 5.3D, 5.4).

The relatively lower coding capability of CT, FA-II, and MS afferents might relate to their functional roles in signaling contact modalities less reflected in the applied six social touch expressions. CT afferents are traditionally thought to signal affective touch, more specifically pleasantness elicited by slow and gentle stroking [7], [80], in parallel with Aβ afferents serving as discriminators for physical contact properties [109]. We indeed found that CT afferents can successfully identify stroking contact (Fig. 5.3D), yet could not further differentiate contact between love and calming expressions (Fig. 5.4). More specifically, gentle stroking was deployed for both expressions but with different contact rhythms and routes, i.e., love: continuous back-forth stroking, calming: four separate one-direction stroking. Meanwhile, although CT afferents have been recorded with relatively small receptive fields [106], Olausson et al., [110] reported

that neuronopathic patients lacking Aβ afferents exhibited a poor ability to localize tactile stimuli based on CT afferents alone. Such weak contribution of CT afferents to localization perception, along with their low sensitivity to very fast movements [9], suggests that the combination of Aβ afferents might be needed to inform subtle contact differences. Surprisingly, CT afferents also respond very well to fast vertical tapping contact (Fig. 5.8). While CT afferents have been reported to respond well to von Frey indentation [111], human tapping affords much higher levels of force in a faster and repetitious manner. However, more detailed contact differences between the tapping of attention and happiness were not captured. For the other two subtypes, FA-II afferents respond to high-frequency vibration in discriminative touch, such as contact delivered to a site remote to the afferent's receptive field center [105]. However, they filter low frequency stimuli [39] that carry most of the information adhering to social touch. MS afferents respond to muscle extension and flexion associated with our proprioceptive sensation [112] and while they could discriminate the lower level gestures (Fig. 5.3D), their relatively low firing rates (Fig. 5.3A-5.3C) suggest that our social touch stimuli are not optimal stimuli.

5.5.3 Temporal Envelope of Firing Pattern as Potential Social Touch Encoding Strategy

By leveraging machine learning classification models, we identified the most informative firing patterns of SA-II and HFA afferents in encoding touch expressions. Those firing patterns and their corresponding contact patterns suggest their coding strategies relate to perceptual discrimination. More specifically, instead of the full 10 s of contact, we found that an average of 3-4 s provides enough information for single units to differentiate the six expressions (Fig. 5.5D). Also, as window position did not have a critical impact, it suggests that afferents respond in a consistently informative way throughout the course of contact, where the accumulation of a sufficient amount of information would be the key for social touch processing. Indeed, this time duration of 3-4 s aligns with the cortical response time of brush-delivered affective touch [113], facial EMG response time in natural social touch that reflects emotional processing [18], and the acceptable response time of humanoid robots being touched by a human [114]. However, this time duration is significantly longer than that reported in encoding precisely-controlled single stimulus features. Based on a population simulation of peripheral tactile afferents, tens of milliseconds were found to be sufficient in encoding stimulus directions [115]. Similarly, with ensembles of recorded single afferents, tens of milliseconds neural responses were also suggested to be effective in encoding controlled force, torque, force direction, and shape on finger pads [116], [117]. Such a difference in time course highlights the complexity of human social touch, where social meanings may be integrated from specific spatiotemporal contact interactions. For example, attention was expressed as separate rounds of

repeated fast tapping versus happiness was expressed as continuous tapping with multiple fingers tickling back and forth on the forearm. While afferent firing at tens of milliseconds can be comparable between the two expressions, they begin to reflect the contact rhythms of expressions in the time scale of multiple seconds (Fig. 5.6A, 5.6B). In comparison, controlled single stimulus features carry less information and thus could be identified with much shorter neural responses especially using a population model [115]. As single units were tested in our case, we expect that population responses of single or multiple afferent subtypes might encode social touch expressions in shorter durations.

Furthermore, 10 to 20 ms SD random shifts applied to the spike timing cause little effect on the classification of the expressions, although greater shifts can change the firing envelope of one expression to be confused with another. It appears that the spike timing precision needed in encoding human social touch is relatively lower than encoding controlled stimulus features. For instance, when classifying well-controlled scanned textures and vibratory stimuli, the optimal spike timing precision is around 1 to 10 ms [94], [118]. Although the distance of transforming one spike train exactly to another [119] was used in aforementioned studies, we directly added artificial jitter to spike times [120]–[122] given the variation of human contact delivery. It was believed that spike-timing jitter would blur the transmitted information of the stimulus [120], [121], [123]. For encoding controlled audio amplitudes, milliseconds or even sub-milliseconds of added artificial jitter can significantly decrease the accuracy of transmitted information [122]. Therefore, in human social touch, the relatively higher tolerance to spike-timing jitter suggests that the coarser level of temporal pattern might play a role. We found that by adding spike timing jitter, the envelope of the firing pattern can be drastically changed, which may be closely related to macro level touch interaction of gestures (Fig. 5.7D), instead of cell level dynamics of signal transmission. It also aligns with the finding that the SVM model using aggregated firing features provided comparable classification performance as the time-series CNN model (Fig. 5.4). It implies that detailed spike-to-spike temporal coding may not contribute to the core information in human social touch scenarios. Meanwhile, rate coding of aggregated features might not capture the whole dynamic details. Here we hypothesize that the temporal envelope of the firing pattern, which falls between the precise temporal coding and the summarized rate coding, could be a valuable metric in encoding social touch expressions, where the window length would have a large impact. It also offers references for future designs of social touch devices, including potential durations and resolutions for haptic rendering.

5.5.4 Limitations and Future Works

The slowly-adapting type I (SA-I) afferent is another Aβ subtype that is likely to play a significant role in encoding social touch stimuli. In general, SA-I afferents contribute to our abilities in fine touch discrimination [124]. In our study, the population of SA-I afferents (n=2) was not large enough to include. Our speculation is that SA-I afferents might behave akin to SA-II afferents, due to similar adaptation characteristics. Additionally, SA-I afferents exhibit a very large dynamic range of sensitivity, as compared to SA-II afferents, combined with very low absolute thresholds [125]. Such sensitivity should benefit discriminability in general, yet if SA-I afferents are too sensitive, this may be too variable a response that buries the core contact information carried in social touch. In this way, SA-II afferents might offer advantages because they have relatively dampened responses to dynamic stimuli compared to SA-I afferents. Indeed, less sensitive subtypes in high threshold mechanoreceptors are shown to better encode noxious forces than the more sensitive ones [91]. However, further follow up work is required to understand the response characteristics of the SA-I subtype to social touches.

Since peripheral afferents convey all mechanical sensory inputs to the nervous system, one perspective is that the expressions simply reflect arbitrary collections of different mechanical inputs. However, social meanings assigned to the six expressions together with the discriminability differences across those subtypes can be interpreted as the evidence for early tuning of the nervous system to facilitate interpretation of social touch. Our study concerns to what extent the first stages of the nervous system would provide the scaffolding for the complex neural processing of social touch. We have shown here that at least two afferent subtypes, SA-II and HFA, provide more information than others. As different subtypes are believed to be responsible for certain mechanical features, our results imply that mechanical tuning properties of those two subtypes are particularly well suited for the contact dynamics embedded in social touch expressions. We predict from our results that these two subtypes would have a stronger influence than other classes in the neural pathway of social touch. Such findings also provide insights into haptic rendering of social touch, where contact stimuli preferential for SA-II and HFA afferents could be prioritized. Meanwhile, while single units appear to hold discriminative capacity, afferent subtypes are likely to interplay in a cohesive way in generating population responses [95], [126], from which our perception and discrimination are gleaned. Our findings regarding single unit responses provide the foundation for such future explorations, where empirical or mathematical studies of higher-order nervous structures would be needed to unravel the population processing of social touch communication.

Additionally, at the single-unit level, it is possible that SA-II and HFA afferents may struggle to distinguish different sets of touch expressions than those we used, and other subtypes may excel. However, it is empirically challenging to include a large set of emotional messages in human touch microneurography experiments while maintaining the data size for effective analysis. The six emotional messages adopted here were reported to be easily recognizable through touch [1]–[4], [18], while many others are difficult to communicate using touch alone. In our study, only one expression was used per emotional message and was constrained to be delivered on the forearm. The forearm was chosen for the benefits of microneurography setup as well as for being the body portion widely acceptable and studied in social touch scenarios [35], [45], [63], [127], [128]. The specific expression was derived from the commonly adopted touch behaviors of that emotion that is understandable by human receivers [4], [18]. Among the selected six touch expressions, a wide range of contact dynamics were included with varying velocities, movement directions, contact areas, indentation depths, etc., [18], [72]. That said, it may be beneficial to vary expressions per emotion in future studies, which could also take into account individual differences in touch delivery [84] and emotion perception [18].

Meanwhile, with the expressions connected to specific social meanings, the underlying emotional contexts could be moderated. In particular, the perception of pleasantness (valence), emotional arousal, and dominance [50], [129] were not fully explored in this study. Part of the reasons was to avoid the high task load of participants if psychophysical and microneurography experiments were conducted together. Based on the dataset of emotional ratings for English words [129], happiness and attention afford high arousal and were found both delivered by fast tapping contact. We might assume that neural responses to fast contact velocities are related to high arousal percepts. However, other contact characteristics, e.g., force, indentation, contact area might also contribute [72]. Therefore, precise contact quantification needs to be introduced to uncover further details of how emotional contexts of physical touch delivery are encoded by peripheral afferents [71].

Overall, in this work, through microneurography recordings of single peripheral afferents elicited by naturalistic, human-delivered social touch, we found that Aβ afferents, especially SA-II and HFA subtypes, can effectively encode social touch expressions. Indeed, the responses of single afferents match the discriminative accuracy of human perceptual recognition. More specifically, the analysis of spike firing patterns using time-series machine learning classification indicates that a duration of 3-4 s of spike firing provides sufficient discriminatory information in social touch, with high tolerance to shifts in spike-timing

of 10-20 ms, suggesting the time scales relevant for the peripheral encoding of social touch interactions are distinct from millisecond accuracy requisite in discriminative touch interactions.

5.6 Supplemental Materials

A

Partial η^2 Effect Sizes for Fig. 5.3A, 5.3B

Mean IFF	SA-II	HFA	Field	CT	FA-II	MS
Tapping - Stroking	0.52	0.53	0.00059	0.24	0.33	0.23
Stroking - Holding	0.66	0.8	0.36	0.52	0.32	0.23
Tapping - Holding	0.72	0.47	0.56	0.048	6.1E-5	0.12

# of Spikes	SA-II	HFA	Field	CT	FA-II	MS
Tapping - Stroking	0.51	0.68	0.4	1.1E-5	0.32	0.32
Stroking - Holding	0.6	0.27	0.078	0.32	0.42	0.0022
Tapping - Holding	3.9E-5	0.75	0.39	0.36	0.18	0.38

B

LMEM Test Results and Partial η^2 Effect Sizes for Fig. 5.3C

Tapping	SA-II	HFA	Field	CT	FA-II	MS
SA-II		0.12	0.026	* 0.37	8.8 E-5	**** 0.7
HFA			0.017	*** 0.52	0.043	**** 0.75
Field				* 0.37	0.0097	*** 0.57
CT					0.20	0.0069
FA-II						** 0.32

Stroking	SA-II	HFA	Field	CT	FA-II	MS
SA-II		0.09	0.07	*** 0.68	** 0.6	**** 0.76
HFA			0.0018	*** 0.63	*** 0.57	**** 0.71
Field				** 0.47	* 0.42	*** 0.55
CT					0.066	*** 0.58
FA-II						*** 0.6

Holding	SA-II	HFA	Field	CT	FA-II	MS
SA-II		* 0.34	* 0.47	** 0.54	** 0.71	**** 0.75
HFA			0.0098	0.056	* 0.31	** 0.36
Field				0.043	** 0.49	*** 0.5
CT					* 0.46	** 0.43
FA-II						0.012

Figure 5.S1. (**A**) Partial η^2 effect sizes for the LMEM tests reported in Fig. 5.3A, 5.3B. (**B**) LMEM test results (upper line in each cell) and the corresponding partial η^2 effect sizes (bottom line in each cell) for the pairwise comparison reported in Fig. 5.3C. *$p < 0.05$, **$p < 0.01$, ***$p < 0.001$, ****$p < 0.0001$.

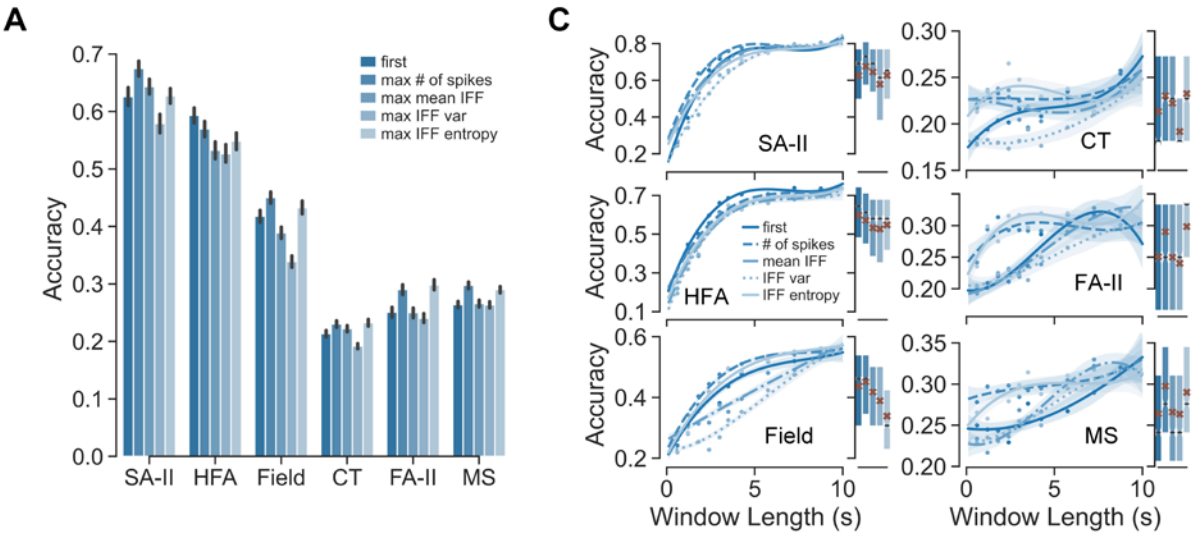

B

SA-II ****	first	count	mean	var	entropy
first	0.63	***	-	****	-
count		0.67	***	****	****
mean			0.64	****	-
var				0.58	***
entropy					0.63

HFA ****	first	count	mean	var	entropy
first	0.59	**	****	****	****
count		0.57	**	***	-
mean			0.53	-	-
var				0.53	-
entropy					0.55

Field ****	first	count	mean	var	entropy
first	0.42	****	***	****	-
count		0.45	****	****	*
mean			0.39	****	****
var				0.34	****
entropy					0.43

CT ****	first	count	mean	var	entropy
first	0.21	***	*	****	****
count		0.23	-	****	-
mean			0.22	****	-
var				0.19	****
entropy					0.23

FA-II ****	first	count	mean	var	entropy
first	0.25	****	-	-	****
count		0.29	****	****	-
mean			0.25	-	****
var				0.24	****
entropy					0.30

MS ****	first	count	mean	var	entropy
first	0.26	****	-	-	****
#		0.30	****	****	-
mean			0.27	-	****
var				0.26	****
entropy					0.29

Figure 5.S2. (**A**) Classification accuracies across window position metrics averaged over all window lengths for each afferent subtype. (**B**) *p < 0.05, **p < 0.01, ***p < 0.001, ****p < 0.0001 were derived by Mann–Whitney U tests with Benjamini-Hochberg post-hoc correction. (**C**) Classification accuracies across window position metrics along with the increase of window length. Curves were fitted using third-order polynomial functions, points denote means of 10 evenly-binned data. Bar plots show distributions of classification accuracies over all window lengths per window position metric, and brown cross markers denote means per window position metric.

Overall Conclusions

In this dissertation, we focused on human social touch communication and uncovered its details regarding touch delivery, emotional perception, and the underlying peripheral neural coding mechanism. This effort contributes to the understanding of social touch and aids in future haptics design, where the precise nature of social touch can be optimally mimicked and rendered remotely.

Quantified human-to-human physical contact in social touch communication

To decompose how the variation of physical contact evokes different perceptional responses, the complex and subtle details of human-delivered touch need to be precisely measured. In our first chapter, we developed a 3D visual tracking system using a time-of-flight depth camera to measure the physical skin contact between the bare hand of a toucher and the forearm of a receiver. More specifically, the toucher's hand was tracked as a posed and positioned 3D hand mesh using deep neural network, while the receiver's forearm was segmented as a detailed 3D point cloud. Contact detected between the 3D hand and forearm was then quantified through six time-series attributes using a customized point-cloud contact model. The tracking performance of the system was systematically validated using independent higher-resolution direct measurements, including electromagnetic tracker, force mat sensor, and laser displacement sensor. Additionally, the system was also evaluated specifically for its applicability and effectiveness in social touch interactions by classifying touch gestures, emotional messages, and individual touchers. In this way, we demonstrated that the proposed system is capable of capturing information that human receivers typically perceive during affective touch communication. This suggests that the tracking system could also be beneficial for related research areas involving human-human interactions, such as physical therapy and human-robot interaction.

Identified subtle contact changes and corresponding emotional perceptions across social contexts

In our daily social interactions, we routinely communicate distinct social and emotional intentions through even very nuanced touch. Meanwhile, our emotional communication is also influenced by social factors, such as the different relationship statuses. In our second chapter, we investigated how contact attributes are varied to express different emotional meanings, and how such subtle contact changes influence emotional perception. Psychophysical experiments were conducted with couples and strangers, in which touchers delivered cued emotional messages to the receiver's forearm. The touchers' contact delivery was quantified using our developed tracking system, while the emotional recognition accuracy and

perceived emotional valence and arousal were recorded from receivers. Through statistical analyses, we identified that even when using the same touch gesture, touchers could still convey distinct social messages by varying the magnitudes of their skin-to-skin contact in a subtle but significant way. Besides improving receivers' recognition of cued messages, this subtle tuning also correlates with receivers' perception of underlying valence and arousal. Moreover, we found that romantically involved couples perceive social touch as emotionally more pleasant and intense compared to the touch from strangers. Our analyses suggest that this perception discrepancy could be related to fine-tuning of the partner's contact, such as specific stroking velocities that preferentially activate C-tactile afferents, longer contact durations, and larger contact areas. However, despite the significant influences discussed above, we also found that relationship status has the least impact on contact delivery compared to other factors, such as touch gestures, emotional messages, and individual differences. This finding provides insights into when relationship status should be considered in future haptic design.

Investigated peripheral neural coding of human social touch expressions

Our sensation of touch relies on mechanosensitive sensory neurons, such as HFA, PC, Field, SAI, SAII, and CT afferents in human hairy skin. The role of these peripheral neurons in encoding social touch expressions under complex, natural conditions is not yet fully understood. To address this gap, we conducted microneurography experiments for the first time to record and analyze the responses of single units during human social touch interactions. By examining predefined, standard emotional expressions, we found that the firing properties of these neurons during human social touch closely align with those previously reported using controlled mechanical stimuli, validating our new experimental design with human touch stimuli. We then modeled the neurons' decoding of social touch by classifying standard touch expressions with both feature-based and time-series classification models. Results show that single units of multiple mechanoreceptive Aβ subtypes, especially slowly adapting type II (SA-II) and fast-adapting hair follicle afferents (HFA), can reliably differentiate social touch expressions at accuracies similar to human recognition performance. We identified the most informative firing patterns of SA-II and HFA afferents, which suggest that average firing durations of 3-4 seconds provide sufficient discriminative information. These two subtypes also exhibit robust tolerance to spike-timing shifts of up to 10-20 ms, varying with touch gestures due to their specific firing properties. Overall, our findings indicate that SA-II and HFA afferents can differentiate skin contact in social touch at time scales relevant for such interactions—1-2 orders of magnitude longer than those for non-social touch.

Publications

[J1] **S. Xu**, S. Hauser, S. Nagi, J. Jablonski, M. Rezaei, E. Jarocka, A. Marshall, H. Olausson, S. McIntyre, G. Gerling. Mechanoreceptive Aβ primary afferents discriminate naturalistic social touch inputs at a functionally relevant time scale. IEEE Trans. Affective Computing, 2024. [DOI]

[J2] **S. Xu**, C. Xu, G. Gerling. Social and emotional touch between romantic partners is affectively more pleasant due to finely tuned contact interactions. *IEEE Trans. Haptics*, 2023. [DOI]

[J3] Y. Moayedi, **S. Xu**, S. Obayashi, B. Hoffman, G. Gerling, E. Lumpkin. The cellular basis of mechanosensation in mammalian tongue. *Cell Reports,* 2023. [DOI]

[J4] **S. Xu**, C. Xu, S. McIntyre, H. Olausson, G. Gerling. 3D visual tracking to quantify physical contact interactions in human-to-human touch. *Front. Physiol.,* 2022. [DOI]

[J5] **S. Xu**, C. Xu, S. McIntyre, H. Olausson, G. Gerling. Subtle contact nuances in the delivery of human-to-human touch distinguish emotional sentiment. *IEEE Trans. Haptics,* 2022. [DOI]

[C1] **S. Xu**, S. Sykes, P. Abtahi, T. Grossman, D. Walden, M. Glueck, C. Rognon, Designing haptic feedback for sequential gestural inputs. *ACM CHI Conf. Hum. Factors Comput. Syst*. (*CHI'24*), 2024. [DOI]

[W1] **S. Xu**, S. Hauser, S. Nagi, S. McIntyre, H. Olausson, G. Gerling. A multivariate modeling approach to deciphering peripheral nerve signaling underlying naturalistic human touch. *IEEE Haptics Symp.*, (WIP), 2020.

References

[1] M. J. Hertenstein, D. Keltner, B. App, B. A. Bulleit, and A. R. Jaskolka, “Touch communicates distinct emotions,” *Emotion*, vol. 6, no. 3, pp. 528–533, Aug. 2006, doi: 10.1037/1528-3542.6.3.528.

[2] M. J. Hertenstein, R. Holmes, M. Mccullough, and D. Keltner, “The Communication of Emotion via Touch,” *Emotion*, vol. 9, no. 4, pp. 566–573, 2009, doi: 10.1037/a0016108.

[3] E. H. Thompson and J. A. Hampton, “The effect of relationship status on communicating emotions through touch,” *Cogn. Emot.*, vol. 25, no. 2, pp. 295–306, Feb. 2011, doi: 10.1080/02699931.2010.492957.

[4] S. C. Hauser, S. McIntyre, A. Israr, H. Olausson, and G. J. Gerling, “Uncovering Human-to-Human Physical Interactions that Underlie Emotional and Affective Touch Communication,” in *2019 IEEE World Haptics Conference (WHC)*, 2019, pp. 407–412, doi: 10.1109/WHC.2019.8816169.

[5] C. Lo, S. T. Chu, T. B. Penney, and A. Schirmer, “3D Hand-Motion Tracking and Bottom-Up Classification Sheds Light on the Physical Properties of Gentle Stroking,” *Neuroscience*, vol. 464, pp. 90–104, Sep. 2021, doi: https://doi.org/10.1016/j.neuroscience.2020.09.037.

[6] M. Salvato *et al.*, “Data-driven sparse skin stimulation can convey social touch information to humans,” *IEEE Trans. Haptics*, 2021, doi: 10.1109/TOH.2021.3129067.

[7] F. McGlone, J. Wessberg, and H. Olausson, “Discriminative and Affective Touch: Sensing and Feeling,” *Neuron*, vol. 82, no. 4. Cell Press, pp. 737–755, 21-May-2014, doi: 10.1016/j.neuron.2014.05.001.

[8] F. McGlone, A. B. Vallbo, H. Olausson, L. Loken, and J. Wessberg, “Discriminative touch and emotional touch,” *Can. J. Exp. Psychol.*, vol. 61, no. 3, pp. 173–183, Sep. 2007, doi: 10.1037/CJEP2007019.

[9] L. S. Löken, J. Wessberg, I. Morrison, F. McGlone, and H. Olausson, “Coding of pleasant touch by unmyelinated afferents in humans,” *Nat. Neurosci.*, vol. 12, no. 5, pp. 547–548, May 2009, doi: 10.1038/nn.2312.

[10] R. Ackerley, H. Backlund Wasling, J. Liljencrantz, H. Olausson, R. D. Johnson, and J. Wessberg, “Human C-tactile afferents are tuned to the temperature of a skin-stroking caress,” *J. Neurosci.*, vol. 34, no. 8, pp. 2879–2883, Feb. 2014, doi: 10.1523/JNEUROSCI.2847-13.2014.

[11] H. E. Van Stralen, M. J. E. van Zandvoort, S. S. Hoppenbrouwers, L. M. G. Vissers, L. J. Kappelle, and H. C. Dijkerman, “Affective touch modulates the rubber hand illusion,” *Cognition*, vol. 131, no. 1, pp. 147–158, Apr. 2014, doi: 10.1016/j.cognition.2013.11.020.

[12] S. Yohanan and K. E. MacLean, “The Role of Affective Touch in Human-Robot Interaction: Human Intent and Expectations in Touching the Haptic Creature,” *Int. J. Soc. Robot.*, vol. 4, no. 2, pp. 163–180, Apr. 2012, doi: 10.1007/s12369-011-0126-7.

[13] R. Andreasson, B. Alenljung, E. Billing, and R. Lowe, “Affective Touch in Human–Robot Interaction: Conveying Emotion to the Nao Robot,” *Int. J. Soc. Robot.*, vol. 10, no. 4, pp. 473–491, Sep. 2018, doi: 10.1007/s12369-017-0446-3.

[14] M. M. Jung, X. L. Cang, M. Poel, and K. E. Maclean, “Touch challenge’15: Recognizing social touch gestures,” in *Proceedings of the 2015 ACM International Conference on Multimodal Interaction (ICMI)*, 2015, pp. 387–390, doi: 10.1145/2818346.2829993.

[15] D. Silvera-Tawil, D. Rye, and M. Velonaki, “Interpretation of Social Touch on an Artificial Arm Covered with an EIT-based Sensitive Skin,” *Int. J. Soc. Robot.*, vol. 6, no. 4, pp. 489–505, Nov. 2014, doi: 10.1007/s12369-013-0223-x.

[16] M. Rezaei, S. S. Nagi, C. Xu, S. McIntyre, H. Olausson, and G. J. Gerling, “Thin Films on the Skin,

but not Frictional Agents, Attenuate the Percept of Pleasantness to Brushed Stimuli," in *2021 IEEE World Haptics Conference (WHC)*, 2021, pp. 49–54, doi: 10.1109/WHC49131.2021.9517259.
[17] S. C. Hauser, S. S. Nagi, S. McIntyre, A. Israr, H. Olausson, and G. J. Gerling, "From Human-to-Human Touch to Peripheral Nerve Responses," in *2019 IEEE World Haptics Conference (WHC)*, 2019, pp. 592–597, doi: 10.1109/WHC.2019.8816113.
[18] S. McIntyre *et al.*, "The language of social touch is intuitive and quantifiable," *Psychol. Sci.*, 2021.
[19] A. K. Suresh, J. M. Goodman, E. V. Okorokova, M. Kaufman, N. G. Hatsopoulos, and S. J. Bensmaia, "Neural population dynamics in motor cortex are different for reach and grasp," *Elife*, vol. 9, pp. 1–16, Oct. 2020, doi: 10.7554/ELIFE.58848.
[20] F. Mueller *et al.*, "Real-time pose and shape reconstruction of two interacting hands with a single depth camera," *ACM Trans. Graph.*, vol. 38, no. 4, p. 13, Jul. 2019, doi: 10.1145/3306346.3322958.
[21] A. Tagliasacchi, M. Schröder, A. Tkach, S. Bouaziz, M. Botsch, and M. Pauly, "Robust Articulated-ICP for Real-Time Hand Tracking," *Comput. Graph. Forum*, vol. 34, no. 5, pp. 101–114, Aug. 2015, doi: 10.1111/cgf.12700.
[22] T. Nath, A. Mathis, A. C. Chen, A. Patel, M. Bethge, and M. W. Mathis, "Using DeepLabCut for 3D markerless pose estimation across species and behaviors," *Nat. Protoc.*, vol. 14, no. 7, pp. 2152–2176, Jul. 2019, doi: 10.1038/s41596-019-0176-0.
[23] R. B. Rusu and S. Cousins, "3D is here: Point Cloud Library (PCL)," *Proc. IEEE Int. Conf. Robot. Autom.*, 2011, doi: 10.1109/ICRA.2011.5980567.
[24] J. Taylor *et al.*, "Efficient and precise interactive hand tracking through joint, continuous optimization of pose and correspondences," in *ACM Transactions on Graphics*, 2016, vol. 35, no. 4, pp. 1–12, doi: 10.1145/2897824.2925965.
[25] J. A. Russell, "A circumplex model of affect," *J. Pers. Soc. Psychol.*, vol. 39, no. 6, pp. 1161–1178, Dec. 1980.
[26] A. Gallace and C. Spence, "The science of interpersonal touch: An overview," *Neuroscience and Biobehavioral Reviews*, vol. 34, no. 2. Pergamon, pp. 246–259, 01-Feb-2010, doi: 10.1016/j.neubiorev.2008.10.004.
[27] A. W. Goodwin and H. E. Wheat, "Physiological Responses of Sensory Afferents in Glabrous and Hairy Skin of Humans and Monkeys," *Senses A Compr. Ref.*, vol. 6, pp. 39–54, Jan. 2008, doi: 10.1016/B978-012370880-9.00344-3.
[28] A. B. Vallbo, H. Olausson, J. Wessberg, and N. Kakuda, "Receptive field characteristics of tactile units with myelinated afferents in hairy skin of human subjects.," *J. Physiol.*, vol. 483, no. 3, pp. 783–795, Mar. 1995, doi: 10.1113/JPHYSIOL.1995.SP020622.
[29] S. C. Hauser *et al.*, "Human social touch as encoded by first-order Aβ and C-tactile afferents," *under Rev.*, 2021.
[30] C. J. Cascio, D. Moore, and F. McGlone, "Social touch and human development," *Dev. Cogn. Neurosci.*, vol. 35, pp. 5–11, Feb. 2019, doi: 10.1016/j.dcn.2018.04.009.
[31] J. A. Coan, H. S. Schaefer, and R. J. Davidson, "Lending a hand: Social regulation of the neural response to threat," *Psychol. Sci.*, vol. 17, no. 12, pp. 1032–1039, Dec. 2006, doi: 10.1111/j.1467-9280.2006.01832.x.
[32] Å. Vallbo, L. Löken, and J. Wessberg, "Sensual touch: A slow touch system revealed with microneurography," in *Affective Touch and the Neurophysiology of CT Afferents*, 2016, pp. 1–30.
[33] P. Bucci *et al.*, "Sketching CuddleBits: Coupled Prototyping of Body and Behaviour for an Affective Robot Pet," in *Proceedings of the 2017 CHI Conference on Human Factors in Computing Systems*, 2017, pp. 3681–3692.
[34] M. Y. Tsalamlal, N. Ouarti, J.-C. Martin, and M. Ammi, "Haptic communication of dimensions of emotions using air jet based tactile stimulation," *J. Multimodal User Interfaces 2014 91*, vol. 9,

no. 1, pp. 69–77, Sep. 2014, doi: 10.1007/S12193-014-0162-3.
[35] M. Teyssier, G. Bailly, C. Pelachaud, and E. Lecolinet, “Conveying Emotions Through Device-Initiated Touch,” *IEEE Trans. Affect. Comput.*, pp. 1–1, Jul. 2020, doi: 10.1109/TAFFC.2020.3008693.
[36] X. Zheng, M. Shiomi, T. Minato, and H. Ishiguro, “What Kinds of Robot’s Touch Will Match Expressed Emotions?,” *IEEE Robot. Autom. Lett.*, vol. 5, no. 1, pp. 127–134, Jan. 2020, doi: 10.1109/LRA.2019.2947010.
[37] G. K. Essick *et al.*, “Quantitative assessment of pleasant touch,” *Neurosci. Biobehav. Rev.*, vol. 34, no. 2, pp. 192–203, Feb. 2010, doi: 10.1016/J.NEUBIOREV.2009.02.003.
[38] M. J. Hertenstein, “Touch: Its communicative functions in infancy,” *Hum. Dev.*, vol. 45, no. 2, pp. 70–94, 2002.
[39] K. O. Johnson, “The roles and functions of cutaneous mechanoreceptors,” *Curr. Opin. Neurobiol.*, vol. 11, no. 4, pp. 455–461, Aug. 2001, doi: 10.1016/S0959-4388(00)00234-8.
[40] Y. Zhou, M. Habermann, W. Xu, I. Habibie, C. Theobalt, and F. Xu, “Monocular Real-time Hand Shape and Motion Capture using Multi-modal Data,” in *Proceedings of the IEEE/CVF Conference on Computer Vision and Pattern Recognition (CVPR)*, 2020, pp. 5346–5355.
[41] J. Romero, D. Tzionas, and M. J. Black, “Embodied hands: modeling and capturing hands and bodies together,” *ACM Trans. Graph.*, vol. 36, no. 6, Nov. 2017, doi: 10.1145/3130800.3130883.
[42] C. Xu, H. He, S. C. Hauser, and G. J. Gerling, “Tactile Exploration Strategies with Natural Compliant Objects Elicit Virtual Stiffness Cues,” *IEEE Trans. Haptics*, vol. 13, no. 1, pp. 4–10, Jan. 2020, doi: 10.1109/TOH.2019.2959767.
[43] C. Xu, Y. Wang, and G. J. Gerling, “An elasticity-curvature illusion decouples cutaneous and proprioceptive cues in active exploration of soft objects,” *PLoS Comput. Biol.*, vol. 17, no. 3, p. e1008848, Mar. 2021, doi: 10.1371/JOURNAL.PCBI.1008848.
[44] V. Russo, C. Ottaviani, and G. F. Spitoni, “Affective touch: A meta-analysis on sex differences,” *Neuroscience and Biobehavioral Reviews*, vol. 108. Elsevier Ltd, pp. 445–452, 01-Jan-2020, doi: 10.1016/j.neubiorev.2019.09.037.
[45] J. T. Suvilehto *et al.*, “Cross-cultural similarity in relationshipspecific social touching,” *Proc. R. Soc. B Biol. Sci.*, vol. 286, no. 1901, p. 20190467, Apr. 2019, doi: 10.1098/rspb.2019.0467.
[46] C. Xu, Y. Wang, and G. J. Gerling, “Individual Performance in Compliance Discrimination is Constrained by Skin Mechanics but Improved under Active Control,” *2021 IEEE World Haptics Conf. WHC 2021*, pp. 445–450, Aug. 2021, doi: 10.1109/WHC49131.2021.9517269.
[47] R. M. Peters, E. Hackeman, and D. Goldreich, “Diminutive Digits Discern Delicate Details: Fingertip Size and the Sex Difference in Tactile Spatial Acuity,” *J. Neurosci.*, vol. 29, no. 50, pp. 15756–15761, Dec. 2009, doi: 10.1523/JNEUROSCI.3684-09.2009.
[48] X. L. Cang, P. Bucci, A. Strang, J. Allen, K. Maclean, and H. Y. S. Liu, “Different strokes and different folks: Economical dynamic surface sensing and affect-related touch recognition,” in *ICMI 2015 - Proceedings of the 2015 ACM International Conference on Multimodal Interaction*, 2015, pp. 147–154, doi: 10.1145/2818346.2820756.
[49] C. Huang, Q. Wang, M. Zhao, C. Chen, S. Pan, and M. Yuan, “Tactile Perception Technologies and Their Applications in Minimally Invasive Surgery: A Review,” *Front. Physiol.*, vol. 11, p. 1601, Dec. 2020, doi: 10.3389/FPHYS.2020.611596.
[50] J. A. Russell and A. Mehrabian, “Evidence for a three-factor theory of emotions,” *J. Res. Pers.*, vol. 11, no. 3, pp. 273–294, Sep. 1977, doi: 10.1016/0092-6566(77)90037-X.
[51] I. Croy, A. Bierling, U. Sailer, and R. Ackerley, “Individual Variability of Pleasantness Ratings to Stroking Touch Over Different Velocities,” *Neuroscience*, vol. 464, pp. 33–43, Jun. 2021, doi: 10.1016/J.NEUROSCIENCE.2020.03.030.
[52] R. Ackerley, I. Carlsson, H. Wester, H. Olausson, and H. Backlund Wasling, “Touch perceptions

across skin sites: Differences between sensitivity, direction discrimination and pleasantness," *Front. Behav. Neurosci.*, vol. 8, no. FEB, p. 54, Feb. 2014, doi: 10.3389/FNBEH.2014.00054.
[53] M. Yao and R. Wang, "Neurodynamic analysis of Merkel cell–neurite complex transduction mechanism during tactile sensing," *Cogn. Neurodyn.*, vol. 13, no. 3, pp. 293–302, Jun. 2019, doi: 10.1007/S11571-018-9507-Z/FIGURES/8.
[54] J. Liljencrantz and H. Olausson, "Tactile C fibers and their contributions to pleasant sensations and to tactile allodynia," *Front. Behav. Neurosci.*, vol. 8, no. MAR, p. 37, Mar. 2014, doi: 10.3389/FNBEH.2014.00037.
[55] Y. S. Sefidgar, K. E. MacLean, S. Yohanan, H. F. M. H. Van Der Loos, E. A. Croft, and E. J. Garland, "Design and Evaluation of a Touch-Centered Calming Interaction with a Social Robot," *IEEE Trans. Affect. Comput.*, vol. 7, no. 2, pp. 108–121, Apr. 2016, doi: 10.1109/TAFFC.2015.2457893.
[56] M. Van Puyvelde, L. Collette, A. S. Gorissen, N. Pattyn, and F. McGlone, "Infants autonomic cardio-respiratory responses to nurturing stroking touch delivered by the mother or the father," *Front. Physiol.*, vol. 10, no. AUG, p. 1117, 2019, doi: 10.3389/FPHYS.2019.01117.
[57] C. A. Moyer, J. Rounds, and J. W. Hannum, "A Meta-Analysis of Massage Therapy Research," *Psychol. Bull.*, vol. 130, no. 1, pp. 3–18, Jan. 2004, doi: 10.1037/0033-2909.130.1.3.
[58] B. App, D. N. McIntosh, C. L. Reed, and M. J. Hertenstein, "Nonverbal Channel Use in Communication of Emotion: How May Depend on Why," *Emotion*, vol. 11, no. 3, pp. 603–617, Jun. 2011, doi: 10.1037/a0023164.
[59] A. Schirmer, C. Reece, C. Zhao, E. Ng, E. Wu, and S.-C. Yen, "Reach out to one and you reach out to many: Social touch affects third-party observers," *Br. J. Psychol.*, vol. 106, no. 1, pp. 107–132, Feb. 2015, doi: 10.1111/BJOP.12068.
[60] A. Saarinen, V. Harjunen, I. Jasinskaja-Lahti, I. P. Jääskeläinen, and N. Ravaja, "Social touch experience in different contexts: A review," *Neurosci. Biobehav. Rev.*, vol. 131, pp. 360–372, Dec. 2021, doi: 10.1016/J.NEUBIOREV.2021.09.027.
[61] A. Sorokowska *et al.*, "Affective Interpersonal Touch in Close Relationships: A Cross-Cultural Perspective," *Personal. Soc. Psychol. Bull.*, vol. 47, no. 12, pp. 1705–1721, Dec. 2021, doi: 10.1177/0146167220988373/ASSET/IMAGES/LARGE/10.1177_0146167220988373-FIG2.JPEG.
[62] S. McIntyre *et al.*, "Affective touch communication in close adult relationships," in *2019 IEEE World Haptics Conference (WHC)*, 2019, pp. 175–180, doi: 10.1109/WHC.2019.8816093.
[63] J. T. Suvilehto, E. Glerean, R. I. M. Dunbar, R. Hari, and L. Nummenmaa, "Topography of social touching depends on emotional bonds between humans," *Proc. Natl. Acad. Sci. U. S. A.*, vol. 112, no. 45, pp. 13811–13816, Nov. 2015, doi: 10.1073/PNAS.1519231112/SUPPL_FILE/PNAS.1519231112.SAPP.PDF.
[64] R. Beßler, J. Bendas, U. Sailer, and I. Croy, "The 'Longing for Interpersonal Touch Picture Questionnaire': Development of a new measurement for touch perception," *Int. J. Psychol.*, vol. 55, no. 3, pp. 446–455, Jun. 2020, doi: 10.1002/IJOP.12616.
[65] A. Schirmer, C. Cham, Z. Zhao, and I. Croy, "What Makes Touch Comfortable? An Examination of Touch Giving and Receiving in Two Cultures," *Personal. Soc. Psychol. Bull.*, Jun. 2022, doi: 10.1177/01461672221105966/ASSET/IMAGES/LARGE/10.1177_01461672221105966-FIG5.JPEG.
[66] A. Schirmer, M. H. Chiu, and I. Croy, "More Than One Kind: Different Sensory Signatures and Functions Divide Affectionate Touch," *Emotion*, 2021, doi: 10.1037/EMO0000966.
[67] L. Nummenmaa *et al.*, "Social touch modulates endogenous μ-opioid system activity in humans," *Neuroimage*, vol. 138, pp. 242–247, Sep. 2016, doi: 10.1016/J.NEUROIMAGE.2016.05.063.
[68] T. Strauss, A. Bytomski, and I. Croy, "The Influence of Emotional Closeness on Interindividual Touching," *J. Nonverbal Behav.*, vol. 44, no. 3, pp. 351–362, Sep. 2020, doi: 10.1007/S10919-020-00334-2/FIGURES/2.
[69] L. P. Kirsch, X. E. Job, M. Auvray, and V. Hayward, "Harnessing tactile waves to measure skin-to-

skin interactions," *Behav. Res. Methods*, vol. 53, no. 4, pp. 1469–1477, Aug. 2021, doi: 10.3758/S13428-020-01492-3/FIGURES/4.
[70] M. M. Bradley and P. J. Lang, "Measuring emotion: The self-assessment manikin and the semantic differential," *J. Behav. Ther. Exp. Psychiatry*, vol. 25, no. 1, pp. 49–59, Mar. 1994, doi: 10.1016/0005-7916(94)90063-9.
[71] S. Xu, C. Xu, S. McIntyre, H. H. Olausson, and G. J. Gerling, "3D Visual Tracking to Quantify Physical Contact Interactions in Human-to-Human Touch," *Front. Physiol.*, vol. 13, p. 778, Jun. 2022, doi: 10.3389/FPHYS.2022.841938/BIBTEX.
[72] S. Xu, C. Xu, S. Mcintyre, H. Olausson, and G. J. Gerling, "Subtle Contact Nuances in the Delivery of Human-to-Human Touch Distinguish Emotional Sentiment," *IEEE Trans. Haptics*, 2021, doi: 10.1109/TOH.2021.3137833.
[73] H. B. Mann and D. R. Whitney, "On a Test of Whether one of Two Random Variables is Stochastically Larger than the Other," *Ann. Math. Stat.*, vol. 18, no. 1, pp. 50–60, Jun. 1947, doi: 10.1214/AOMS/1177731909.
[74] J. Cohen, *Statistical power analysis for the behavioral sciences*. Academic press, 2013.
[75] Y. Benjamini and Y. Hochberg, "Controlling the False Discovery Rate: A Practical and Powerful Approach to Multiple Testing," *J. R. Stat. Soc. Ser. B*, vol. 57, no. 1, pp. 289–300, Jan. 1995, doi: 10.1111/J.2517-6161.1995.TB02031.X.
[76] A. Kuznetsova, P. B. Brockhoff, and R. H. B. Christensen, "lmerTest Package: Tests in Linear Mixed Effects Models," *J. Stat. Softw.*, vol. 82, no. 13, pp. 1–26, Dec. 2017, doi: 10.18637/JSS.V082.I13.
[77] M. S. Ben-Shachar, D. Lüdecke, and D. Makowski, "effectsize: Estimation of Effect Size Indices and Standardized Parameters Aims of the Package," *J. Open Source Softw.*, vol. 5, no. 56, 2020, doi: 10.21105/joss.02815.
[78] M. J. Hertenstein, J. M. Verkamp, A. M. Kerestes, and R. M. Holmes, "The Communicative Functions of Touch in Humans, Nonhuman Primates, and Rats: A Review and Synthesis of the Empirical Research," *Genet. Soc. Gen. Psychol. Monogr.*, vol. 132, no. 1, pp. 5–94, 2006, doi: 10.3200/MONO.132.1.5-94.
[79] L. F. Barrett, "The theory of constructed emotion: an active inference account of interoception and categorization," *Soc. Cogn. Affect. Neurosci.*, vol. 12, no. 1, pp. 1–23, Jan. 2017, doi: 10.1093/SCAN/NSW154.
[80] H. Olausson, J. Wessberg, I. Morrison, F. McGlone, and Å. Vallbo, "The neurophysiology of unmyelinated tactile afferents," *Neurosci. Biobehav. Rev.*, vol. 34, no. 2, pp. 185–191, Feb. 2010, doi: 10.1016/J.NEUBIOREV.2008.09.011.
[81] J. H. Kryklywy, M. R. Ehlers, A. K. Anderson, and R. M. Todd, "From Architecture to Evolution: Multisensory Evidence of Decentralized Emotion," *Trends Cogn. Sci.*, vol. 24, no. 11, pp. 916–929, Nov. 2020, doi: 10.1016/J.TICS.2020.08.002.
[82] H. Olausson *et al.*, "Unmyelinated tactile afferents signal touch and project to insular cortex," *Nat. Neurosci.*, vol. 5, no. 9, pp. 900–904, Jul. 2002, doi: 10.1038/nn896.
[83] C. Triscoli, H. Olausson, U. Sailer, H. Ignell, and I. Croy, "CT-optimized skin stroking delivered by hand or robot is comparable," *Front. Behav. Neurosci.*, vol. 7, no. DEC, p. 208, Dec. 2013, doi: 10.3389/fnbeh.2013.00208.
[84] S. Xu, C. Xu, and G. J. Gerling, "Social and Emotional Touch between Romantic Partners is Affectively More Pleasant due to Finely Tuned Contact Interactions," *IEEE Trans. Haptics*, 2023, doi: 10.1109/TOH.2023.3293070.
[85] V. E. Abraira and D. D. Ginty, "The sensory neurons of touch," *Neuron*, vol. 79, no. 4. pp. 618–639, 21-Aug-2013, doi: 10.1016/j.neuron.2013.07.051.
[86] F. Vega-Bermudez and K. O. Johnson, "SA1 and RA receptive fields, response variability, and population responses mapped with a probe array," *J. Neurophysiol.*, vol. 81, no. 6, pp. 2701–

2710, 1999, doi: 10.1152/JN.1999.81.6.2701/ASSET/IMAGES/LARGE/9K0690258012.JPEG.
[87] K. O. Johnson and S. S. Hsiao, “Neural mechanisms of tactual form and texture perception,” *Annu. Rev. Neurosci.*, vol. 15, pp. 227–250, 1992, doi: 10.1146/ANNUREV.NE.15.030192.001303.
[88] D. M. Owens and E. A. Lumpkin, “Diversification and Specialization of Touch Receptors in Skin,” *Cold Spring Harb. Perspect. Med.*, vol. 4, no. 6, p. a013656, Jun. 2014, doi: 10.1101/CSHPERSPECT.A013656.
[89] A. B. Vallbo’ and R. S. Johansson, “Properties of cutaneous mechanoreceptors in the human hand-related to touch sensation,” *Hum. Neurobiol*, vol. 3, pp. 3–14, 1984.
[90] G. Macefield, S. C. Gandevia, D. Burke, G. Macefield, S. C. Gandevia, and D. Burke, “Perceptual responses to microstimulation of single afferents innervating joints, muscles and skin of the human hand.,” *J. Physiol.*, vol. 429, no. 1, pp. 113–129, Oct. 1990, doi: 10.1113/JPHYSIOL.1990.SP018247.
[91] S. S. Nagi *et al.*, “An ultrafast system for signaling mechanical pain in human skin,” *Sci. Adv.*, vol. 5, no. 7, 2019, doi: 10.1126/SCIADV.AAW1297/SUPPL_FILE/AAW1297_SM.PDF.
[92] J. Ochoa and E. Torebjörk, “Sensations evoked by intraneural microstimulation of single mechanoreceptor units innervating the human hand.,” *J. Physiol.*, vol. 342, no. 1, pp. 633–654, Sep. 1983, doi: 10.1113/JPHYSIOL.1983.SP014873.
[93] I. Birznieks, H. E. Wheat, S. J. Redmond, L. M. Salo, N. H. Lovell, and A. W. Goodwin, “Encoding of tangential torque in responses of tactile afferent fibres innervating the fingerpad of the monkey,” *J. Physiol.*, vol. 588, no. 7, pp. 1057–1072, Apr. 2010, doi: 10.1113/JPHYSIOL.2009.185314.
[94] A. I. Weber *et al.*, “Spatial and temporal codes mediate the tactile perception of natural textures,” *Proc. Natl. Acad. Sci. U. S. A.*, vol. 110, no. 42, pp. 17107–17112, Oct. 2013, doi: 10.1073/PNAS.1305509110/SUPPL_FILE/PNAS.201305509SI.PDF.
[95] H. P. Saal and S. J. Bensmaia, “Touch is a team effort: interplay of submodalities in cutaneous sensibility,” *Trends Neurosci.*, vol. 37, no. 12, pp. 689–697, Dec. 2014, doi: 10.1016/J.TINS.2014.08.012.
[96] J. Gautrais and S. Thorpe, “Rate coding versus temporal order coding: A theoretical approach,” *BioSystems*, vol. 48, no. 1–3, pp. 57–65, 1998, doi: 10.1016/S0303-2647(98)00050-1.
[97] Å. B. Vallbo, H. Olausson, and J. Wessberg, “Unmyelinated afferents constitute a second system coding tactile stimuli of the human hairy skin,” *J. Neurophysiol.*, vol. 81, no. 6, pp. 2753–2763, 1999, doi: 10.1152/jn.1999.81.6.2753.
[98] B. B. Edin, “Quantitative analysis of static strain sensitivity in human mechanoreceptors from hairy skin,” *J. Neurophysiol.*, vol. 67, no. 5, pp. 1105–1113, 1992, doi: 10.1152/jn.1992.67.5.1105.
[99] D. T. Blake, K. O. Johnson, and S. S. Hsiao, “Monkey cutaneous SAI and RA responses to raised and depressed scanned patterns: Effects of width, height, orientation, and a raised surround,” *J. Neurophysiol.*, vol. 78, no. 5, pp. 2503–2517, 1997, doi: 10.1152/JN.1997.78.5.2503/ASSET/IMAGES/LARGE/JNP.NO62F16.JPEG.
[100] F. McGlone and D. Reilly, “The cutaneous sensory system,” *Neurosci. Biobehav. Rev.*, vol. 34, no. 2, pp. 148–159, Feb. 2010, doi: 10.1016/J.NEUBIOREV.2009.08.004.
[101] B. B. Edin and A. B. Vallbo, “Dynamic response of human muscle spindle afferents to stretch,” *J. Neurophysiol.*, vol. 63, no. 6, pp. 1297–1306, 1990, doi: 10.1152/jn.1990.63.6.1297.
[102] L. J. von Buchholtz, N. Ghitani, R. M. Lam, J. A. Licholai, A. T. Chesler, and N. J. P. Ryba, “Decoding Cellular Mechanisms for Mechanosensory Discrimination,” *Neuron*, vol. 109, no. 2, pp. 285-298.e5, Jan. 2021, doi: 10.1016/J.NEURON.2020.10.028.
[103] L. Bai *et al.*, “Genetic Identification of an Expansive Mechanoreceptor Sensitive to Skin Stroking,” *Cell*, vol. 163, no. 7, pp. 1783–1795, Dec. 2015, doi: 10.1016/J.CELL.2015.11.060.
[104] R. S. Johansson, “Tactile sensibility in the human hand: receptive field characteristics of mechanoreceptive units in the glabrous skin area.,” *J. Physiol.*, vol. 281, no. 1, pp. 101–125, Aug.

1978, doi: 10.1113/JPHYSIOL.1978.SP012411.
[105] B. B. Edin and J. H. Abbs, “Finger movement responses of cutaneous mechanoreceptors in the dorsal skin of the human hand,” *https://doi.org/10.1152/jn.1991.65.3.657*, vol. 65, no. 3, pp. 657–670, 1991, doi: 10.1152/JN.1991.65.3.657.
[106] J. Wessberg, H. Olausson, K. W. Fernström, and Å. B. Vallbo, “Receptive field properties of unmyelinated tactile afferents in the human skin,” *J. Neurophysiol.*, vol. 89, no. 3, pp. 1567–1575, Mar. 2003, doi: 10.1152/jn.00256.2002.
[107] L. Li and D. D. Ginty, “The structure and organization of lanceolate mechanosensory complexes at mouse hair follicles,” *Elife*, vol. 2014, no. 3, Feb. 2014, doi: 10.7554/ELIFE.01901.001.
[108] B. B. Edin, G. K. Essick, M. Truisson, and K. A. Olsson, “Receptor encoding of moving tactile stimuli in humans. I. Temporal pattern of discharge of individual low-threshold mechanoreceptors,” *J. Neurosci.*, vol. 15, no. 1, pp. 830–847, Jan. 1995, doi: 10.1523/JNEUROSCI.15-01-00830.1995.
[109] I. Morrison, L. S. Löken, and H. Olausson, “The skin as a social organ,” *Exp. Brain Res.*, vol. 204, no. 3, pp. 305–314, Jul. 2010, doi: 10.1007/S00221-009-2007-Y/FIGURES/2.
[110] H. Olausson *et al.*, “Functional role of unmyelinated tactile afferents in human hairy skin: Sympathetic response and perceptual localization,” *Exp. Brain Res.*, vol. 184, no. 1, pp. 135–140, Jan. 2008, doi: 10.1007/S00221-007-1175-X/TABLES/2.
[111] S. J. Middleton *et al.*, “Nav1.7 is required for normal C-low threshold mechanoreceptor function in humans and mice,” *Brain*, vol. 145, no. 10, pp. 3637–3653, Oct. 2022, doi: 10.1093/BRAIN/AWAB482.
[112] J. Wessberg and A. B. Vallbo, “Coding of pulsatile motor output by human muscle afferents during slow finger movements.,” *J. Physiol.*, vol. 485, no. 1, pp. 271–282, May 1995, doi: 10.1113/jphysiol.1995.sp020729.
[113] I. Gordon, A. C. Voos, R. H. Bennett, D. Z. Bolling, K. A. Pelphrey, and M. D. Kaiser, “Brain mechanisms for processing affective touch,” *Hum. Brain Mapp.*, vol. 34, no. 4, pp. 914–922, Apr. 2013, doi: 10.1002/HBM.21480.
[114] M. Shiomi, T. Minato, and H. Ishiguro, “Subtle Reaction and Response Time Effects in Human-Robot Touch Interaction,” *Lect. Notes Comput. Sci. (including Subser. Lect. Notes Artif. Intell. Lect. Notes Bioinformatics)*, vol. 10652 LNAI, pp. 242–251, 2017, doi: 10.1007/978-3-319-70022-9_24/FIGURES/6.
[115] H. P. Saal, B. P. Delhaye, B. C. Rayhaun, and S. J. Bensmaia, “Simulating tactile signals from the whole hand with millisecond precision,” *Proc. Natl. Acad. Sci. U. S. A.*, vol. 114, no. 28, pp. E5693–E5702, Jul. 2017, doi: 10.1073/PNAS.1704856114/SUPPL_FILE/PNAS.1704856114.SM02.AVI.
[116] H. Khamis, I. Birznieks, and S. J. Redmond, “Decoding tactile afferent activity to obtain an estimate of instantaneous force and torque applied to the fingerpad,” *J. Neurophysiol.*, vol. 114, no. 1, pp. 474–484, May 2015, doi: 10.1152/JN.00040.2015/ASSET/IMAGES/LARGE/Z9K0151531330007.JPEG.
[117] R. S. Johansson and I. Birznieks, “First spikes in ensembles of human tactile afferents code complex spatial fingertip events,” *Nat. Neurosci.*, vol. 7, no. 2, pp. 170–177, Jan. 2004, doi: 10.1038/nn1177.
[118] E. L. Mackevicius, M. D. Best, H. P. Saal, and S. J. Bensmaia, “Millisecond Precision Spike Timing Shapes Tactile Perception,” *J. Neurosci.*, vol. 32, no. 44, pp. 15309–15317, Oct. 2012, doi: 10.1523/JNEUROSCI.2161-12.2012.
[119] J. D. Victor and K. P. Purpura, “Metric-space analysis of spike trains: theory, algorithms and application,” *Netw. Comput. neural Syst.*, vol. 8, no. 2, pp. 127–164, 1997, doi: 10.1088/0954-898X_8_2_003.
[120] S. Schreiber, J. M. Fellous, D. Whitmer, P. Tiesinga, and T. J. Sejnowski, “A new correlation-based measure of spike timing reliability,” *Neurocomputing*, vol. 52–54, p. 925, Jun. 2003, doi:

10.1016/S0925-2312(02)00838-X.
[121] T. Gollisch, “Estimating receptive fields in the presence of spike-time jitter,” *Netw. Comput. Neural Syst.*, vol. 17, no. 2, pp. 103–129, Jun. 2006, doi: 10.1080/09548980600569670.
[122] A. Rokem, S. Watzl, T. Gollisch, M. Stemmler, A. V. M. Herz, and I. Samengo, “Spike-timing precision underlies the coding efficiency of auditory receptor neurons,” *J. Neurophysiol.*, vol. 95, no. 4, pp. 2541–2552, Apr. 2006, doi: 10.1152/JN.00891.2005/ASSET/IMAGES/LARGE/Z9K0040673230011.JPEG.
[123] R. Lestienne, “Spike timing, synchronization and information processing on the sensory side of the central nervous system,” *Prog. Neurobiol.*, vol. 65, no. 6, pp. 545–591, Dec. 2001, doi: 10.1016/S0301-0082(01)00019-3.
[124] R. S. Johansson, U. Landström, and R. Lundström, “Sensitivity to edges of mechanoreceptive afferent units innervating the glabrous skin of the human hand,” *Brain Res.*, vol. 244, no. 1, pp. 27–32, Jul. 1982, doi: 10.1016/0006-8993(82)90900-3.
[125] M. Knibestöl and B. Vallbo, “Single Unit Analysis of Mechanoreceptor Activity from the Human Glabrous Skin,” *Acta Physiol. Scand.*, vol. 80, no. 2, pp. 178–195, Oct. 1970, doi: 10.1111/J.1748-1716.1970.TB04783.X.
[126] G. Corniani, M. A. Casal, S. Panzeri, and H. P. Saal, “Population coding strategies in human tactile afferents,” *PLoS Comput. Biol.*, vol. 18, no. 12, pp. 1–24, Dec. 2022, doi: 10.1371/journal.pcbi.1010763.
[127] M. Y. Tsalamlal, M. A. Amorim, J. C. Martin, and M. Ammi, “Combining Facial Expression and Touch for Perceiving Emotional Valence,” *IEEE Trans. Affect. Comput.*, vol. 9, no. 4, pp. 437–449, Oct. 2018, doi: 10.1109/TAFFC.2016.2631469.
[128] S. I. Askari, V. J. Harjunen, M. M. Spape, A. Haans, N. Ravaja, and W. A. Ijsselsteijn, “Receiving a Mediated Touch From Your Partner vs. a Male Stranger: How Visual Feedback of Touch and Its Sender Influence Touch Experience,” *IEEE Trans. Affect. Comput.*, vol. 14, no. 2, pp. 1044–1055, Apr. 2023, doi: 10.1109/TAFFC.2021.3085185.
[129] A. B. Warriner, V. Kuperman, and M. Brysbaert, “Norms of valence, arousal, and dominance for 13,915 English lemmas,” *Behav. Res. Methods*, vol. 45, no. 4, pp. 1191–1207, Dec. 2013, doi: 10.3758/s13428-012-0314-x.